Nucleation and crystallization of poly(lactic acid)

Yury Yuryev

A Thesis

in

The Department

of

Mechanical and Industrial Engineering

Presented in Partial Fulfillment of the Requirements

For the Degree of

Doctor of Philosophy (Mechanical Engineering) at

Concordia University

Montreal, Quebec, Canada

November, 2011

CONCORDIA UNIVERSITY

SCHOOL OF GRADUATE STUDIES

This is to certify that the thesis prepared

By: **Yury Yuryev**

Entitled: **Nucleation and crystallization of poly(lactic acid)**

and submitted in partial fulfillment of the requirements for the degree of

DOCTOR OF PHILOSOPHY (Mechanical Engineering)

complies with the regulations of the University and meets the accepted standards with respect to originality and quality.

Signed by the final examining committee:

Dr. M. Elektorowicz _____ Chair

Dr. João Soares _____External Examiner

Dr. M. Nokken _____External to Program

Dr. M.D. Pugh _____Examiner

Dr. M. Medraj _____ Examiner

Dr. P. Wood-Adams _____Thesis Supervisor

Approved by Dr. W-F. Xie_____
Graduate Program Director

Dr. Robin A.L. Drew_____
Dean of Faculty of Engineering & Computer Science

Abstract

Nucleation and crystallization of poly(lactic acid)

Yury Yuryev, Ph.D.

Concordia University, 2011

Poly(lactic acid) is one of the most promising "green" polymers, having huge potential for use as a packaging and construction material. The lack of knowledge about polylactide-specific crystallization behaviour is one of the barriers to widespread industrial use.

In the present thesis, different aspects of one of the most important phenomena in polylactide crystallization were studied. In the series of articles included in this thesis, parameters of quiescent and field-induced crystallization were investigated. Significant attention was paid to the spherulitic morphology, growth rates, and stereocomplexation phenomenon that are intrinsic to polylactide, due its optical activity. A novel technique for growth rate measurements based on ultrafast heating and cooling of cast films, was suggested and validated.

Melt crystallization of polylactide was studied using rheological methods. A new advanced model allowing the relation of complex viscosity to melt crystallinity was proposed and verified. The physical cross-linking phenomenon was introduced and quantified in the frame of the proposed model. Also, a new technique allowing the determination of the induction time of crystallization was presented and successfully

validated. A proposed technique allowed dramatically improved precision of the measurement of induction time for both quiescent and field-induced crystallization.

The phenomena of surface crystallization that had previously gone unexamined by the research community were investigated in detail. A theoretical model was suggested and its predictions were supported by extensive computer simulations. The simulation program used for research was developed during this study. It was found that surface crystallization can have an immense effect on crystallization kinetics and dramatically distort the observed thermal analysis results. Custom-designed experiments allowed the application of these results to polylactide crystallization.

Extensive studies of shear-induced crystallization were done in this work. The novel techniques developed in the research allowed for a better understanding of the field-induced phenomenon. New techniques allowing the implementation of rheological measurements to discover and quantitatively assess electric field-induced polylactide crystallization were investigated in this study as well. It was shown that a DC electric field significantly promotes homogeneous nucleation of polylactide and enhances crystallization. An explanation to this observation based on the dipole moments of repeat units in the polylactide chain was offered and validated.

Contributions of Author

This thesis contains chapters that present results that have been published in the form of unaltered original journal articles as well as material that is in preparation for submission or already submitted. The complete citations for these papers and the chapters in which they appear are provided below:

CHAPTER 2, 3: Yury Yuryev, Paula Wood-Adams, Marie-Claude Heuzey, Charles Dubois, Josee´ Brisson "Crystallization of polylactide films: An atomic force microscopy study of the effects of temperature and blending." Published in: *Polymer*; 2008; 49; 2306-2320. As well as new results, this article contains some material published in the M.A.Sc thesis by Yury Yuryev "Application of Atomic Force Microscopy for the Study of Crystalization Kinetics and Morphology of L-and D- Polyactide Blends in Solution Cast Thin Films" (ISBN: 9780494207697).

CHAPTER 5: Yury Yuryev, Paula Wood-Adams "Rheological properties of crystallizing polylactide: Detection of induction time and modeling the evolving structure and properties." Published in: *Journal of Polymer Science: Part B: Polymer Physics;* 2010; 48, 812–822.

CHAPTER 7: Yury Yuryev, Paula Wood-Adams "Effect of Surface Nucleation on

Isothermal Crystallization Kinetics: Theory, Simulation and Experiment." Published in: *Polymer;* 2011; 52; 708-717.

CHAPTER 9: Yury Yuryev, Paula Wood-Adams "Crystallization of poly(L-/D-lactide) in the presence of electric fields." Accepted to *Macromolecular Chemistry and Physics* for publication.

Appendix 1: "Monte Carlo Simulation of polymer crystallization" contains excerpts from the article by Yury Yuryev and Paula Wood-Adams "A Monte Carlo Simulation of Homogeneous Crystallization in Confined Spaces: Effect of Crystallization Kinetics on the Avrami Exponent". Published in: *Macromolecular Theory and Simulations;* 2010, 19, 278–287.

All the papers presented in this thesis were co-authored and reviewed prior to submission to publication by Dr. Paula Wood-Adams, my supervisor. The first paper was co-authored by Dr. Marie-Claude Heuzey (École Polytechnique de Montréal, Montreal, Québec), Dr. Charles Dubois (École Polytechnique de Montréal, Montreal, Québec) and Dr. Josee Brisson (Département de chimie, Faculté des sciences et de génie, Université Laval, Québec,) who provided valuable input to the ideas and content in the article. All of the remaining work and manuscript preparation were performed by the author of this thesis.

Acknowledgements

I would like to thank my supervisor Dr. Paula Wood-Adams for her continuous support and guidance during my time at Concordia University. In addition to the time she spent with me, providing valuable explanations about the numerous technical and theoretical questions I had, I especially appreciated her positive and encouraging attitude towards my work.

I am grateful to the following people for the help they provided over the course of this research project: Dr. Mamoun Medraj who provided a valuable support when I needed it the most, Dr. Marie-Claude Heuzey École Politechnique de Montréal, Dr. Charles Dubois of École Politechnique de Montréal and Dr. Josée Brisson of Université Laval.

Final heartfelt thanks go to my wife Jana for her unconditional love and moral support. I would also like to deeply thank my parents, Galina and Vitaly, my friends Ark, Heng and Ramin.

You all helped me to make the most of my experience in Canada.

Thank you.

Statement of Originality

I hereby certify that all of the work described within this thesis is the original work of the author. Any published (or unpublished) ideas and techniques from the works of other authors are fully acknowledged in accordance with the standard referencing practices.

September 2011

Yury Yuryev

Table of Contents

List of Figures……...……xiv

List of Tables…….....xxiii

Nomenclature……..……xxiv

CHAPTER 1 Introduction…….….1

1.1 Thesis objectives……2

1.2 Thesis organization……3

CHAPTER 2 Poly(lactide) crystallization …….5

2.1 Crystalline modifications of polylactide……5

2.2 Crystallization kinetics and spherulitic morphology of poly(lactide)……6

2.3 Stereocomplexation phenomenon in poly(lactide) crystallization…….7

CHAPTER 3 Crystallization of polylactide films: An atomic force microscopy study of the effects of temperature and blending……..10

3.1 Introduction ……10

3.2 Experimental ……...15

3.2.1 Materials and sample preparation…….15

3.2.2 Heating/cooling of samples……...19

3.2.3 Technique for the measurement of spherulite size……...20

3.2.4 Influence of the heating/cooling cycle on spherulite growth measurements……...22

3.2.5 Generality of experimental technique……...25

3.3 Results and discussion…….27

3.3.1 Isothermal spherulite growth rate…….27

3.3.2 The crystalline morphology of polylactides…….31

3.3.3 Stereocomplexation phenomenon in polylactide blends and its influence on spherulite growth……..35

3.4 Conclusions……..46

CHAPTER 4 Degradation and rheology of poly(lactide) ……...48

CHAPTER 5 Rheological properties of crystallizing polylactide: Detection of induction time and modeling the evolving structure and properties ……53

5.1 Introduction…….53

5.2 Experimental……56

5.3 Results and discussion…….59

5.3.1 The exponential decay model of polylactide thermal degradation……..59

5.3.2 The determination of induction time of homogeneous crystallization using the standardized residuals technique……61

5.3.3 Rheological properties and crystallization at the initial stages…….67

5.3.4 The Physical Crosslink Model……..74

5.3.5 Gelation and the transition to solid-like behavior…….77

5.4 Conclusions……..82

CHAPTER 6 The surface crystallization phenomenon in polymer crystallization …….84

CHAPTER 7 Effect of surface nucleation on isothermal crystallization kinetics: theory, simulation and experiment……...……..86

7.1 Introduction……..86

7.2 Experimental methods…….92

7.3 Numerical methods……..97

7.4 Kinetics of surface crystallization: theory and simulation…….100

7.5 Results and discussion……...108

7.5.1 Experimental results……108

7.5.2 Monte-Carlo simulation of crystallization kinetics of the samples of different thickness……114

7.6 Conclusions……118

CHAPTER 8 Overview of polymer crystallization induced by electric field……119

8.1 Thermodynamics of polymer crystallization…….119

8.2 Nucleation and crystal growth in homogeneous polymer systems……...120

8.3 Effect of the electric field on polymer nucleation…….122

8.4 Effect of electric field on morphology and growth rate of polymer crystalline structures……123

8.5 Dipoles in A1-type polymers and dynamic properties of polymer chains…….....……125

CHAPTER 9 Crystallization of poly(L-/D-lactide) in the presence of electric fields……..……130

9.1 Introduction ……...130

9.2 Experimental section ……..……133

9.3 Results and discussion…….……..135

9.3.1 Effect of the electric field on induction time for crystallization….137

9.3.2 Effect of electric field on the complex viscosity of crystallizing

polylactide ……..138
9.3.3 The crystal structure as determined by XRD analysis ……..140
9.3.4 The crystalline morphology as observed using optical microscopy……...141
9.3.5 Estimation of nucleation rate from viscosity……..144
9.3.6 Estimation of nucleation rate from viscosity……..146
9.4 Conclusion…….149
CHAPTER 10 Flow-induced crystallization of linear polylactide observed by rheology……..150
10.1 Introduction…….150
10.2 Experimental……153
10.3 Results and discussion…….154
10.3.1 Specifics of the geometry of the measuring system in context of the shear-induced crystallization experiments…….154
10.3.2. The effect of the surface crystallization on rheology of the crystallizing melt……...158
10.3.3 The standardized residuals approach to crystallization onset determination: practice and rheological data evaluations……..160
10.3.4 An induction time of the polylactide crystallization under continuous constant shear……..163
10.3.5 An induction time of the polylactide crystallization under step shear……..166
10.4. Conclusion…….168
CHAPTER 11 Conclusions, contributions and recommendations for

the future work…….169

11.1 Conclusions……..169

11.2 Contributions……...172

11.3 Recommendations for the future work……174

Appendix 1 Monte Carlo Simulation of polymer crystallization……176

Description of the subroutines…….175

Subroutine A1……...…177

Subroutine A2……...…177

Nucleation……..……..178

Subroutine A3……..……178

Growth Simulation……...……179

Subroutine A4……..……179

Subroutine A5……..……179

Subroutine A6……..……180

Subroutine A7……..……181

Crystallization data post-processing……...….181

Crystallization parameters and data handling……..…181

REFERENCES……...…….183

List of Figures

Figure 2.1 The chemical structure of polylactide……...5

Figure 3.1 The development sequence of crystalline structure on the surface of the (a) premelted and (b) solution cast films of poly(L/D-lactide) at 110 ºC. The upper row images show the polymer surface prior to isothermal crystallization, the middle and lower rows show the same samples crystallized for 2 and 4 minutes, respectively. The round elevated area on the left images is an amorphous area remaining after a spherulite formed in the casting step was melted in the premelting step. The 100 μm AFM height images are shown……...18

Figure 3.2 AFM height image of solution cast poly(L/D-lactide) film (left) and spherulite cross-section (right). These spherulites are about 25 μm in size and are typical for the both polylactides under investigation in solution cast films. Image size is 50 μm. Note clearly distinguishable spherulite borders which make accurate size measurements possible. ……..21

Figure 3.3 The AFM height images of the same area of the same poly(L-lactide) sample subjected to crystallization at 130 ºC in (a) one fast heating/cooling cycle for 100 seconds; (b) two cycles (150 seconds in total); (c) three cycles (200 seconds in total) and (d) four cycles (250 seconds in total) . (e) Sample crystallized at 130 ºC in one cycle for 250 seconds is considered to be the reference point. All images are 100 μm scans.……..24

Figure 3.4 Influence of fast heating/cooling cycle on spherulite size and growth rate measurements of poly(L-lactide). The comparison of the spherulite sizes of the samples

subjected to multiple fast heating/cooling cycle with those of the samples subjected to only one cycle at 110 ºC (a), 130 ºC (b) and 150 ºC (c).……...25

Figure 3.5 Morphology of isotactic polystyrene crystallized at 170 ºC for 65 min……..26

Figure 3.6 Spherulite size vs. isothermal crystallization time for poly(L/D-lactide) at various temperatures (a)–(c). Error bars indicate one standard deviation. (d) Spherulite radius growth rate vs. isothermal crystallization temperature. Error bars indicate standard error in the slope from least squares regression of data in (a)–(c)……...28

Figure 3.7 Spherulite size vs. isothermal crystallization time for poly(L-lactide) at various temperatures (a) – (c). Error bars indicate one standard deviation. (d) Spherulite radius growth rate vs. isothermal rystallization temperature. Error bars indicate standard error in the slope from least squares regression of data in (a) – (c)……...29

Figure 3.8 Morphology of surface crystallinity of poly(L-lactide) formed (a) at 90 ºC for 1.5 min (50 μm height image); (b) at 120 ºC for 4 minutes (100 μm height image) and (c) morphology of surface crystallinity of poly(L/D-lactide) formed at 160 ºC for 60 minutes (100 μm height image)……..……..…32

Figure 3.9 The crystalline morphology of the poly(L-lactide) samples crystallized at low supercooling. Crystallization temperatures, times and AFM height image scales are: (a) 170 ºC, 120 minutes, 20 μm ; (b) 165 ºC, 30 minutes, 50 μm; (c) 165 ºC, 90 minutes, 100 μm; (d) 170 ºC, 120 minutes, 8 μm; (e) 165 ºC, 60 minutes, 30 μm; (f) 165 ºC, 25 minutes, 15 μm.……..33

Figure 3.10 Second runs DSC curves for the blends of (a) poly(L/D-lactide) and (b) poly(L-lactide) with varying poly(D-lactide) content. Heating rate is 5 °C/min. Curves were shifted vertically for clarity ……..36

Figure 3.11 Enthalpy of stereocomplex melting for polylactide blends. Filled symbols are for blends of poly(L/D-lactide) with poly(D-lactide) and open symbols are for blends of poly(L-lactide) with poly(D-lactide). Extracted from data in Figure 3.10…….38

Figure 3.12 Isothermal spherulite radius growth rates for poly(L/D-lactide) and its blends with poly(D-lactide). ……40

Figure 3.13 Isothermal spherulite radius growth rates for poly(L-lactide) and its blend with poly(D-lactide)……..41

Figure 3.14 Reduced spherulite growth rate at 110°C (solid lines) and 120°C (dashed lines). Note that 110 ºC is in regime III and 120 ºC is in regime II……..42

Figure 4.1 The Arrhenius equation fits for polylactide at $t=0$ and $t=\infty$. Only data points for temperatures higher than 160 °C are used……50

Figure 5.1 The complex viscosity of L 9000 polylactide and exponential decay fits…..60

Figure 5.2 The complex viscosity of homogeneously nucleated L 9000 polylactide at different temperatures. The solid lines are corresponding fits according to Equation 5.2..…….62

Figure 5.3 The standardized residuals of complex viscosity, storage G′ and loss G′′ modulii at 1 Hz during homogeneous crystallization at (a) 140 °C and 155 °C (b). The vertical lines at 2400 s (140 °C) and 35100 s (150 °C) show the induction points.……..65

Figure 5.4 The standardized residuals for complex viscosity at 155 ºC based on model fits using various data sets: up to 30000 s: no crystallization; up to 35100 s: until onset of crystallization; and up to 40000 s: beyond onset of crystallization……...…66

Figure 5.5 Comparison of induction times of homogeneous crystallization of polylactide determined from rheological data and DSC measurements. Error bars for rheological data represent 1 standard deviation from 3 measurements at each point. Error bars for DSC data were determined using the confidence band technique for scarce data…….66

Figure 5.6 The Avrami fit for isothermal DSC data used in the determination of nucleation rate.……...69

Figure 5.7 The enhancement of viscosity during homogeneous crystallization of polylactide at different temperatures. The curves represent the filler effect estimated using Equation 5.8.……71

Figure 5.8 Effect of physical crosslinks on the viscosity of crystallizing polylactide at different temperatures. The *Y* axis is the ratio between real viscosity and the viscosity after taking into account only the filler effect using Equation 5.8. Curves represent the best fits of Equation 5.10.……..72

Figure 5.9 Physical entanglement factor δ at different temperatures.……...73

Figure 5.10 The fit of the proposed model (Equation 5.11).…….73

Figure 5.11 A schematic illustration of physical crosslink effect.……75

Figure 5.12 A series of frequency sweeps of crystallizing polylactide at 140 °C interpolated to the same moment in time. (a) Complex viscosity η^* and (b) storage modulus G'. Note that induction takes place at 2400 s at this temperature and φ is the volume fraction crystallinity corresponding to the time of the sweep.……..78

Figure 5.13 Relationship between equilibrium modulus and volume fraction crystallinity at 140°C. Symbols are raw experimental data, and the straight line emphasizes the proportionality between G_e and φ^3. Inset shows $G'(t)$ for 3 frequencies…….……81

Figure 7.1 Temperature protocol for DSC experiments. The sample was first heated to 200°C (30°C above the melting point) at 20°C/min (1) then held at 200°C for 5 minutes to erase the thermal history (2). Next, the sample was rapidly cooled at 50°C/min (3) to the isothermal crystallization temperature (4) and held for a predetermined time. Next, the sample was rapidly heated at 50°C/min to 150°C to avoid secondary crystallization (5) and finally heated to 200°C at 5°C/min (6).…….95

Figure 7.2 An example of shifted baseline and crystallization heat curve (a 77 μm sample at 130°C is shown). The sharp endotherm at about 10 minutes, present in the baseline and in the experimental data, is due to the thermal response of the apparatus.……96

Figure 7.3 Illustration of the first 2 stages of surface induced crystallization.…..……..101

Figure 7.4 Kinetics of surface crystallization for different surface nucleation concentration. Data points are the simulation results for d=500 μm and G=1.715 μm/min. Doted lines are fits of simulated crystallization data for the first stage of crystallization using Equation (7.7). ……..……102

Figure 7.5 An illustration of the concept of equivalent spherical segment. Image is a 100 μm by 100 μm AFM height image of a poly(L/D-lactide) film, surface crystallized at 120°C on a glass surface and having local nucleation density of 1.3×10^9 m^{-2}. The dashed circle represents an equivalent diameter c_e corresponding to this nucleation concentration. The confinement interfaces show up as the dark lines bordering the crystallites.……...104

Figure 7.6 The simulated crystallization kinetics (symbols) and corresponding analytical functions Eqsuations 12 and 13 (solid lines). The three crystallization stages are denoted in roman numerals. Data for d=500 μm and G=1.715 μm/min are shown. The best fit value of f is 0.48……..106

Figure 7.7 Simulated crystallization rate curves showing 3 different types of crystallization: pure surface nucleation (N_s= 10^8 m^{-2}, $\tau_{½}$=4874 s), pure bulk nucleation (N=10^8 $s^{-1}m^{-3}$, $\tau_{½}$=4242 s), and mixed nucleation (N_s= 10^8 m^{-2} and N=10^8 $s^{-1}m^{-3}$, $\tau_{½}$=3533 s). Data are the simulation results for d=500 μm and G=1.715 μm/min.……107

Figure 7.8 Experimental half-times of crystallization of poly(L-lactide) sandwiched between aluminium surfaces.……...109

Figure 7.9 The experimental spherulitic growth rate of the poly(L/D-lactide) used in thist study. Data are taken from Yuryev et al. [78] The square symbols highlight the experimental conditions of this study..……110

Figure 7.10 The simulation of bulk crystallization kinetics of the system having N=1×10^8 $s^{-1}m^{-3}$ with different growth rates. The dashed lines represent the half-time $\tau_{½}$ of crystallization..……112

Figure 7.11 The experimental crystallization kinetics data of the poly(L/D-lactide) samples of different thickness in contact with aluminum surface at a) 100°C b) 110°C; c) 120°C; d) 130°C. These curves were calculated from the DSC traces as explained in the Experimental Methods section. Points have been thinned by a factor of 3000 to 24000 to allow for clear viewing of the behaviour.……113

Figure 7.12 The experimental data (symbols) and Monte-Carlo simulation results (solid lines). The dashed lines represent corresponding $\tau_{1/2}(d=\infty)$ lines.……..117

Figure 8.1 Steps in polymer crystallite growth. The orientation of polymer chains is critical for homogeneous nucleation. Sketch was adapted from Hoffman et al.[137]....121

Figure 8.2 Schematic illustration of electric field effect on mesomorphic layer formation. The polymer chains conformation in absence of electric field (a) and local orientation of chains in electric field (b).……...123

Figure 8.3 Schematic illustration classifying the dipoles of polymer chains. The circles indicate atoms in the chain backbone. Type-A and type-B dipoles, both attached to the chain backbone, are parallel and perpendicular to the backbone. The type-C dipole is attached to the side group.……...126

Figure 9.1 The polylactic acid chain representation showing the directions of dipole moment of the repeat unit. P_A and P_B are the parallel and transverse dipole vectors respectively and the dashed line represents the virtual backbone. Schematic illustration from work by Ren et al.[161]……...136

Figure 9.2 The effect of static electric fields of different intensity on relative complex viscosity of the polylactide melt at: a) 145 °C, b) 147.5 °C, c) 150 °C..…….139

Figure 9.3 An overlap of the XRD profiles of the polylactide samples subjected to crystallization for 9000 s at 147.5 °C without applied electric field (dotted blue line) and under the influence of 240 kV/m electric field (solid red line).……...141

Figure 9.4 Optical micrographs of polylactide crystallized at 147.5 °C for 60 minutes: a) 240 kV/m electric field applied; b) no electric field (10X magnification).…….142

Figure 9.5 Crystallinity, $\phi(t)$, in the absence of electric field. Symbols represent values estimated from complex viscosity $\eta^*(t)$ and curves represent crystallinity determined from DSC experiments using Avrami equation..…….146

Figure 9.6 Example of linear relation between $ln(1/(1-\phi))$ and t^4 at 150°C……..147

Figure 9.7 Nucleation rates N ($m^{-3} \cdot s^{-1}$) as a function of electric field intensity E.…….148

Figure 10.1 Photograph of polylactide sample subjected to shear-induced crystallization in plate-plate geometry. The crystallization starts at sample's edges (white area) and propagates to the centre over the time. The sample's central area subjected to lower shear remains amorphous and transparent for significantly longer time..……..…155

Figure 10.2 The comparison of development of the reduced zero shear complex viscosity of L 9000 polylactide subjected to 1 s^{-1} shear for 120 s at 155 °C measured using different measuring system geometries. The SAOS frequency is 1 Hz and strain is 5%. The viscosity curve of not sheared polylactide had been obtained using plate-plate geometry and given for reference..……..157

Figure 10.3 The standardized residuals of viscosity curves from Figure 10.2 derived from the exponential decay fits. The induction time of quiescent crystallization of polylactide at 155 °C is 35100 s.……....162

Figure 10.4 Induction time of the quiscent polylactide crystallization observed by rheology and DSC. Data are taken from reference [134] ……..163

Figure 10.5 The relative induction time of polylactide crystallization depending on continuous hear rate at different temperatures. The Y axis represents the reduced induction time under continuous shear expressed as ratio of the induction time under shear to quiescent induction time and the X axis is the shear rate. .....….165

Figure 10.6 The relative induction time after the application of step shear. The temperature was 145 °C. The X axis represents the product of the shearing time and the shear rate. The dashed lines represent a reduced induction time for continuous shear……..……167

Figure A1.1 A simplified algorithm of the Monte Carlo simulation……..176

List of Tables

Table 2.1 Crystalline structures of the pure polylactide enantiomers and L-/D-lactide stereocomplex……...…8

Table 7.1 The effect of surface nucleation concentration on the Avrami parameters for the initial stage of surface induced crystallization.……..……103

Table 7.2 The surface crystallization of poly(L/D-lactide) simulation results at different temperatures.……117

Table 9.1 Effect of applied electric field on induction time t_i (s) of the polylactide crystallization. The induction time determined from rheological measurements using 0.5 mm gap. The induction times for the 1 mm gap are also shown to demonstrate the effect of heterogeneous surface crystallization on induction time.……137

Nomenclature

A	Area (m^2)
b	Kuhn length (m)
C	Viscosity decay coefficient (Pa)
c_e	Equivalent diameter (m)
d	Thickness (m)
E	Electric field intensity (V/m)
e_i	Real residual
f	Equivalency coefficient
ΔH_∞	Ultimate heat of crystallization (J/mol)
ΔH_f	Crystal heat of fusion (J/mol)
G	Growth rate (m/s)
G'	Storage modulus (Pa)
G''	Loss modulus (Pa)
G'_0	Initial storage modulus (Pa)
G'_∞	Final plateau of storage modulus (Pa)
Ge	Equilibrium modulus (Pa)
ΔG^*	Critical excess free energy due to the creation of a nucleus (Pa)
k	Crystallization constant
l_g^*	Lamellar thickness (m)
M_n	Number-averaged molecular weight
$\overline{M}_{da}$	Average length of dangling arms

M	Molecular weight
M_e	Entanglement molecular weight
M_w	Weight-average molecular weight
M_C	Critical molecular weight
N_0	Molecular weight of the precursor
N_s	Surface nucleation concentraton (m^{-2})
N	Nucleation rate ($m^{-3}s^{-1}$)
n	Avrami exponent
P	Polarization
P_{gel}	Fraction of all chain segments that are attached to the gel
P_E	Component of polarization in the direction of electric field
Q	Heat flow of crystallization (W/g)
r	*R*adius of the nuclei (m)
R^2	Adjusted coefficient of determination
r_i	Standardized residuals
$S(t)$	Evolution of interfacial area (m^2)
ΔS	Change of the entropy
t_i	Induction time (s)
T	Temperature (K)
ΔT	Degree of supercooling (K)
$T_m^{\ 0}$	Equilibrium melting temperature (K)
Tg	Glass transition temperature (K)
$T_g(0)$	Glass transition temperature in absence of crosslinking (K)

Greek symbols

α	Fraction of transformed material
γ	Shear rate (s^{-1})
γ_{cs}	Crystal-substrate interfacial free energy (J/m^2)
γ_{cm}	Crystal-melt interfacial free energy (J/m^2)
γ_{ms}	Melt-substrate interfacial free energy (J/m^2)
δ	Physical entanglement factor (m^{-1})
ε^*	Complex dielectric constant
$\varepsilon'(\omega)$	Dynamic dielectric constant
$\varepsilon''(\omega)$	Dielectric loss
ε_∞	High-frequency dielectric constant
$\Delta\varepsilon$	Dielectric relaxation intensity
η^*	Complex viscosity (Pa·s)
$\eta^*_{t=\infty}$	Limiting complex viscosity at long times (Pa·s)
η^*_0	Zero-shear complex viscosity (Pa·s)
η_{cryst}	Complex viscosity of the crystallizing polymer (Pa·s)
η_{melt}	Complex viscosity of the completely molten polymer (Pa·s)
$\lambda(t)$	Fraction of untransformed (i.e. amorphous) material
μ	Dipole moment
$\upsilon(t,\tau)$	Volumetric growth rate of crystalline structure (s^{-1})
ρ_c	Density of crystalline phase (kg/m^3)
ρ_l	Density of melt (kg/m^3)

σ_e	Fold energy (J/m^2)
σ	Crystal surface energy (J/m^2)
$\Delta\sigma$	Surface to the interfacial free energy difference (J/m^2)
$\Delta\sigma'$	Interfacial free energy difference for homogeneously nucleated crystal-melt interface (J/m^2)
τ	Thermal degradation time constant (s)
$\tau_{1/2}$	Half time of crystallization (s)
ϕ	Volumetric fraction filler
$\Phi(t)$	Normalized dielectric relaxation function
φ_{da}	Volume fraction of dangling arms in the amorphous region
χ	Number of crosslinks per gram
ω	Angular frequency (rad/s)

Abbreviations

AFM	Atomic Force Microscopy
CLF	Contour Length Fluctuations
DSC	Differential Scanning Calorimetry
IF	Immersion factor
FIC	Flow-Induced Crystallization
HDPE	High Density Poly(ethylene)
PDLA	D-Poly(lactic) acid
PE	Poly(ethylene)

PEO	Poly(ethylene oxide)
PLA	Poly(lactic) acid
PLLA	L-Poly(lactic) acid
PP	Poly(propylene)
PS	Poly(styrene)
SAOS	Small Angle Oscillatory Shear
SAXS	Small Angle X-Ray Scattering
SEC	Size-Exclusion Chromatography
UV	Ultraviolet
XRD	X-Ray Diffraction

CHAPTER 1

Introduction

Polylactide (PLA) is one of the most promising new materials for packaging applications. Lactic acid is produced by the fermentation of corn and other plant materials, and is therefore a renewable resource. PLA degradation does not produce toxic by-products and, depending on conditions, takes place over a period of 20 days to 3 years [1]. At the same time, PLA combines good processability and packaging properties. Polymerization technology for this new polymer is well developed, and several companies have started semi-industrial commercial production of PLA.

Since PLA is a relatively new material, it provides an extensive field for research. Especially interesting directions of research include crystallinity development, mechanical properties and surface structure of films under different conditions, aging, and degradation, as well as means of controlling crystallinity. Depending on application, crystallinity could be desirable or not. For example, high crystallinity must be avoided for injection-molded preforms that are intended for subsequent blow molding, since rapid crystallization of the polymer would affect the stretching of the preform and optical clarity of the end product. In contrast, increased crystallinity would be necessary in articles for which good thermal stability is important. Crystallization of PLA articles can be facilitated by annealing at temperatures between *Tg* and the melting point to enhance their thermal stability [2].

While crystallization is observed when polymer melt is undisturbed, the presence of the external fields could dramatically facilitate this process. Therefore, it is important

to establish the effects of external fields on polylactide crystallization. These external fields include shearing and electric fields. While flow-induced crystallization is studied relatively well for a wide range of polymers, the effects of electric fields on crystallization are not so well known. The non-zero dipole moment of the polylactide repeat unit makes its crystallization potentially sensitive to the presence of external electric fields.

1.1 Thesis Objectives

Presently, the main objective of this work is to study the effects of external field forces on polylactide crystallization. The focus was decided to be two main phenomena involving crystallization under external fields: flow-induced crystallization and electric field-induced crystallization. Apart from morphological changes, field-induced crystallization is characterized by increased nucleation rate. On the macroscopic scale, this phenomenon results in decreased induction time and enhanced crystallization. While shear-induced crystallization is very well known and can be witnessed in the majority of polymer processing technologies, the effect of electric fields on polylactide crystallization were largely unknown to the scientific community. Therefore, the study of the effects of the electric field on polylactide crystallization was set as one of the primary objectives.

It was found that many aspects of polylactide crystallization still remained unknown and many problems needed to be resolved in order to contribute to the main

objectives. Therefore, the following problems needed to be explored as secondary thesis objectives:

- Polylactide spherulitic growth rate, morphology, and dependency on temperature and stereocomplexation. This task required the development and application of techniques for growth rate measurement, applicable for a wide range of crystallization temperatures;
- Developing a reliable and sensitive technique for crystallization onset determination (detection of induction time);
- Developing a technique allowing the use of rheological measurements for the crystallization studies and creating a model allowing the relation of complex viscosity to melt crystallinity;
- Studying effects with significant impact on the observed crystallization (including surface nucleation and setup gap effects) and developing the approaches needed for offsetting of their influence;
- Developing an advanced computational approach for crystallization kinetics evaluation using a Monte Carlo simulation.

1.2 Thesis Organization

The present thesis consists of eleven chapters. Chapter 1 gives an introduction to the topic and explains the scope of this work. Chapter 2 briefly introduces Chapter 3, which represents the article containing an extensive study of the quiescent crystallization of polylactide. In this chapter, various aspects of polylactide crystallization, including

growth rate, spherulitic morphology, and stereocomplexation, were studied using novel research techniques. Chapters 4 and 5 represent the introduction to and article on the rheology of crystallizing polylactide, respectively. The model presented here relates the rheological parameters of the melt to its apparent crystallinity and a novel technique allowing precise determination of induction time. Chapters 6 and 7 are dedicated to extensive studies of the surface crystallization phenomenon of polylactide. After a brief overview in Chapter 6, an article-based Chapter 7 provides insight into the theoretical aspects of surface crystallization and demonstrates the effect of surface crystallization on overall crystallization kinetics experimentally. Chapter 7 introduces the advanced computer simulation of the surface crystallization as well. Chapters 8 and 9 are dedicated to the studies of the effect of the electric field on the crystallization of polylactide. Chapter 8 provides an overview of previous studies in this field, and Chapter 9 is dedicated to a novel experimental study of electric field-induced crystallization. Chapter 10 provides an insight into flow-induced crystallization of polylactide observed by using rheological techniques, including various influential factors affecting the observations. Chapter 11 gives an overview of this research project and some recommendations for future studies.

CHAPTER 2

Poly(lactide) Crystallization

2.1 Crystalline Modifications of Polylactide

Poly(lactic acid) is a thermoplastic aliphatic polyester made from renewable resources, such as corn, tapioca or sugarcanes (Figure 2.1).

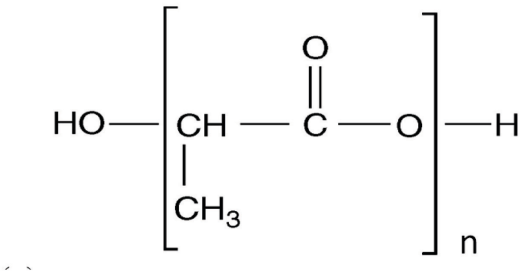

Figure 2.1. The chemical structure of polylactide.

There are three known structural modifications of polylactide crystals. They are characterized by the different helix conformations and cell symmetries that develop with different thermal and/or mechanical treatments. The α form develops during melt or cold crystallization and from solution-spinning processes at low drawing temperatures and/or low hot-draw ratios [3]. De Sanctis and Kovacs [4] first determined the chain conformation of the α phase to be a left-handed 10_3 helix packed into an orthorhombic unit cell. Extra (001) reflections have also been observed in the XRD experiments, suggesting possible deviation from a pure 10_3 helix conformation [3].

Eling et al. [5] first observed the β modification. This modification develops upon mechanical stretching of the more stable α form or during the solution-spinning processes conducted at high temperatures and/or high hot-draw ratios [6]. Little is known regarding

the crystal structure of the β modification. Hoogsten et al. [3] suggested an orthorhombic unit cell with a = 1.031 nm, b = 1.821 nm, and c = 0.900 nm, and a chain conformation having left-handed 3_1 helices. Alternatively, Brizzolara et al. proposed an orthorhombic unit cell with two parallel chains [7]. A third crystal modification of PLA (γ form) develops upon epitaxial crystallization. Presumably it has two antiparallel helices packed in an orthorhombic unit cell [8].

2.2 Crystallization Kinetics and Spherulitic Morphology of Polylactide

The crystallization kinetics from melt processing for polylactide has been the focus of studies by many researchers. Polylactide crystallizes at a wide range of temperatures and its bulk crystallization rates were determined over the range from 70ºC to 165ºC [9]. The maximum crystallization rate was observed around 100ºC. Some researchers reported a peculiar behavior in the spherulitic growth rate of polylactide, which resulted in discontinuity in the growth kinetics around 110-120ºC. This discontinuity has been attributed to a transition in regimes II–III growth of spherulites that was observed in the same temperature range [10].

The morphology of the growing spherulites seems to vary in the whole explored temperature range, even during the very rapid increase of linear growth rate below 120ºC. Similarly, spherulites grown isothermally at various temperatures do not show any noteworthy morphological difference; therefore, the abrupt increase in crystallization rate cannot be ascribed to changes in morphology occurring during growth at different temperatures. The discontinuity in the crystallization rate of PLLA around 120ºC is

mainly related to a drastic variation in crystal growth rate and is not affected by abrupt changes in nucleation behavior. The sudden change in crystallization rate may be due to growth in a different crystal modification, which might be favored at temperatures below 120ºC [10]. The discontinuity in crystallization rate of PLLA reported above has sometimes been correlated with a transition in crystallization regime, observed in the same temperature range [11].

2.3 Stereocomplexation Phenomenon in Polylactide Crystallization

The optically active polymers have *meso* and *racemic* group placements of the repeat units. These terms are related to their optical orientation. While meso placement corresponds to the same position of two neighboring optically active centers, racemic placement assumes that they are opposite. Because the lactic acid is optically active, blends of L- and D-polylactides are able to crystallize with the formation of a *stereocomplex*. Ikada et al. [12] first reported the formation of a stereocomplex from the blends of poly(L-lactide) and poly(D-lactide). Subsequent research showed that nonequimolar blends can exhibit both homopolymer and stereocomplex crystallization [13]. While both L- and D-lactide are able to crystallize individually in an orthorhombic crystalline form, L-lactide and D-lactide repeat units can also form stereocomplex crystals having a triclinic crystalline form, which is the lowest crystallographic symmetry possible (Table 2.1). This kind of crystallization takes place via the side by side packing mechanism and, as a result, the stereocomplex has a significantly higher density and melting point than homocrystallites. The stereocomplex has a dramatic influence on the

rheological behavior of the polymer blends because of its significantly higher melting point. The formation of the stereocomplex can cause *gelation* even at the melt temperature of the orthorhombic crystals [13]. This stereocomplexation strongly influences the crystallization behavior of L- and D-polylactide blends and their spherulitic morphology. For the last two decades, stereocomplexation phenomena have been studied by many researchers, and the conditions and kinetics of the stereocomplexation were explored. Studies of polylactide blends showed that stereocomplexation can occur even with as little as 10 wt% poly(D-lactide) present in a blend [13].

Table 2.1. Crystalline structures of the pure polylactide and L-/D-lactide stereocomplex [14,15].

	Pure L- and D- polylactide	L-/D-stereocomplex
	Orthorombic	Triclinic
Lattice dimension	a=1.07 nm	a=0.916 nm
	b=0.645 nm	b=0.916 nm
	c=2.78 nm	c=0.87 nm
Lattice angle	$\alpha = 90^{o}$	$\alpha = 98^{o}$
	$\beta = 90^{o}$	$\beta = 69.5^{o}$
	$\gamma = 90^{o}$	$\gamma = 121.2^{o}$
Conformation	10/3 helix	3/1 helix
Melting point	130 –185 C^{o}	230 – 279 C^{o}

The stereocomplex formation is affected by many factors, such as the blending ratio and optical purity of the enantiomers, as well as molecular weight. Experimental conditions such as temperature and the nature of the solvent, and even the blending mode, can influence stereocomplex formation. For the preferable stereocomplex formation, low molecular weight and the presence of sufficiently long sequences of both L-lactide and D-lactide units are important [16,17]. Stereocomplex crystallites are predominantly formed in blends of low molecular weight polymers; therefore, for solution cast blends, the most important factor for stereocomplexation is the polymer's molecular weight. Blends of polymers having high molecular weight yield mostly mixtures of the L- and D-lactide homocrystallites [18]. Two main factors prevent stereocomplexation in high molecular weight blends: 1) microscopic phase separation as the concentration of the solution increases during casting, resulting in the suppression of racemic crystallization in phases that are rich in one of the enantiomers that leads to prevailing homocrystallization; 2) there is evidence that the racemic crystallization rate is slower than the homocrystallization rate. Regardless of crystallization conditions, the molecular weight also affects stereocomplexation and its influence is stronger than that of homocrystallization. The crystallites in films cast from blends of polylactides having molecular weights higher than 60,000 consist mostly of homopolymers [19]. While L- and D-polylactides form spherulites of relatively large size, the presence of a small amount of stereocomplex decreases their size. This observed suppressed-spherulite formation in L-/D-polylactide blends may be attributed to the gelation. This can explain the superior properties of the blended film because stereocomplexation suppresses the formation of large spherulites that give poor mechanical properties to the polymer [20].

CHAPTER 3

Crystallization of Polylactide Films: An Atomic Force Microscopy Study of The Effects of Temperature and Blending

3.1. Introduction

Surface crystallinity on films of poly(L-lactide), poly(L/D-lactide) and their blends with poly(D-lactide) was studied. The isothermal spherulitic growth rate and its dependence on temperature were studied using tapping mode atomic force microscopy and *ex situ* isothermal crystallization. Using this technique, it is possible to extend spherulitic growth rate measurements to the region of significantly higher supercooling where nucleation concentration makes the use of *in situ* hot stage optical microscopy impossible. It was confirmed that while a poly(L-/D- lactide) copolymer exhibits the typical "bell" shaped crystallization rate - temperature dependence, poly(L-lactide) exhibits a nonsymmetrical behavior having two crystallization rate maxima at 105 ºC and 130 ºC. As expected, the spherulitic growth rate of poly(L-lactide) was significantly higher than that of poly(L/D-lactide). The different types of crystalline formations exhibited at the surface of polylactide films are shown and discussed. The crystalline long spacing of poly(L-lactide) was also measured directly using tapping mode AFM and found to be 19 nm at 165-170 ºC. At low supercooling, several different scenarios of individual crystal formation were observed: purely flat-on stacks, purely edge-on stacks and scenarios where edge-on crystals flip to flat-on crystals and vice versa, where flat-on crystals yield edge-on sprouts. The preferred direction of growth of lamellae of both

poly(L-lactide) and poly(D-lactide) was found to be counter-clockwise relative to the free surface.

Finally, the crystallization kinetics of blends of poly(L-lactide) and poly(L/D-lactide) with poly(D-lactide) were studied. In such blends a triclinic stereocomplex crystalline structure forms as well as the usual pseudo-orthorhombic α-crystals formed between chains of like chirality. The presence of the stereocomplex crystals affects both the nucleation and growth of the α-crystals. In fact depending on the stereocomplex content and the crystallization temperature the α-crystallization can either be enhanced or inhibited. Interestingly it was found that the presence of the stereocomplex had a much stronger effect on the α-crystallization of poly(L/D-lactide) than on the α-crystallization of poly(L-lactide).

One of the most promising biodegradable polymers for commodity and speciality applications is polylactide (PLA), which is synthesized from lactic acid. Despite the fact that polylactide has been known for many decades, many of its properties, especially those related to its crystallization behavior, remain insufficiently explored. In this work we aim to provide certain missing understanding of the crystallization behavior and crystalline morphology of optically pure poly(L-lactide), poly(L/D-lactide) and of blends of these polymers with poly(D-lactide).

Individual optically pure polylactide isomers crystallize in a pseudo-orthorhombic crystalline form with a 10/3 helix conformation [21] while chains of different enantiomers form a triclinic stereocomplex with 3/1 helix conformation [22] having a higher melting temperature. The melting point of the stereocomplex is about 230 ºC as compared to 180 ºC for the pseudo-orthorombic crystalline form [23]. The stereocomplex

forms under the side by side packing mechanism and therefore, it has a significantly higher density and melting point than the other crystal form. The stereocomplex can also have a dramatic influence on the rheological behavior of polylactide blends because of its significantly higher melting point as compared to the orthorhombic crystals. In fact, the formation of the stereocomplex can cause *gelation* at the normal melt temperature [13]. The formation of the triclinic stereocomplex in blends of poly(L-lactide) and poly(D-lactide) also strongly affects its crystallization behavior and morphology. Recently in was found that even 0.5 wt% poly(D-lactide) in poly(L-lactide) can result in the formation of stereocomplex [24] which then affects the crystallization. In our experiments we also observed gelation in concentrated dichloromethane solutions of poly(L/D-lactide) and poly(D-lactide) blends when the blend concentration of poly(D-lactide) exceeded 2 wt%. The exact effect of the stereocomplex presence on the crystallization kinetics of the pseudo-orthorombic α-crystalline form has not been reported on in detail. In this work we examine this aspect.

The crystallization of polylactides is characterized by fast spherulitic growth and high achievable overall crystallinity up to 87.5 % [25]. Unusual isothermal spherulite growth rate data have been reported for poly(L-lactide) [26, 27]. Di Lorenzo [28] found that the isothermal spherulite growth rate curve of pure poly(L-lactide) displays two maxima: a broad maximum around 130 ºC and another sharper peak at 115 ºC. Thus, the G vs. T plot significantly deviates from the typical bell-shaped curve [28]. This peculiar crystallization behavior was also noted by Tsuji et al. [29] who performed an extensive study of crystallization behaviors of the optically pure poly(L-lactide) and of the copolymer poly(L/D-lactide). In particular the unusual crystallization behavior was

observed only for essentially pure poly(L-lactide) of intermediate molecular weight (30 – 100 kg/mol). Interestingly, they observed the typical "bell-shaped" spherulite growth rate dependence for poly(L/D-lactide) copolymers.

One of the most widely used spherulite growth rate measurement techniques is the hot stage polarized light optical microscopy. There are several commercially available setups allowing in situ spherulite growth measurements. Being a relatively simple technique, hot stage optical microscopy is precise and reliable only for relatively high crystallization temperatures where spherulite growth rate and especially nucleation density are low. High growth rates and/or high nucleation density significantly decrease the accuracy of in situ measurements and make studies impossible at a certain degree of undercooling. The major drawback of *in situ* hot stage optical microscopy is its low cooling rate (maximum 20 °C/min, though some setups allow cooling rate to 100 °C/min) which cannot prevent crystallization from starting before the isothermal treatment temperature of interest is reached [30]. Consequently, a significant range of crystallization temperatures cannot be studied using an *in situ* hot stage and the applicability of this method is limited to the range of medium to high temperatures. Other techniques have been used to minimize these limitations and increase sample cooling rate. These techniques include using *ex-situ* sample melting and two chamber gas heating and cooling. Non-isothermal techniques similar to those described by Ding and Spruiell, Wagner and Phillios [31,32] also have been developed. Polylactide exhibits high nucleation density at temperatures below 120 ºC which makes it difficult to study its crystallization using hot stage optical microscopy. Therefore the unusual crystallization

behavior has been studied using indirect measurements making studies of the crystallization behavior of polylactide at high supercooling especially important.

In situ hot stage atomic force microscopy is also a popular tool for studying crystallization [33]. This technique allows not only the study of spherulite growth but also provides valuable information on crystalline morphology at scales inaccessible in optical microscopy. Nevertheless, the *in situ* AFM technique is limited to very low growth rates and very low undercooling crystallization due to the scanning nature of the AFM which makes the time resolution extremely poor. Additionally, it has been shown that the probe tip can itself influence the crystallization being observed during *in situ* AFM studies [34].

Here we study the crystallization behavior and morphology of polylactide films using atomic force microscopy and *ex situ* crystallization. This AFM technique for studying crystallization involves using sufficiently thin polymer films that the crystallization in the surface normal direction is constrained but that in the surface parallel directions proceeds as in the bulk. Because the surface normal crystallization is constrained, peaks are formed at the center of spherulites and troughs are formed at the edges. This aspect of the morphology allows us to very accurately measure the sperulitic dimensions as explained later. We have also developed a technique to locate the same spherulite on a film after removing the sample from the microscope to allow for the ex situ thermal treatments. Previous work has showed that from the point of view of orientation of lamellae, the crystallization behavior in polylactide films with thickness down to 30-80 nm is not different from that of the bulk material [34]. For this reason we can extrapolate the results of our studies on films of about 500–700 nm to bulk behavior.

By definition, *ex situ* crystallization studies require intermediate cold periods when the sample is in the glassy state and can be imaged in the absence of ongoing crystallization. We note that polylactide is an excellent candidate for such studies because its glass transition temperature of 60 ºC is above room temperature. Therefore crystalline structures are very stable in this polymer at room temperature and different stages of crystallization can easily be "frozen in" and imaged.

We begin by explaining in detail and validating the experimental technique since it is not a standard approach for studying crystallization kinetics (Section 3.2). Next we consider the kinetics and morphology of the individual polymers (Sections 3.3.1 and 3.3.2) and finally we discuss the kinetics of the blended systems (Section 3.3.3).

3.2. Experimental

3.2.1 Materials and Sample Preparation

Three polylactide samples were used; the first, supplied by Biomer, was a poly(L/D-lactide) copolymer containing 2 % of D-lactide (L 9000). The other two were optically pure resins supplied by PURAC; a poly(L-lactide) (Purasorb PL) and a poly(D-lactide) (Purasorb PD). The molecular weight distributions were analyzed by gel permeation chromatography using a Varian liquid chromatograph equipped with refractive index, UV, light scattering and viscosity detectors. Trichloromethane at 35 °C was used as the eluent and the SEC columns were from Supelco (G6000-4000-2000 HXL). It was found that the poly(L/D-lactide) has a number average molecular weight of 50,000 and a polydispersity index of 2.0. The optically pure PLLA has a number average

molecular weight of 59,500 and a polydispersity index of 1.8. The optically pure PDLA has a number average molecular weight of 84,500 and a polydispersity index of 1.7.

For the crystallization kinetics studies, samples were prepared using the solution casting technique with dichloromethane, supplied by ACROS, as a solvent. The polymer was dissolved in dichloromethane at a concentration of 0.1 wt% and then cast onto a thin glass substrate (a 6 mm by 6 mm piece of microscope slide of 150 μm thickness supplied by Fisher Scientific). The samples were dried at room temperature under controlled evaporation conditions which allowed a film to form over 1–2 hours. Dichloromethane has a very high volatility and evaporation of a drop of solution under normal ambient conditions takes less than 40 s resulting in a film with a very rough surface not suitable for subsequent AFM imaging. For this reason, the casting was performed in a closed chamber nearly saturated with solvent vapor. The films cast under these conditions have a smooth surface and are ideally suited for AFM imaging. The thickness of the films was measured by profiling the film surface in the vicinity of a sharp cut using AFM and was found to be in the range of 500–600 nm.

It was established experimentally that heating the film for 3 minutes at temperature higher than the melting point is enough to erase the effect of the casting process on subsequent surface crystallization. In particular, the concentration of crystallization nuclei is much higher in the cast films than in the films that were melted after casting. By melting the film and evaporating any residual solvent from the surface and immediate subsurface regions, the nuclei density is decreased drastically allowing longer times for spherulite growth before impingement in the subsequent crystallization studies. We refer to this step as “premelting”. The heating and cooling for the premelting

step were performed very quickly (method explained in following section) to prevent crystallization during cooling. Additionally, the premelting step was performed under a nitrogen atmosphere to prevent polymer decomposition. The difference between premelted and solution cast film crystallization behavior can be readily seen in Figure 3.1. Note the difference in nuclei density in the premelted series as compared to the cast series. Additionally, note that the residual solvent in the cast films does not significantly affect the spherulite growth rate; the size of the spherulites after 2 minutes of crystallization is 6.9±0.3 and 7.0±0.3 μm for the premelted and cast films respectively.

AFM imaging of numerous premelted film surfaces showed no traces of crystallinity validating our quenching procedure which is explained in more detail in the next section. According to the nominal melting temperatures of the polymers under investigation, the premelting temperature was chosen to 182 ºC for poly(L/D-lactide) and its blends and 192 ºC for poly(L-lactide) and its blends.

The high nucleation density and high spherulite growth rate in polylactides at high supercooling puts a strict limitation on the crystallization time available before spherulite impingement. The only way to observe isothermal crystallization under these circumstances is to bring the sample to and from the crystallization temperature at a very high heating/cooling rate. Quenching is a well known technique used to "freeze" polymer's crystalline structure for subsequent studies by using very high cooling rates. It is also possible to perform the opposite fast heating if certain conditions are met. First, the heating environment should be preheated and equilibrated at the target temperature.

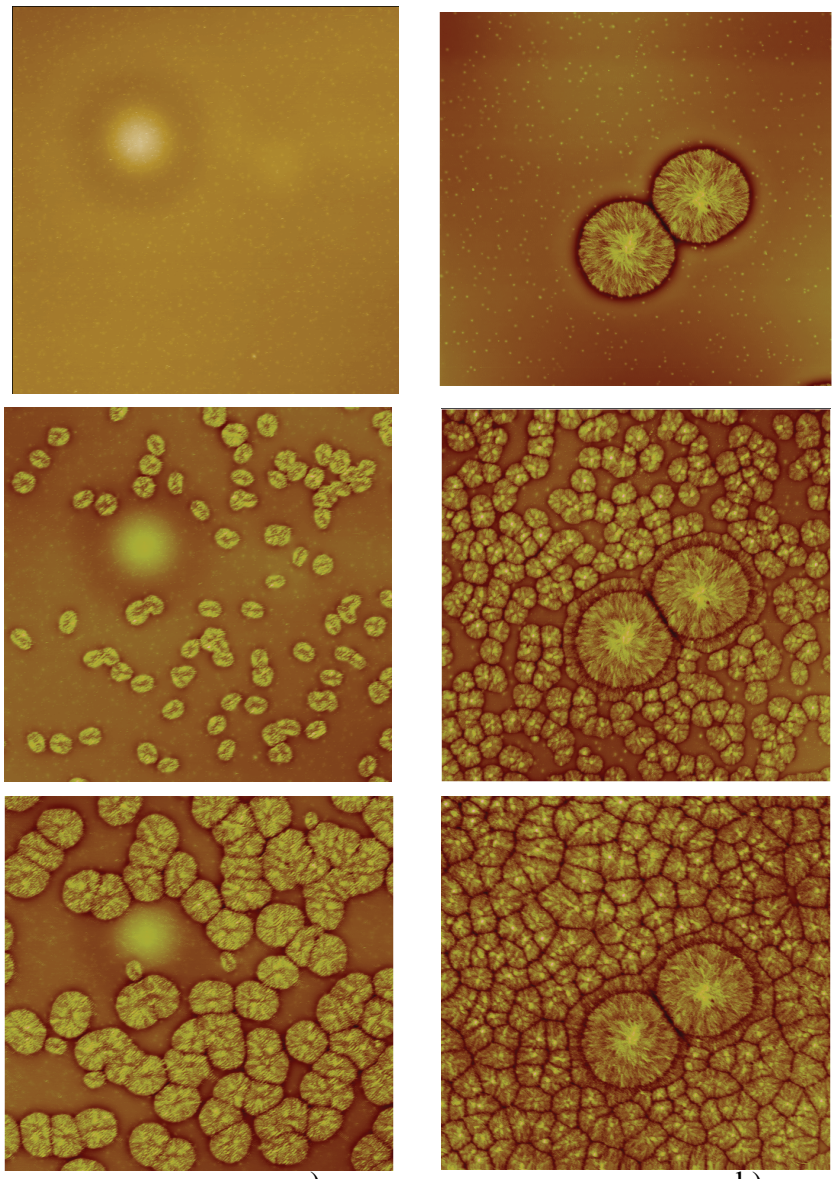

Figure 3.1. The development sequence of crystalline structure on the surface of the (a) premelted and (b) solution cast films of poly(L/D-lactide) at 110 ºC. The upper row images show the polymer surface prior to isothermal crystallization, the middle and lower rows show the same samples crystallized for 2 and 4 minutes, respectively. The round elevated area on the left images is an amorphous area remaining after a spherulite formed in the casting step was melted in the premelting step. The 100 μm AFM height images are shown.

Second, the weight of the sample should be several orders less than that of the heating media. Third, the sample must have a high surface to weight ratio for maximum heat exchange rate.

3.2.2. Heating/cooling of Samples

For the crystallization experiments, a preheated and thermally stabilized heating chamber of a modular compact rheometer MCR 500 by Anton Paar was used. Prior to experiments the heating chamber was stabilized at the target temperature with ± 0.1 °C tolerance. Heated nitrogen was flowing into the chamber (1.1 m^3/h) facilitating convective heat transfer with the sample. The preheated gas flow also allows the system to rapidly compensate for the heat loss that occurs during sample insertion. During the experiments, the sample (film and substrate) was placed on a hot surface inside the chamber and after the desired crystallization time was quickly removed and placed on metallic plate at room temperature for cooling. A heat transfer calculation showed that at 150 °C the sample reaches the heating media temperature in less than 2 seconds. Such a high heating rate is possible due to the small sample weight (typically less than 9 μg) and the high surface area to weight ratio. The heat transfer to the sample occurs by forced convection from the preheated gas and by conduction from the hot metal surface on which it was sitting. A precisely calibrated thermocouple was placed inside the metal immediately under the sample. After reaching steady state, the temperature was kept constant within ± 0.1 °C by the controller.

During sample insertion some of the hot gas escapes from the heating chamber causing a temporary temperature drop which is compensated for by the controller. The maximum temperature drop ranged from 0.44 °C for a 110 °C set point to 1.05 °C for a 170 °C set point and returned to within ±0.3 °C in 54 and 82 seconds respectively. Note that at the lower temperatures, where we will observe the maximum spherulite growth rate, the temperature drop is the smallest. Additionally the oscillations around the set point approximately compensate for each other. We therefore consider this temperature drop to be negligible in regards to the overall measurement accuracy.

It was found that, for small samples, cooling in air at room temperature on the surface of a room temperature metal plate gives cooling rates comparable to our heating rates. In such conditions, the sample cools to below the glass transition temperature (~60 °C) in less than 2 seconds.

3.2.3. Technique for the Measurement of Spherulite Size

A Digital Instrument's Nanoscope IIIa MultiMode SPM atomic force microscope was used in tapping mode for these studies. The ultra sharp NSC15/AlBS cantilevers used for scanning were obtained from MikroMash. The typical resonance frequency of the tips was approximately 300 kHz and the characteristic force constant was approximately 40 N/m. The small radius of the tips ($R < 10$ nm) allowed scanning with high image resolution. Image analysis was then performed to measure the sizes of the crystalline features. Prior to the experiments, the dimensional precision of the AFM was calibrated and verified using a reference silicon grid with 10 μm mesh (supplied by

Digital Instruments Company). The scan rate ranged from 0.5 Hz to 1.0 Hz. For all scans only the highest 512 by 512 resolution was used.

The crystalline sizes in polymer films can be conveniently measured using cross-sectional analysis of height images (Figure 3.2) because of the trough that surrounds each spherulite in thin films. We found that in films thicker than about 1.5–2 μm this interface becomes increasingly blurred thus decreasing the precision of the spherulite size measurement. Additionally it was almost impossible even to find surface crystallinity in films thicker than 5–8 μm as the crystalline structure tends to be submerged under a layer of amorphous polymer at these thicknesses.

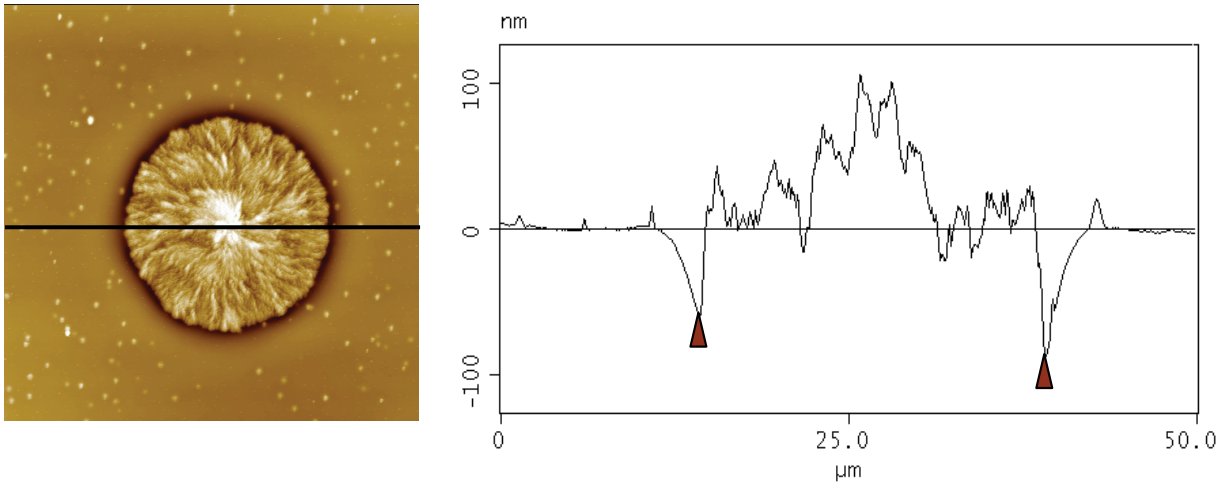

Figure 3.2. AFM height image of solution cast poly(L/D-lactide) film (left) and spherulite cross-section (right). These spherulites are about 25 μm in size and are typical for the both polylactides under investigation in solution cast films. Image size is 50 μm. Note clearly distinguishable spherulite borders which make accurate size measurements possible.

For each temperature at each crystallization time at least 14–30 crystalline features were measured and averaged. In the case of spherulites, the radius was

determined from the diameter measurement and used in the calculation of the growth rates. For the axialitic crystalline structures, size measurements were taken along lamellae, i.e. along the growth directions, and half of this dimension was used in the calculation of the growth rate. For the high temperature crystalline structures, growth rate measurements were determined from the radius of the circle inside which the crystalline structure was inscribed. To determine the variation in spherulite size over time at least three different crystallization times were used. In order to increase the reliability of our data, the measurements of spherulite size were performed on 3–5 AFM images obtained from different locations on each sample. Even our small samples had a surface more than a thousand times the largest AFM scan area. Since scanning is performed on stable, already crystallized samples below the glass transition temperature; this method allows enough time and surface area to perform numerous measurements thus increasing measurement accuracy. Even for the high supercooling range where the nucleation density is very high, it is possible to find enough unconstrained crystalline structures to perform accurate measurements.

3.2.4. Influence of the Heating/cooling Cycle on Spherulite Growth Measurements

The most important issue in *ex situ* crystalization studies such as ours is whether or not the exposure to multiple heating and cooling cycles affects the crystallization rates. In order to evaluate this we undertook 3 series of experiments (1 series at each of 110°C, 130°C, and 150 °C) under 2 conditions (single cycle and multiple cycles). Samples were subjected to repeated fast heating/cooling cycles according to the techniques described above and then compared to samples subjected to only 1 cycle. The difference in the

spherulite sizes and morphology of these samples provides key information on the effects of each cycle on polylactide crystallization. Images for the series of experiments at 130°C are shown in Figure 3.3. The numerical results for this study are presented in Figure 3.4. In order to improve the precision of this study we used an in-house developed technique to repeatedly find the same region on the film for the AFM scanning. All multiple cycle measurements were performed on the same set of spherulites and in the same growth directions. We consider first the sequence of images presented in Figure 3.3 all collected at 130°C. The first four images (a-d) show the development of the same spherulites over 1 through 4 heating and cooling cycles reaching in Figure 3.3(d) a total crystallization time of 250 seconds. It is apparent that demarcations exist in the spherulites for each crystallization cycle. This phenomenon is relatively common in samples exposed to such fast heating/cooling cycles as explained by Fraschini et al. [35]. Figure 3.3(e) shows another sample which was exposed to only 1 cycle with a total crystallization time of 250 seconds. By visual inspection we can see that the size of the spherulites in Figures 3.3(d) and 3.3(e) are very similar. We now consider the final results of this study which are shown in Figure 3.4. The difference between the final spherulite size in the multicycle sample and the one cycle sample is in each case less than 5%, which is lower than the standard deviation of our results (10%). Therefore we consider that the effect of multiple heating/cooling cycles on the spherulite size is negligible. Additionally based on these results, we consider that the intermediate glassy periods do not affect the crystallization which will proceed in essentially the same manner as crystallization from the melt. All of the following kinetics studies were done using multiple heating/cooling cycles on the same sample.

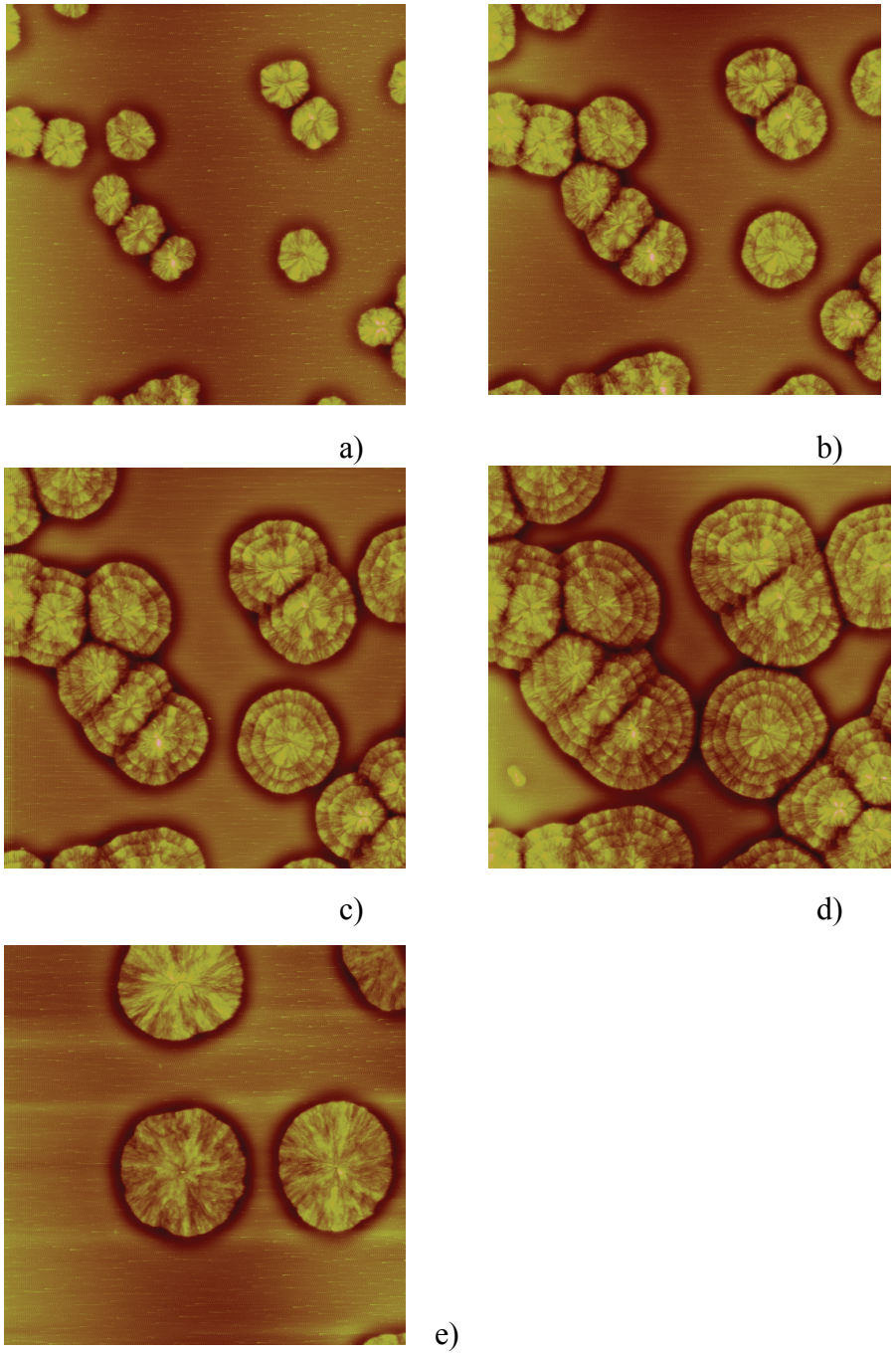

Figure 3.3. The AFM height images of the same area of the same poly(L-lactide) sample subjected to crystallization at 130 ºC in (a) one fast heating/cooling cycle for 100 seconds; (b) two cycles (150 seconds in total); (c) three cycles (200 seconds in total) and (d) four cycles (250 seconds in total); (e) Sample crystallized at 130 ºC in one cycle for 250 seconds is considered to be the reference point. All images are 100 μm scans.

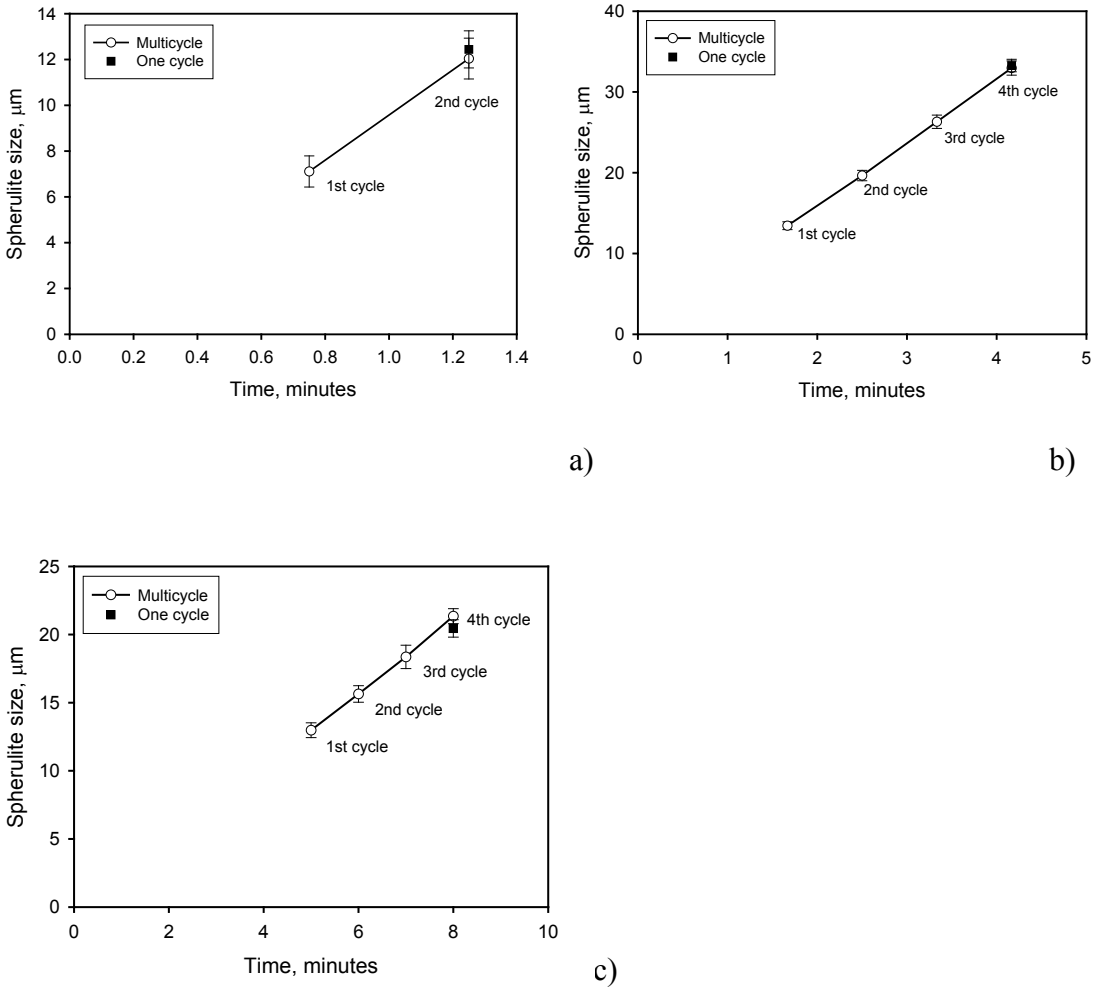

Figure 3.4. Influence of fast heating/cooling cycle on spherulite size and growth rate measurements of poly(L-lactide). The comparison of the spherulite sizes of the samples subjected to multiple fast heating/cooling cycle with those of the samples subjected to only one cycle at 110 ºC (a), 130 ºC (b) and 150 ºC (c).

3.2.5. Generality of Experimental Technique

At this point it is important to consider whether or not our experimental technique for studying crystalization kinetics is generally applicable or if it depends upon the

nucleation behavior of polylactide. Therefore we have performed a limited study with isotatic polystyrene of M_N = 400 kg/mol to ensure that sufficient nucleation would occur over the entire crystallization range and that spherulites would grow from nucleation from the same time. The casting, pre-melting and *ex situ* crystalization were performed in exactly the same manner as with the polylactide. The only proceedural difference was that the PS was melted at 250 ºC and quenched to room temperature before dissolution in dichloromethane at 0.84 wt%. Crystallization was performed for 65 minutes at 130, 135, 140, 150, 160, 170 and 178 ºC. At all temperatures there was sufficient nucleation such that many spherulites could be identified. In fact for 135 ºC and above the entire surface was covered with spherulites. Also, it was clear that all of the spherulites were nucleated at the same time leading to equal diameters. As an example, the morphology of the sample crystalizated at 170 ºC is presented in Figure 3.5. Presumably, since the high degree of nucleation occurs in both polylactide and polystyrene, it is caused by residual solvent which may be increasing the chain mobility and/or acting as heterogeneous nucleation centers.

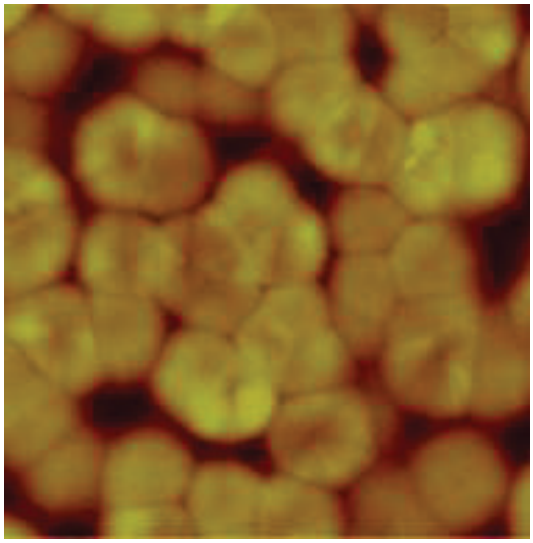

Figure 3.5. Morphology of isotactic polystyrene crystallized at 170 ºC for 65 min.

3.3 Results and Discussion

3.3.1. Isothermal Spherulite Growth Rate

We measured spherulite growth rates of poly(L/D-lactide) in the range of 100 – 160 ºC and of poly(L-lactide) in the range of 100 – 170 ºC. The growth rate curves were constructed from the spherulite size measurements as shown in Figure 3.6 and 3.7. A relatively small standard deviation rarely exceeding 10 % in spherulite size was present in our data. Generally, it can be noted that the intersections of the lines are very close to the origin meaning both very short nucleation time in all polylactide samples and a very fast heating allowing crystallization without delay. This extremely short induction time was also observed by Tsuji et al. [29] for poly(L-lactide) and poly(L/D-lactide).

Previous studies show that the maximum spherulite growth rate of poly(L-lactide) is around 110 – 130 ºC, and that it exhibits a most peculiar, bimodal shape (observed by Di Lorenzo [28] and by Tsuji et al. [29]). The lower temperature peak (at about 110 ºC) has been correlated to a transition in spherulitic growth regimes II to III that was observed in the same temperature range [36] although other explanations of the unusual crystallization behavior of poly(L-lactide) exist as well. Our results perfectly match the results obtained by Tsuji et al. [29]. For the optically pure poly(L-lactide) they reported a spherulite growth rate curve of a similar shape to ours. There is very nice accordance between our data and those from Tsuji et al. [29] in that the peaks occur at the same temperatures for both polymers. We note that our study covers a temperature range that is broader by 20 ºC than that of Tsuji et al. [29] providing additional information at high temperatures.

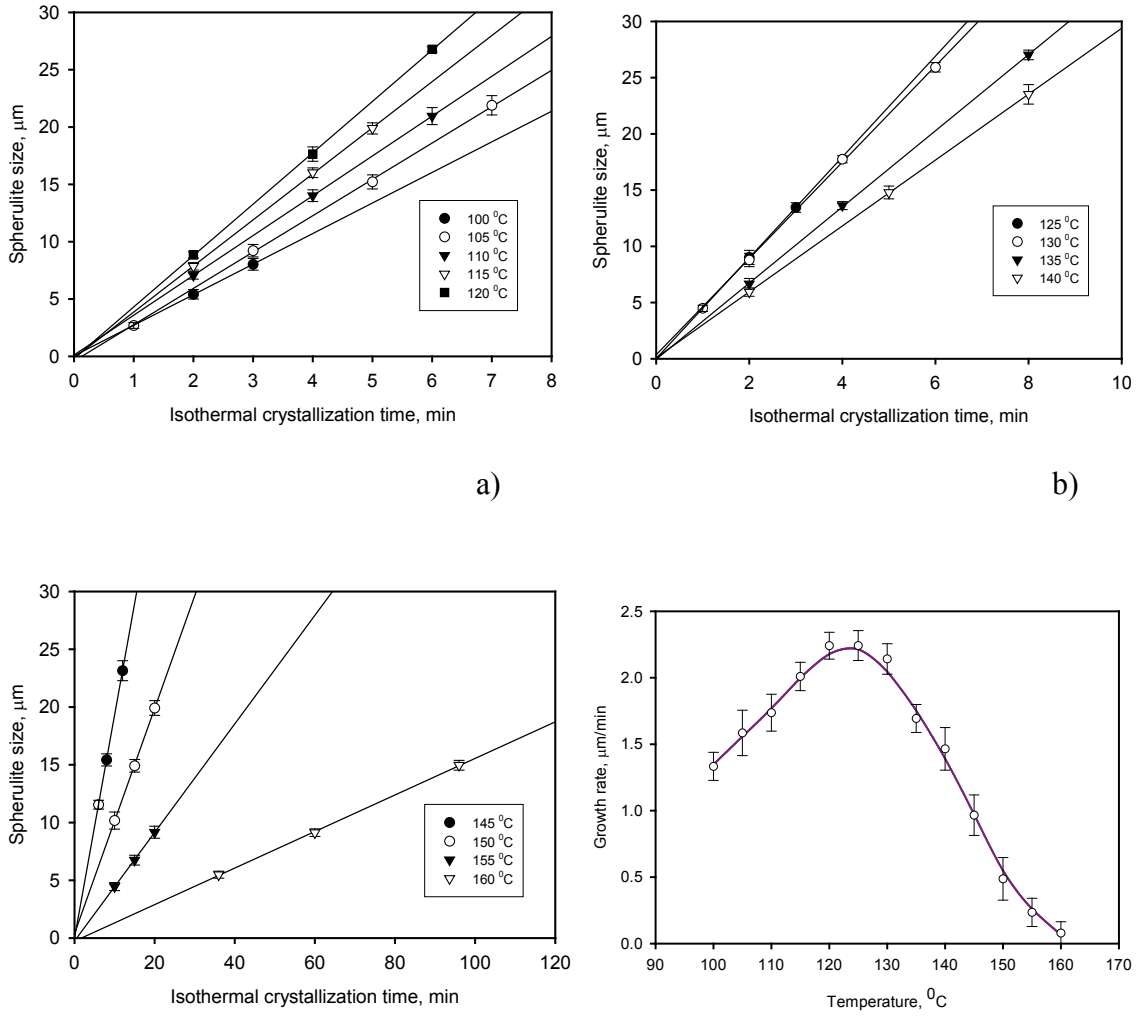

Figure 3.6. Spherulite size vs. isothermal crystallization time for poly(L/D-lactide) at various temperatures (a)–(c). Error bars indicate one standard deviation. (d) Spherulite radius growth rate vs. isothermal crystallization temperature. Error bars indicate standard error in the slope from least squares regression of data in (a)–(c).

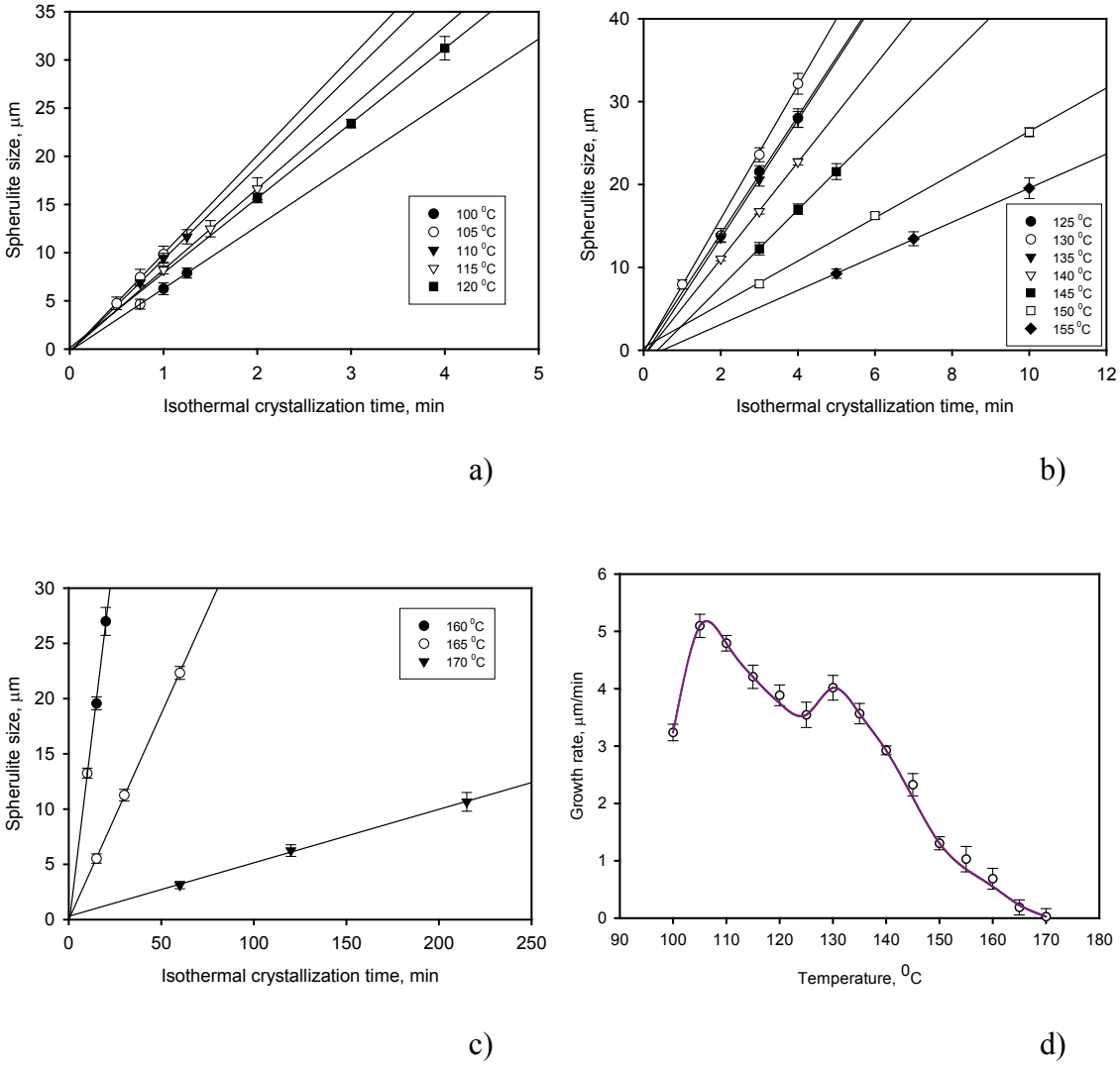

Figure 3.7. Spherulite size *vs*. isothermal crystallization time for poly(L-lactide) at various temperatures (a)–(c). Error bars indicate one standard deviation. (d) Spherulite radius growth rate *vs*. isothermal crystallization temperature. Error bars indicate standard error in the slope from least squares regression of data in (a)–(c).

If we now consider the data of Baratian et al. [37] we can observe that their study did not cover the low temperature where the second peak occurs therefore missing the unexpected second peak. This data set indicates the importance of the lower temperature

range accessible by the *ex-situ* crystallization techniques used in this study and that of Tsuji et al. [29].

Following Abe et al. [36], Tsuji et al. [29] attributed the transition zone between the two peaks to a regime II – regime III transition. According to Abe et al. [36] this effect is related to a change in the isothermal thickening coefficient at the regime transition which favors an accelerated growth rate in regime II under certain conditions. This was first observed and explained for long-chain n-alkanes by Alamo et al. [38]. Note that the transition from regime II to III is not accompanied by any transformations in spherulite morphology. Rather, the most dramatic changes in crystallization morphology of poly(L-lactide) are observed at low supercooling in at temperatures of 160 ºC and above.

Poly(L-lactide) exhibited a spherulite growth rate about two times higher than the poly(L/D-lactide). It is the 2 % D-lactide repeat unit content in the poly(L/D-lactide) which causes this decrease of the spherulite growth rate. The randomly distributed D-lactide repeat units create steric impediments during crystallization thus decreasing the overall spherulite growth rate. This effect is well known and has been quantified by Tsuji et al. [29] for polylactide. The poly(L/D-lactide) copolymers that they studied exhibited crystallization behavior very similar to our sample. We also note that the growth rate curve for our poly(L/D-lactide) exhibited only one maximum again in accordance with the observations of Tsuji et al. [29]. It is clear that the unusually fast spherulite growth at low temperatures is entirely suppressed by even very small amounts of D-lactide units in the chain. Since this unusual behavior has been observed only with optically pure

polylactides of 17,000 ≤ M_N ≥ 104,000 [29, 36] it is likely that L-lactyl sequence lengths of at least 230 (or 17000/M_0) units are necessary for its occurrence.

3.3.2. The Crystalline Morphology of Polylactides

The morphology observed naturally depends on the crystallization temperature. Generally, four typical crystalline forms can be distinguished (Figs. 3.8 and 3.9). As expected, at low temperatures the nucleation concentration is very high and crystallization proceeds in the form of non-oriented lamellae stacks (Figure 3.8(a)), making direct measurements of the crystalline features very difficult at temperatures below 100 ºC. At intermediate temperatures, clearly distinguishable spherulitic structures can be observed (Figure 3.8(b)). Despite the fact that some researchers reported that they were not able to observe the formation of the high-temperature axialites for polylactide [39], in our experiments we observed them at temperatures around 160 ºC (Figure 3.8(c)). At higher temperatures crystalline structures having "truncated lozenge" morphology with distinguishable lamellar structure were observed (Figure 3.9 (a)-(f)). The transformations between the different morphologies take place gradually as isothermal crystallization temperature changes and no specific transformation temperatures were observed. Nevertheless perfectly round spherulites were observed in the temperature range of 110 – 130 º C which is the zone of highest spherulite growth rate.

As expected, nucleation density rapidly decreases at higher temperatures; the nucleation density for the poly(L-lactide) samples crystallized at 170 ºC was estimated to

be $4.2\pm1.6\times10^{14}m^{-3}$. Under these low supercooling conditions, polylactide forms stacked, flat-on and edge-on crystalline structures (Figure 3.9(a)). The nucleation density increases to $3.3\pm1.4\times10^{15}m^{-3}$ at 130 ºC and reaches $1.3\pm0.4\times10^{17}m^{-3}$ at 110 ºC.

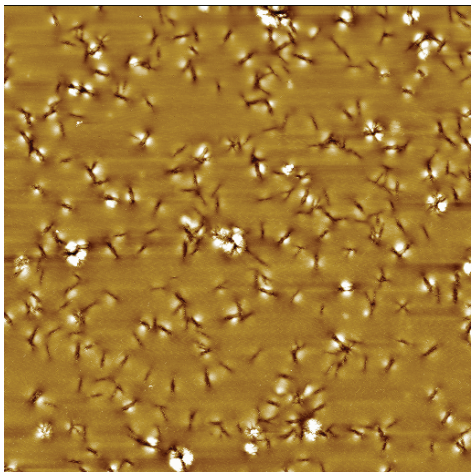

a)

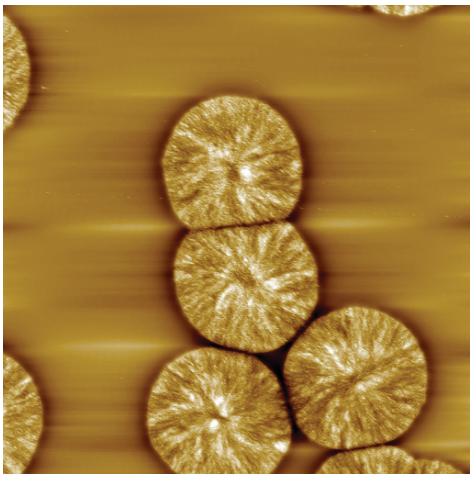

b)

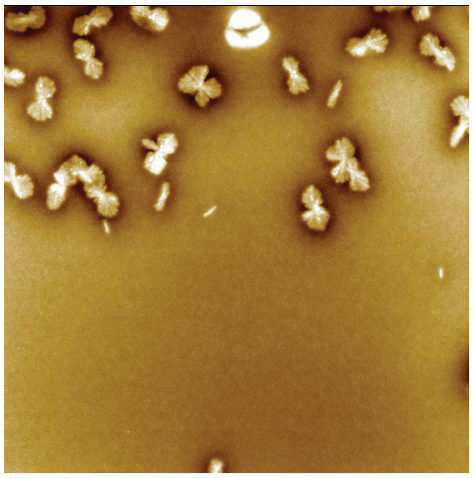

c)

Figure 3.8. Morphology of surface crystallinity of poly(L-lactide) formed (a) at 90 ºC for 1.5 min (50 µm height image); (b) at 120 ºC for 4 minutes (100 µm height image) and (c) morphology of surface crystallinity of poly(L/D-lactide) formed at 160 ºC for 60 minutes (100 µm height image).

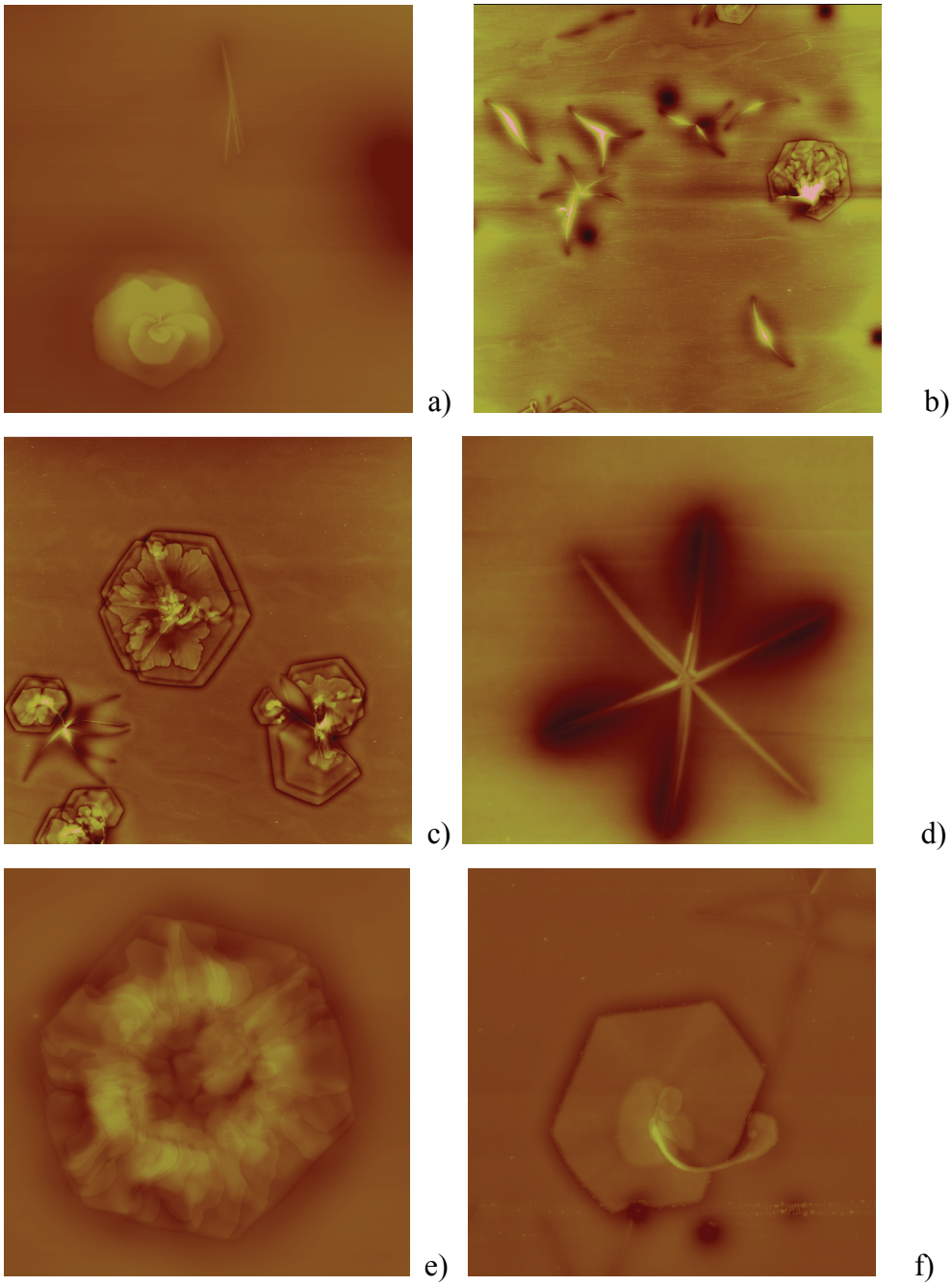

Figure 3.9**.** The crystalline morphology of the poly(L-lactide) samples crystallized at low supercooling. Crystallization temperatures, times and AFM height image scales are: (a) 170 ºC, 120 minutes, 20 µm ; (b) 165 ºC, 30 minutes, 50 µm; (c) 165 ºC, 90 minutes, 100 µm; (d) 170 ºC, 120 minutes, 8 µm; (e) 165 ºC, 60 minutes, 30 µm; (f) 165 ºC, 25 minutes, 15 µm.

Kikkawa et al. [34] proposed that crystallization of polylactide takes place as edge-on crystals only, which can flip later during their growth to a flat-on crystal by a defect obstacle mechanism. We found that at low supercooling this is not the only possible crystallization behavior and in fact different scenarios of individual crystalline structure formation are possible. The crystallization can proceed in the form of a purely flat-on stack (Figs 3.9(a), (c), (e)), purely a edge-on stack (Figs 3.9(a), (b) and d)) and scenarios where edge-on crystals flip to flat-on crystals (Figure 3.9(c)) and the opposite, where flat-on crystals yield edge-on sprouts (Figure 3.9(f)). Interestingly, at 170 ºC no transitions between edge-on and flat-on crystals was observed (Figure 3.9(a)) and crystallization took place in the form of completely flat-on and edge-on lamellae in an approximately equal ratio. At slightly lower crystallization temperatures (165 ºC) the edge-on orientation seemed to be preferable (Figure 3.9(b)). It is interesting that in some cases edge-on stacks also maintained hexagonal symmetry (Figure 3.9(d)). We note that it is possible that the lamellar orientation transitions observed by Kikkawa et al. [34] were caused by the interaction of the AFM tip and growing lamellae during *in situ* scanning since it has been proven that the AFM tip can cause additional nucleation [34]. This is another benefit of the *ex situ* crystallization technique as the imaging takes place below the glass transition where it is certain that no spurious artifacts will be caused.

An important crystallization parameter is the lamellar thickness l_g^* which can be related to thermodynamic properties such as supercooling. Normally, the lamellar thickness decreases with increasing degree of supercooling [40]. The clearly distinguishable lamellar structure of the crystalline formations observed at low supercooling allows the direct measurement of long spacing which is the sum of lamellar

and amorphous layer thickness. It was found that for poly(L-lactide) the average long spacing in the range of 165–170 ºC is 19 ± 2 nm. These values correlate well with experimental SAXS lamellar thickness measurements of 15–20 nm [37] for polylactides at this temperature.

3.3.3. Stereocomplexation Phenomenon in Polylactide Blends and Its Influence on Spherulite Growth

The stereocomplex forms when sequences of different optical isomers are present in a system. It can form in a blend of two optically pure polymers and also in a single poly(L/D-lactide) polymer if sequences of sufficient length of both optical isomers exist. This crystalline form is interesting because its presence can have significant effects on many aspects of the dynamic behavior of polylactide. The stereocomplex melts at about 230ºC and therefore can be present under conditions when the α-crystals are molten (above 170ºC) and when they are crystallizing (between 70ºC and 170ºC). In those situations the stereocomplex particles act as crosslinks which hinder the whole chain coordinated motions required for crystallization and melt flow. Here we are looking at the effect of the stereocomplex particles on the spherulitic growth rates of the α-crystals.

We begin by confirming the presence of the stereocomplex in the blends of our polylactides from a series of DSC analyses. These analyses were performed on blends containing 2, 5, 10, 20 and 50 % poly(D-lactide) in poly(L/D-lactide) and 5, 10, 20 and 50 % poly(D-lactide) in poly(L-lactide) (Figure 3.10). In both the first and second runs,

the blends containing poly(D-lactide) showed a small peak at about 220–230 ºC that does not exist for the pure polymers.

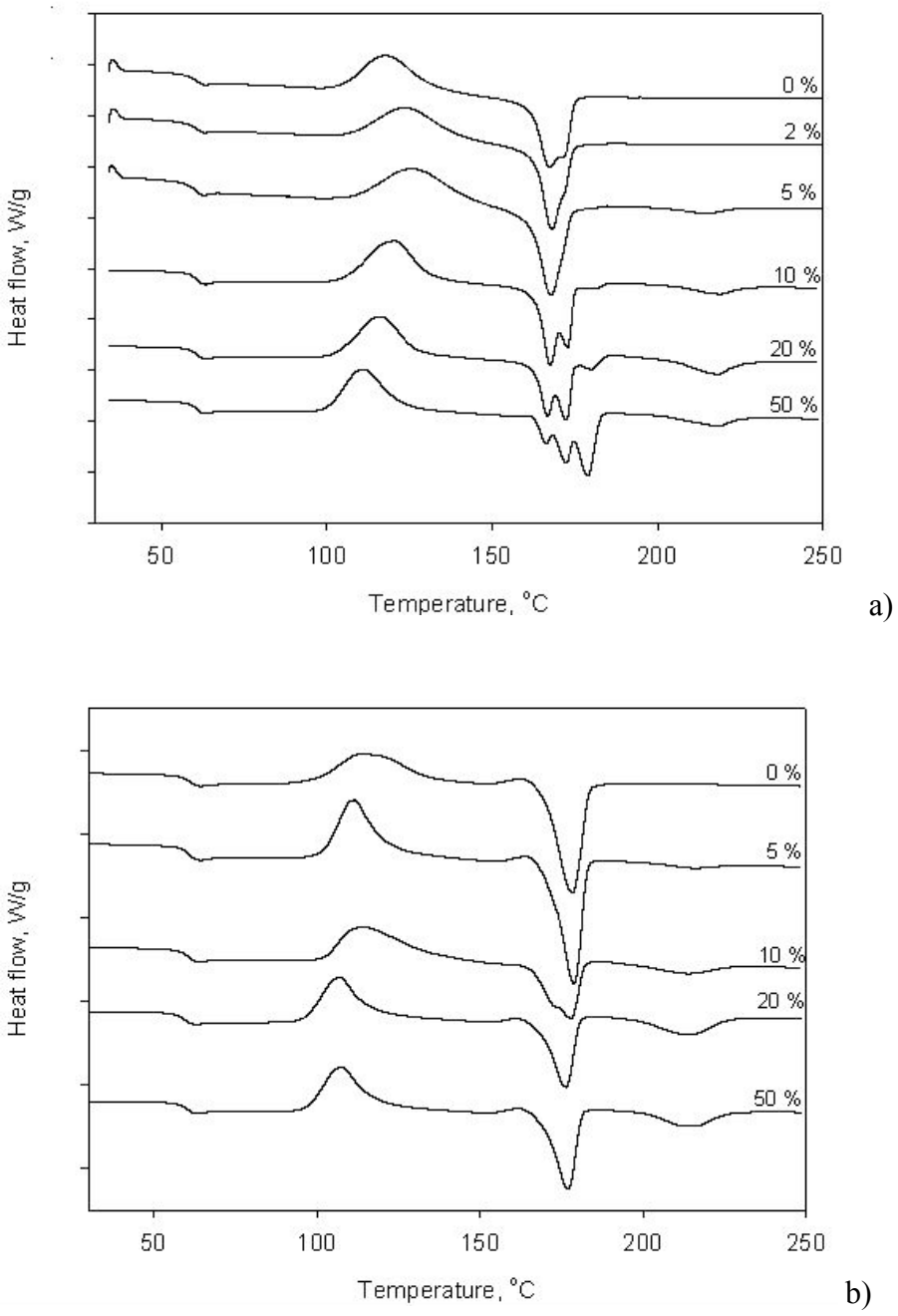

Figure 3.10. Second runs DSC curves for the blends of (a) poly(L/D-lactide) and (b) poly(L-lactide) with varying poly(D-lactide) content. Heating rate is 5 °C/min. Curves were shifted vertically for clarity.

The area under this peak increases as the poly(D-lactide) content increases (up to a maximum) confirming the presence of the stereocomplex as shown in Figure 3.11. Note that the stereocomplex melting peak is not visible in Figure 3.10(a) for the 2% PDLA blend. This is simply a result of the low vertical resolution on the graph and there is actually a very small peak in the data. The heat of fusion of the pure stereocomplex is 142 J/g, indicating that the maximum stereocomplex content observed in our blends is about 10 % by weight. Interestingly, the maximum stereocomplex content occurs at 20 % PDLA in both systems with the maximum being significantly lower in the poly(L/D-lactide) based system. We note that the amounts of stereocomplex observed in the first DSC runs were very similar to those observed in the second runs (Figure 3.10). Therefore we propose that during the following crystallization kinetics studies for the blends the stereocomplex content is given approximately by the data in Figure 3.10 and is likely not changing while the α-crystallization is taking place.

Additionally, for blends contain 10 % or less PDLA there is very little difference between the stereocomplex content in the poly(L/D-lactide) based systems as compared to the of poly(L-lactide) based systems. This indicates that the formation of stereocomplex is not significantly hindered by the presence of the D-lactide units in the copolymer at these PDLA contents. This is particularly interesting as the presence of a small amount of D-lactide units in a L/D copolymer has an enormous effect of the formation of the α-crystal. We will come back to this issue later with an explanation for this behavior.

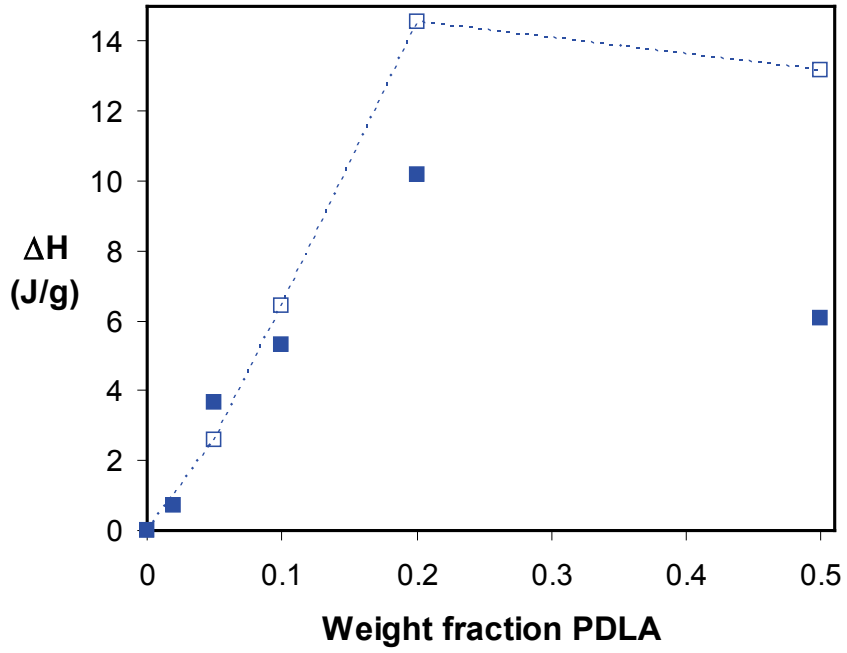

Figure 3.11. Enthalpy of stereocomplex melting for polylactide blends. Filled symbols are for blends of poly(L/D-lactide) with poly(D-lactide) and open symbols are for blends of poly(L-lactide) with poly(D-lactide). Extracted from data in Figure 3.10.

We note that the multiple α-crystal melting peaks on the DSC curves for blends of poly(D-lactide) in poly(L/D-lactide) are related to the difference in the melting temperatures of the two pure polymers and also perhaps to structural reorganization caused by the low heating rate [41]. Since we are using the DSC scans only to observe the stereocomplex melting, these multiple peaks can safely be neglected.

In order to study the influence of stereocomplexation on the spherulite growth rate, we have studied the crystallization kinetics of the blends of polylactides using the techniques described earlier. Note that since our premelting step is performed at 182ºC (blends of poly(L/D-lactide) with PDLA) and 192ºC (blends of PLLA with PDLA) all of

the stereocomplex that is formed during the casting processes remains intact. Additionally during the "premelting" step it is possible that additional stereocomplex is forming. As explained previously, based upon the DSC studies we assume that during the crystallization studies the stereocomplex content is not changing significantly. Therefore we can observe the effect of the presence of stereocomplex particles on the crystallization of the α form separate from any potential effects of the competing crystallization mechanisms occurring at the same time. This work is complementary to that of Anderson and Hillmyer [24] who showed that small amounts of stereocomplex can act as very effective primary nucleating agents and that of Yamane and Sasai [13] who demonstrated unequivocally that the stereocomplex acts as a primary nucleating agent and that it increases the spherulitic growth rate at 120ºC. Yamane and Sasai did not study this effect at other temperatures, nor did they examine the differences between poly(L-lactide) and poly(L/D-lactide). Now by examining in detail its effect on the spherulite growth rate at all temperatures in both polymers we can complete the picture.

One would expect that the addition of the poly(D-lactide) to the poly(L/D-lactide) would lower its spherulite growth rate for the α-crystals because of the reduction in whole chain mobility caused by the stereocomplex crystals. However, a blend containing 2 % poly(D-lactide) showed a significantly higher maximum spherulite growth rate than the pure poly(L/D-lactide) while the blend with 5 % poly(D-lactide) showed significantly lower growth rate at all temperatures (see Figure 3.12). Additionally crystallization was almost completely suppressed in the blend with 10 % poly(D-lactide).

For the optically pure poly(L-lactide) and its blends with poly(D-lactide) (Figure 3.13), it was found that the shape of the spherulite growth rate curves were significantly

different from the poly(L/D-lactide)'s "bell" shape and had two maxima as explained previously. It is especially interesting that the shapes of the curves for these systems are similar, with the spherulite growth rate for most of the blends being lower than that of the pure poly(L-lactide) at all temperatures. The blend containing 2 wt % poly(D-lactide) showed a peculiar crystallization behavior; in that its spherulite growth rate at 120 ºC was slightly higher than for pure poly(L-lactide). This is somewhat similar to the observed increased maximum growth rate for the blend of poly(L/D-lactide) with 2 % poly(D-lactide) although not as marked. It was found that the global spherulite growth rate maximum is at around 110 ºC and the second local maximum is at around 130 ºC for all poly(L-lactide) with poly(D-lactide) blends. The lines in Figures 3.12 and 3.13 represent cubic spline interpolations of the experimental spherulite growth rate data.

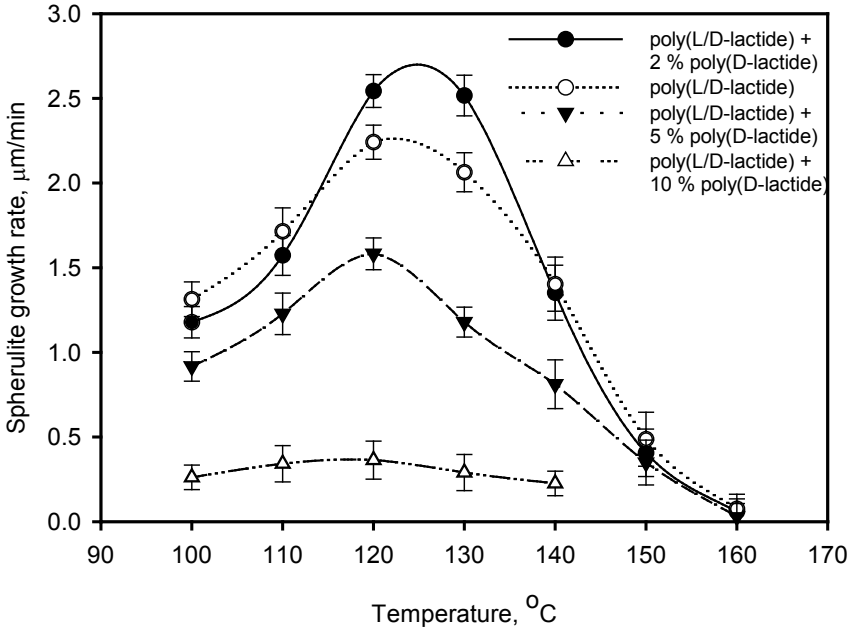

Figure 3.12. Isothermal spherulite radius growth rates for poly(L/D-lactide) and its blends with poly(D-lactide).

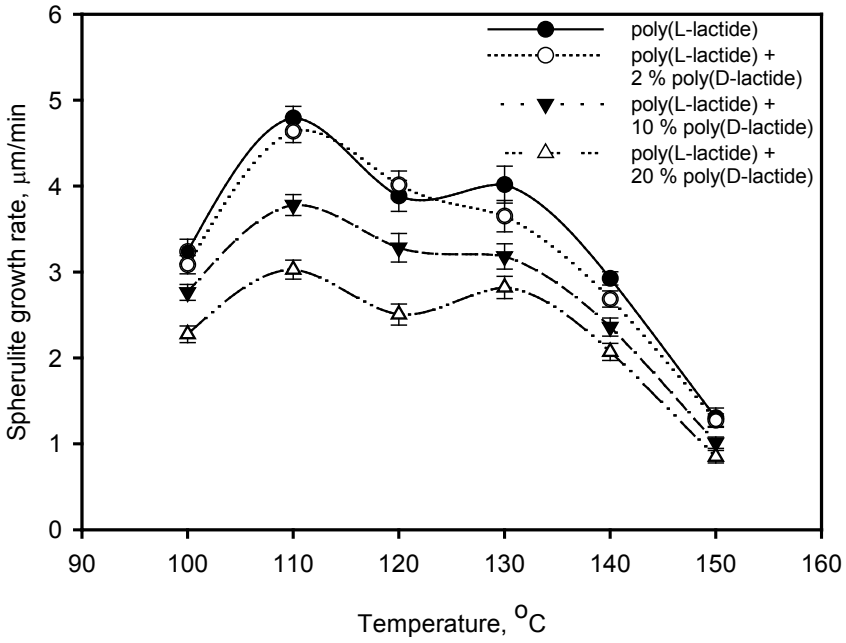

Figure 3.13. Isothermal spherulite radius growth rates for poly(L-lactide) and its blend with poly(D-lactide).

In order to compare the effect of the added PDLA on the spherulite growth rate of the poly(L/D-lactide) to its effect on the spherulite growth rate of the poly(L-lactide) we consider a reduced growth rate, $\frac{G_{x,T}}{G_{0,T}}$, at temperature *T*. Here *x* refers to PDLA content in the blend and the subscript 0 indicates the pure matrix material. The reduced growth rate at 110 and 120 ºC is plotted in Figure 3.14 for both series of blends where we can see clearly the very different impact of PDLA on these two systems. These two temperatures were chosen specifically to illustrate the different effect of the stereocomplex on the growth rate in regime II (120 ºC) and regime III (110 ºC).

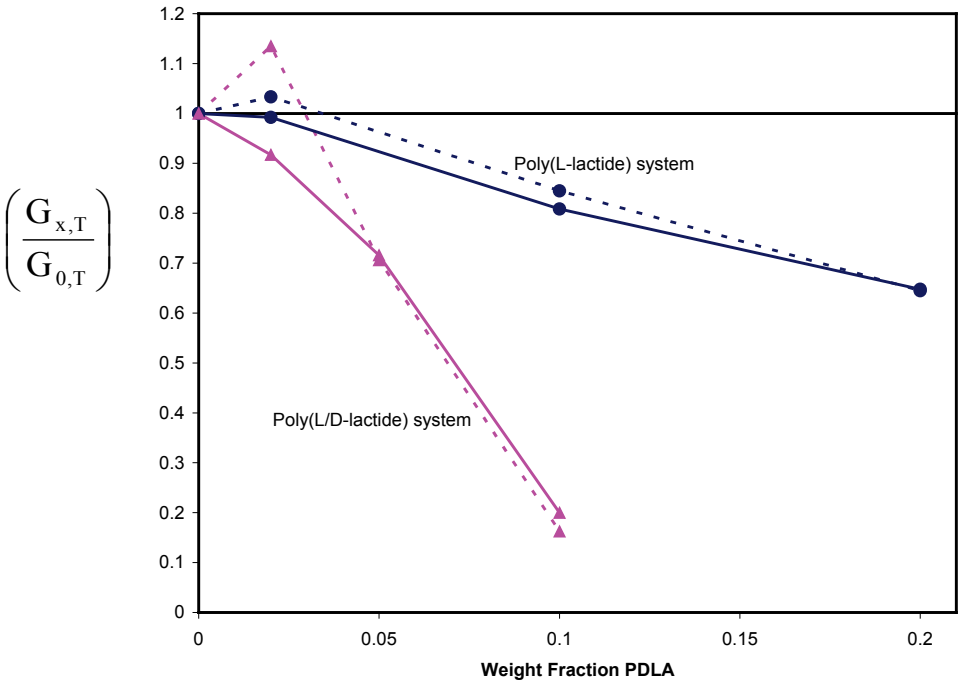

Figure 3.14. Reduced spherulite growth rate at 110°C (solid lines) and 120°C (dashed lines). Note that 110 ºC is in regime III and 120 ºC is in regime II.

At low PDLA content (2 %), the reduced growth rate at 120 ºC is enhanced (i.e. higher than 1) in both systems with a much larger degree of enhancement in the poly(L/D-lactide) system. This can be compared to the behavior at 110 °C where the reduced growth rate is lower than 1 for both systems, again with the impact of the PDLA being larger on the poly(L/D-lactide) system. According to Abe et al. [36] the transition between crystallization regime III (limited by the diffusion of individual chains) to regime II (secondary nucleation rate is larger than rate of diffusion) occurs at about 120 ºC for polylactide and regime II lasts until about 145 ºC [36]. Clearly the rate of diffusion of individual chains is decreased by the presence of stereocomplex crystals (as is discussed in more depth in the following paragraphs) explaining the observed reduction

in spherulite growth rate at 110 ºC where diffusion is an important factor. Now at 120 ºC and slightly above, it is possible that the stereocomplex crystallites are increasing the rate of growth nucleation of α-crystals sufficiently to overcome the effect of the reduced diffusion and enhance the overall spherulite growth rate. This effect is only observable at low stereocomplex contents since the reduction in the diffusion rates at higher stereocomplex contents is very large. We note that secondary or growth nucleation is often unaffected by agents which enhance primary nucleation although in some cases there is an effect. For example, Jang et al. [42] have demonstrated that the presence of sodium benzoate in polypropylene increases both primary nucleation and spherulite growth. Additionally, Kim et al. [43] have demonstrated that silica nanoparticles in poly(ethylene 2,6-naphthalate) act as both a primary nucleating agent and an enhancer of spherulitic growth rate. Most importantly, Yamane and Sasai [13] did show that the stereocomplex acts to enhance the spherulitic growth rate at 120ºC. We propose that this increase of growth rate is a direct result of enhanced secondary nucleation. Additionally, since the increase in 120ºC growth rate is much larger in the poly(L/D-lactide) system than that observed in the poly(L-lactide) system we can conclude that there are more stereocomplex particles present in the poly(L/D-lactide) system.

At higher contents, we observe a much stronger reduction in the reduced growth rate of the poly(L/D-lactide) system as compared to the poly(L-lactide system). These results can be understood by noting that the D-lactide units in the poly(L/D-lactide) chains will disrupt the formation of the stereocomplex. Therefore in this system, for the same PDLA content, we expect to have more but smaller stereocomplex crystals than in the poly(L-lactide) system. The reduction in chain mobility due to a network of

stereocomplex particles is dependent on the number of particles and not just the overall mass fraction of stereocomplex. (We recall that according to the DSC results, the mass fraction of stereocomplex present in these two systems is similar at PDLA contents up to 10 %). Therefore we expect that the chain mobility in the poly(L/D-lactide) blend containing 5 % PDLA is significantly lower than in the poly(L-lactide) at 5 % PDLA. This reduction in chain mobility (as compared to the mobility in the absence of stereocomplex particles) results in the lower average, reduced growth rate.

A sparse network of stereocomplex particles would have a significant effect on whole chain coordinated motions, such as reptation, which are required in the crystallization process while having a negligible effect on the local movements associated with the glass transition. In order to illustrate the difference between the separate effects of stereocomplex particles on α-crystallization and glass transition we consider a hypothetical system in which each of the chains was taking part in a single stereocomplex particle, reptation would be entirely suppressed and the dominant mechanism of large scale motion would be contour length fluctuations (CLF). The time scales associated with reptation and CLF are proportional to $(M/M_e)^3$ and $exp(\nu M/M_e)$ respectively [44]. Here M is the molecular weight of the chain of interest and, M_e is the entanglement molecular weight (~4000 g/mol for PLA [45]) and ν is a coefficient of order 1. Clearly CLF is a much slower process than reptation for chains of significant length (eg. if M = 50 kg/mol then CLF is 2 orders of magnitude slower than reptation) and therefore crystallization would proceed much more slowly in our hypothetical system than in a system free of stereocomplex particles. Now we consider the effect of this number of

stereocomplex particles on the glass transition by using the following semi-empirical equation [46]:

$$\frac{T_g(\chi)-T_g(0)}{T_g(0)}=\frac{\chi K M/\gamma}{1-\chi K M/\gamma} \qquad (3.1)$$

Here χ is the number of crosslinks per gram; K is a constant of order 10^{-23} and M/γ is the molecular weight per flexible backbone bond (24 for polylactide). Note that $T_g(0)$ refers to the T_g in the absence of crosslinks. For our hypothetical system described above if the M_N = 50 kg/mol and the density is of order 1 g/mol then the number of crosslinks per gram is of order 10^{19}. With a T_g of 60 ºC in the absence of crosslinks we therefore expect our hypothetical system to have a T_g of about 60.8 ºC. For the blend of 20 % PDLA in poly(L/D-lactide) we have observed a of T_g of 60.5 ºC as compared to the T_g of the pure poly(L/D-lactide) which is 60 ºC. We recall that in this blend the crystallization rate is about 5 times lower than in the pure poly(L/D-lactide). Therefore we conclude that our observation of significantly affected crystal growth rates in the absence of significant changes in the glass transition temperature is consistent for our systems. At this point we compare our results to those of Tsuji and Ikada [47] who studied the thermal properties of a series of 50/50 blends of optically pure PLLA and PDLA of varying molecular weight. They found that for $M_W < 10^5$ and stereocomplex contents of 40 wt% and above an augmentation in T_g of up to 5 ºC occurs and no α-crystallization occurs. Our study demonstrates that at much lower stereocomplex contents and in the absence of significant augmentation of T_g, the spherulite growth rate can be enormously reduced.

3.4. Conclusions

A flexible technique for studying the isothermal crystallization behavior of polylactide was developed. This technique which uses *ex situ* isothermal crystallization is applicable to any polymer amenable to solution casting with a glass transition above room temperature. The efficacy of this technique was demonstrated and the sources and magnitudes of experimental errors were investigated.

Using this technique, we confirmed that while poly(L/D-lactide) copolymers have typical bell-shaped spherulite growth rate temperature dependencies, poly(L-lactide)s deviate from this pattern and show significantly higher spherulite growth rate in the low temperature region. Thus, the poly(L-lactide) spherulite growth rate curve has two maxima: one is higher and sharper at 110 ºC and a second flatter one at 130 ºC. This behavior, previously attributed to a regime II–regime III transition, is not accompanied by any changes in morphology.

The spherulite growth rate in blends of poly(L/D-lactide) and poly(D-lactide) is much more affected by poly(D-lactide) content than in blends of poly(L-lactide) and poly(D-lactide). We have attributed this to the likely presence of more but smaller stereocomplex particles in the poly(L/D-lactide) systems than in the poly(L-lactide). Our hypothesis is that the presence of 2 % D-lactide units in the copolymer chain disrupts the formation of large continuous stereocomplex crystallites but does not hinder the nucleation and initial growth of these crystallites. In a system with more, smaller stereocomplex particles we expect the chain mobility and therefore the spherulite growth rate to be reduced. Additionally in a system with more stereocomplex particles we

expect the rate of primary and growth nucleation rates to be increased. In crystallization regimes I and III the presence of stereocomplex particles tends to reduce the spherulite growth rate because of the reduced chain mobility. In crystallization regime II the presence of many small stereocomplex particles tends to enhance the spherulite growth rate because of enhanced growth nucleation.

The development of the crystalline morphology of polylactides was also investigated and discussed. The long spacing of poly(L-lactide) crystallized at high temperature was found to be 19 ± 2 nm in the 165–170 ºC temperature range. It was also found that the screw dislocations in hedritic structures in polylactides at low supercooling occurred predominately in the clockwise direction relative to the surface of the film. Finally we have found that flat-on and edge-on crystallites form at 170 ºC but transitions between the two types do not occur at this temperature contrary to 165 ºC where edge-on is the preferred orientation and transitions do occur.

Acknowledgements

Purasorb PL and Purasorb PD samples were donated by PURAC and funding was provided by NSERC and PetroCanada.

CHAPTER 4

Degradation and Rheology of Polylactide

The noticeable decrease of the molecular weight of polylactide during melt processing is a well known phenomenon [48,49]. However, there is not much information on the mechanisms of thermal degradation in the range of moderate temperatures where crystallization occurs. Liu et al. [50] showed that the thermal degradation of polylactides is governed by simple exponential relations and significant degradation occurs at temperatures as low as 160°C in nitrogen. Jamshidi et al. [51] and Zhang et al. [52] identified inter- and intramolecular transesterfications as the main mechanisms for the reduction of molecular weight of polylactide above the melting point. They reported that intramolecular transesterfication from the end of the chain (back-biting) or in the middle of the chain leads to the formation of cyclic lactones and shorter linear polyesters. The intermolecular transesterfication with short molecules also causes a decrease in the average molecular weight.

The degree of thermal degradation of polylactide observed in our experiments is far less than reported by Bigg [53]. This can be explained by the fact that the degree of degradation is affected by the presence of low molecular weight chains, which facilitate polymer chain breakage. This suggests that, among many possible degradation mechanisms, only one is dominant in any given conditions. Though many works are dedicated to polylactide degradation, most of them concerned with thermal decomposition at temperatures higher than 250°C. It is suggested by Cam and Marucci [54] that for polylactides of relatively low molecular weight (M_W < 140,000), random

scission (intermolecular ester exchange) prevails over all other degradation mechanisms below 200°C. This can be explained both by the lower activation energy of the reaction and the higher concentration of terminal hydroxyl groups in low molecular weight polylactides. This conclusion is also supported by the fact that even at relatively high temperatures, the drop in zero shear viscosity is limited and relatively small, since the number average molecular weight of polymer melts remains constant and random scission leads only to redistribution of the polymer chain's molecular weight. Nevertheless, the formation of cyclic lactones due to intramolecular transesterfication cannot be completely excluded without experimental proof.

We conducted some limited studies of the degradation of polylactide. The FTIR spectrometry results also support the assumption about the prevalence of intermolecular ester exchange during thermal degradation. The IR spectra in the range of 600-4,000 cm^{-1} of samples degraded at elevated temperatures (190-200°C) for 60,000 s in nitrogen did not show any visible difference from those of samples not subjected to thermal degradation, indicating the absence of cyclic lactones.

We also have studied the influence of small amounts (0.03 – 0.26 wt%) of residual water on zero shear viscosity at different temperatures. Introduction of abovementioned amounts of water leads to the increase of hydroxyl group's concentration from 2 to 9 times. The water content was controlled by different drying conditions and it was found that water presence causes a fast drop in viscosity. This drop occurs before start of viscosity measurements suggesting a high reaction constant of hydrolysis at relatively low temperatures.

We proposed a polylactide degradation model which relates the evolution of the polylactide melts's complex viscosity over the time using an exponential decay equation. This model will be discussed in Chapter 5. To verify the adequacy of our thermal degradation model, parameters were fitted using Arrhenius equation [80] for 160-200 °C temperature range:

$$\frac{\eta_0(T)}{\eta_0(T_0)} = \exp\left[\frac{E_a}{R}\left(\frac{1}{T} - \frac{1}{T_0}\right)\right] \tag{4.1}$$

where E_a is an activation energy for the flow. The results are presented on Figure 4.1.

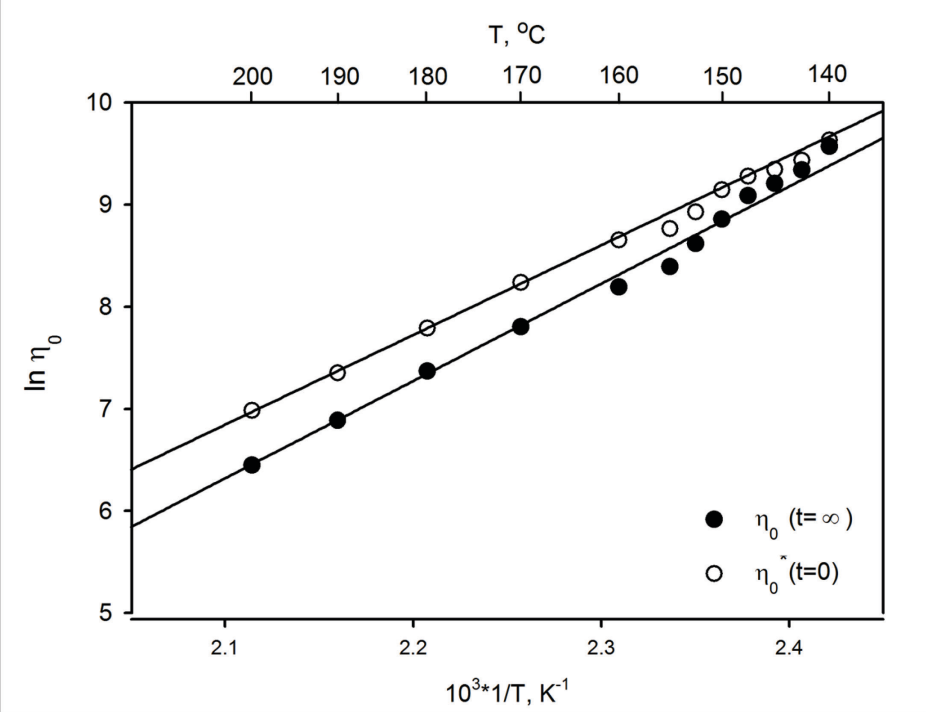

Figure 4.1 The Arrhenius equation fits for polylactide at $t=0$ and $t=\infty$. Only data points for temperatures higher than 160 °C are used.

From Figure 4.1 it was found that activation energy for the flow E_a=73.01k J/mol at $t=0$ and E_a=79.15k J/mol at $t=\infty$. These values are consistent with those previously

reported by S.-Y. Gu et al. [55] Equation (4.1) typically well describes viscosity – temperature dependence for temperatures at least 100 K higher than T_g [56]. The glass transition temperature of the polylactide under investigation was determined by DSC analysis to be 56 °C. As expected, the linear fit is near perfect for temperatures above 160°C and less precise for lower temperature range where temperature dependence of viscosity is strongly affected by free volume increase and Williams-Landel-Ferry equation [56] gives more consistent approximation. It also should be noted that samples at temperatures 160 °C and lower were preheated to 190 °C for short time to avoid immediate heterogeneous crystallization which, in turn, decreases measured complex viscosity at *t=0*.

Rheology, especially small amplitude osciallatory shear (SAOS), provides a very convenient and versatile tool for polymer melt crystallization studies. The advantages are very appealing: 1) it is a well established technique allowing the simultaneous measurement of a range of melt rheological parameters; 2) rheological parameters are very sensitive to crystallinity; 3) rheolodical techniques are nonintrusive to quiescent crystallization when SAOS is used; 4) it allows imposing precisely measured shear rates for predetermined time intervals having very small transition time; and 5) it allows for application of an electric field across the plates during the rheological measurement. In this study it is critical not only to develop research techniques allowing accounting for degradation but also allowing relating melt crystallinity and viscosity. Due to complexity of the viscosity-crystallinity relationship in polymer melts there is no established theory regarding this matter. In the article presented in Chapter 5, we attempted to resolve this problem and developed an approach to observe homogeneous crystallization, which

occurs over very long times, while accounting for the decrease in molecular weight due to thermal degradation. The functional dependencies and techniques presented in Chapter 5 were later applied for studies of flow induced crystallization and the crystallization under the presence of electric field. Therefore, the concepts and models presented in Chapter 5 represent a critical part of this thesis.

CHAPTER 5

Rheological Properties of Crystallizing Polylactide: Detection of Induction Time and Modeling the Evolving Structure and Properties

5.1. Introduction

Polymer crystallization is one of the most significant phenomenon in polymer science and many techniques were used for studying its different aspects. In particular, attempts have been made to retrieve crystallization kinetics from rheological measurements mostly with little quantitative success. A number of equations had been proposed for relating crystallinity and rheological parameters. Khanna [57] used a simple equation to relate the storage modulus to the crystallized volume $\phi(t)$:

$$\phi(t) = \frac{G'_t - G'_0}{G'_\infty - G'_0} \tag{5.1}$$

where G'_0 and G'_∞ are initial and final plateau of storage modulus, respectively. By studying a range of polymers, Kelarakis et al. [58] found that the rates of crystallization from calorimetry and rheometry cannot be described by such a simple relation. The authors showed that at low crystallite volume fraction the storage modulus of some polymers is directly proportional to the degree of crystallinity but at high crystalline volume fractions the proportionality is lost. For many polymers this relation is inconsistent even at low crystallinity. Other more complex models are the Voigt parallel model [59], the Reuss series model [60], the Kerner model [61] and the Budiansky model [62]. Lellinger et al. [63] found that even the most complex Kerner and Budiansky models yield results which are very far from experimental observations. They [63] also

noted that these attempts had very limited success due to the difficulty of determining the onset of crystallization from rheological data.

The most popular method for determining the onset of crystallization involves defining two tangents to the viscosity vs. time curves and then taking their intersection as the induction time [64-66]. A second approach is to define the induction time as the moment when the viscosity of the melt increases by a specified value [67]. Another approach is to define the induction time as the moment when a sudden upturn of viscosity curves is observed [68,69]. Chen et al. [70] defined induction time as the moment of time when the normal force is two times its initial value. They found that in some cases the normal force is a parameter which is more sensitive to onset of crystallization than viscosity. Nevertheless, it should be noted that the measurements of correct normal force represent difficult and nontrivial problem demanding high temperature and instrument precision, especially for cone-plate geometry [71]. Often the induction time values obtained using these techniques are referred as "instrumental" [72], "rheological" [67] or "viscosity" induction time. The use of these techniques results in enormous variation in reported induction times, as the determination of the location of the tangent points and/or the cutoff value of viscosity are somewhat arbitrary. Moreover, in most cases these techniques identify a viscosity at the moment of time when significant crystallinity has already developed, much later than the onset time. Since the evolution of viscosity during crystallization depends both on growth rate and nucleation rate such an "induction time" will not represent the crystallization process. Optical techniques are of course also used for determination of induction time however an arbitrary choice of cutoff value is also made in those techniques. For example, Chaari et al. [73] determined the induction time

as the moment of time when transmittance of the melt decreased by 10%. Eventually the use of any such arbitrary value leads to increased and unpredictable errors in determination of induction time.

Another noteworthy difficulty in relating rheological properties to crystallinity comes from the influence of morphology on the rheological properties. For example, at the same volume fraction crystallinity, a melt with more, smaller crystallites will have a higher viscosity than one with fewer, larger crystallites. In other words, rheological properties depend differently on nucleation rate and growth rate and no simple, general relation with crystallinity content exists. This can be understood by considering that crystallites have two distinct effects on rheological properties. The first is simply due to the presence of solid particles in the melt, referred to here as the filler effect. The second is due to the fact that many chains are partially crystalline and partially amorphous and fully entangled in the amorphous region. These chains cannot relax stress in the same manner as the completely molten chains. Instead they relax by a much slower process similar to star branched polymers. We refer to this effect as the crosslink effect. To use rheological measurements as a quantitative method for observing crystallization, we must account for both of these effects.

The noticeable decrease of molecular weight of polylactide during melt processing is a well known phenomenon [74,49]. However, there is not so much information on the mechanisms of thermal degradation in the range of moderate temperature where crystallization occurs. Liu et al. [75] showed that the thermal degradation of polylactides is governed by simple exponential relations and significant degradation occurs at temperatures as low as 160 °C in nitrogen. Jamshidi et al. [76], and

Zhang et al. [77], identified inter- and intramolecular transesterfications as the main mechanisms for the reduction of the molecular weight of polylactide above the melting point.

In this study we make use of the sensitivity of rheological properties to crystallinity to accurately determine the onset of homogeneous crystallization at low degree of supercooling. To reach this goal we combined an empirical model of thermal degradation with statistical analysis of the rheological data. We also develop a phenomenological model describing the evolution of viscosity of crystallizing polylactide using homogeneous nucleation theory and simple rheological models.

5.2. Experimental

The polylactide sample used was supplied by Biomer (Germany). It is a commercially available poly(L/D-lactide) copolymer containing 2% of D-lactide (L 9000). It was found via gel permeation chromatography measurements that this polymer has a number average molecular weight of 50,000 and a polydispersity index of 2.0. The glass transition of this polymer is 60 °C, and its melting point is 170 °C. its thermal transitions and spherulitic growth rates have previously been described [78].

The pellets were thoroughly dried at 80 °C in a vacuum oven for 24 hours prior to pressing at 185 °C in a Carver hydraulic press. This procedure allowed the decrease of adsorbed water content in the polymer from 0.26 wt% to 0.03 wt% significantly suppressing the influence of hydrolysis during the rheological measurements. Subsequent

experiments showed no noticeable decrease in water content with increase of drying temperatures and times.

The rheological measurements were performed under a nitrogen atmosphere with oxygen content of less than 2.5 ppm in a modular compact rheometer (MCR 500 model of Anton Paar). The use of liquefied nitrogen as source of the protective medium during experiments assures the absence of humidity in the nitrogen. All small amplitude oscillatory shear experiments were done using plate-plate configuration with a 1 mm gap at 5% strain. The small strain value allowed us to avoid shear induced crystallization. We have confirmed that 5% strain remains in the linear viscoelastic region at 1 Hz up to crystallinity content of least 4.5% at 140 °C. Most experiments were performed at a single frequency of 1 Hz, although some frequency sweeps were also performed. The choice of the oscillation frequency is important in these experiments and will be discussed in Sections "The Physical Crosslink Model" and " Gelation and the Transition to Solid-Like Behavior".

Essentially homogeneous crystallization conditions were ensured by a heating of each sample to 190 °C directly inside the rheometer to eliminate any residual crystallinity before dropping the temperature to within the crystallization regime and starting the rheological measurement. This thermal pretreatment was confirmed to be sufficient to remove previous traces of crystallinity by observing that additional annealing did not result in any further increase in induction time. Note that in the absence of the thermal pretreatment, the induction time is essentially zero. Sequential frequency sweeps were performed at 140 °C to observe the frequency dependence of the linear viscoelastic properties during crystallization. In these experiments, 16 sweeps covering a range of

0.01 to 50 Hz were performed during the crystallization process. Each sweep took approximately 500 s and the entire experiment lasted for 9500 s. As the measurement time for each frequency is different, a single sweep contains data for times differing by up to 500 s. In order to recover the behavior at a single time, the raw experimental data were interpolated using Akima cubic spline interpolation [79].

The differential scanning calorimetry (DSC) measurements were done using a ThermalAnalyst Q10 system. The temperature protocol, designed to mimic the conditions in the rheometer, consisted of the heating of the sample up to 190 °C at 5 °C /min, followed by an isothermal hold for 5 min, and then cooling to the target crystallization temperature at 4 °C /min. This procedure ensures that temperature variations in the sample during DSC experiment match those during the rheometrical measurements. The homogeneous crystallization rate of polylactide at high temperatures is very low, resulting in an extremely low heat flow, often approaching the equipment resolution. Also, the thermal degradation enthalpy of reaction significantly contributes to heat flow. In this case it is difficult to retrieve crystallization data from a single isothermal crystallization DSC experiment. Thus, a series of DSC measurements with different isothermal crystallization times were done to determine induction time and crystallization data. The induction time from DSC data was determined as the intersection of the Avrami fit with a line corresponding to ϕ=0.001.

5.3. Results and Discussion

5.3.1 The Exponential Decay Model of Polylactide Thermal Degradation

Thermal degradation occurs with many polymers and mechanisms of this degradation are mainly determined by the chemical structure of polymer chain. The presence of oxygen and water can both significantly increase degradation rate and complicate the mechanisms of degradation in some polymers, particularly polyesters like polylactide. In this study we attempted to limit the degradation processes to thermal degradation by essentially eliminating moisture and oxygen. The degradation processes in polylactide are complex and we do not attempt to provide an insight in this complicated matter, rather in this study we are suggesting a phenomenological model which takes into account effects of both thermal degradation and crystallization phenomena on rheological properties of polymer melt. Thus, this approach is not polymer specific and can be useful for the studies of other crystallizing polymer melts regardless of presence or absence of degradation processes during crystallization. It was found that under these conditions, the complex viscosity of polylactide melts can be precisely described by the following empirical equation:

$$\eta_t^* = \eta_{t=\infty}^* + C\exp(-\frac{t}{\tau}) \tag{5.2}$$

where $\eta^*_{t=\infty}$ is a limiting complex viscosity at long times, C is the viscosity decay coefficient, and τ is the thermal degradation time constant.

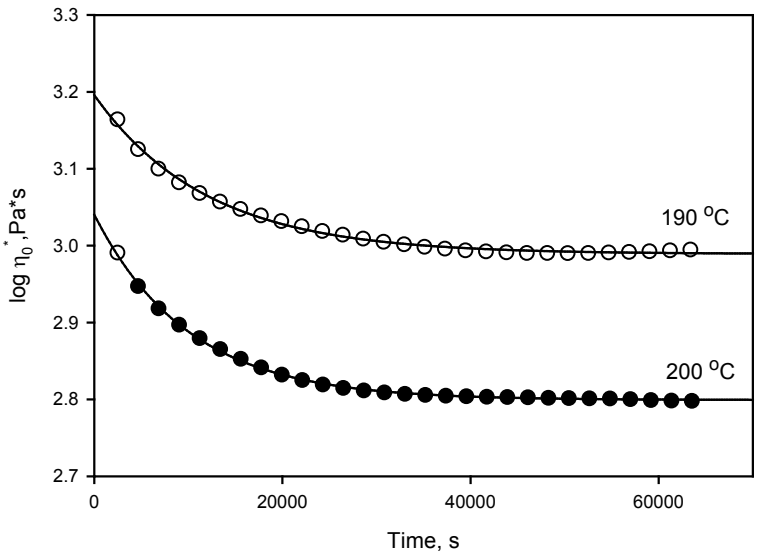

Figure 5.1. The complex viscosity of L 9000 polylactide and exponential decay fits.

The results showed that Equation 5.2 well describes the complex viscosity over a wide range of temperatures from 140 °C to 200 °C (Figure 5.1.) Typical adjusted coefficient of determination R^2 values for the fits using Equation 5.2 at all temperatures were in the range of 0.9988 to 0.999995, which indicates a very good correspondence of the proposed model and the experiments.

The decrease of weight-average molecular weight due to thermal degradation can be estimated from changes in the zero shear viscosity using the following equation [80]:

$$\eta_0 \cong K M_W^{3.4-3.7} \text{ for } M_W > M_C \tag{5.3}$$

where M_C is the critical molecular weight equal to about 8000 for polylactide [81] and K is a constant. It was found by Dorgan et al. [82] that for linear polylactide the exponent is equal to 3.7. Using Equation 5.3, it can be determined that terminal weight-average molecular weight reaches ~86600 for thermal degradation at 200 °C, ~90400 for 155 °C and ~98300 for 140 °C. We note that this approach is exact for the data in Figure 5.1 as 1

Hz is within the terminal zone at these temperatures. At the lower temperatures, 1 Hz is slightly outside of the terminal region and, therefore, Equation 5.3 provides an estimate of the change in weight average molecular weight. As our crystallization studies cover the range of 140–155 °C, we can conclude that the small change in molecular weight from temperature to temperature should have a negligible effect of the interpretation of our results.

5.3.2. The Determination of Induction Time of Homogeneous Crystallization Using the Standardized Residuals Technique

Apart from thermal degradation, the complex viscosity is also affected by crystallization. Even trace amounts of crystallinity can dramatically increase the viscosity of the melt due to its physical crosslink effect and the resulting retardation of the movements of the polymer chains within the entangled system [83]. This effect far exceeds that of the solid filler effect making possible the use of rheological parameters for crystallization studies. The sensitivity of the complex viscosity to melt crystallinity makes it especially convenient for observation of homogeneous crystallization at low degrees of supercooling when spherulite growth rate and nucleation density are extremely low (Figure 5.2).

Homogeneous crystallization conditions are extremely difficult to achieve for many polymers due to the permanent presence of impurities in polymer melts which act as nucleating centres [84]. Nevertheless, if certain precautions are made it is possible to simulate homogeneous crystallization conditions. A distinctive feature of homogeneous

crystallization is the induction time t_0 of crystallization, i.e. the time required for sub-critical clusters to form and develop into nuclei before crystallization starts [85]. It is believed that the induction time is also includes the sum of two characteristic times; first, it is the time necessary for the formation of a number of growing nuclei sufficient to detect them by the available technique and, second, the time required to reach at a constant growth rate [86].

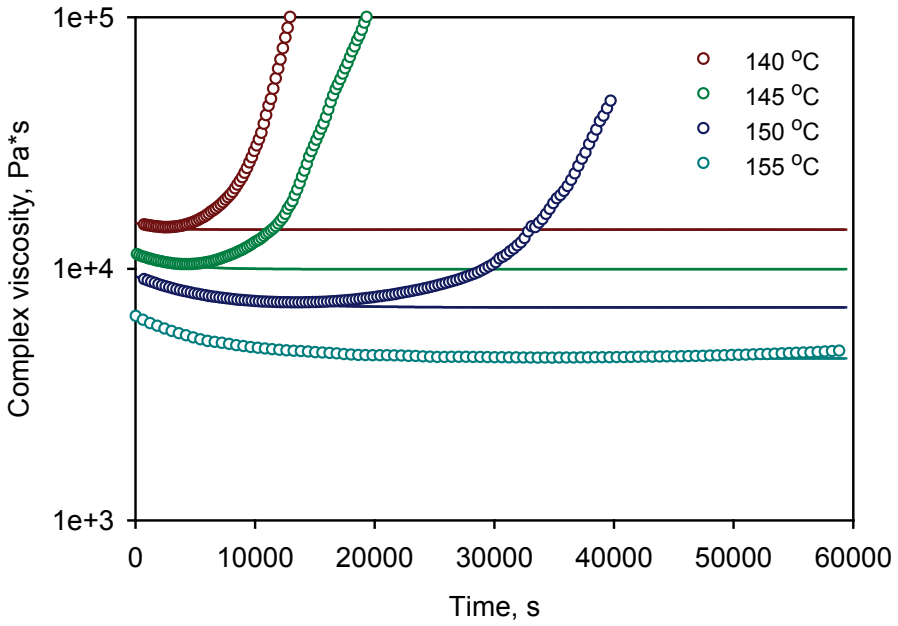

Figure 5.2. The complex viscosity of homogeneously nucleated L 9000 polylactide at different temperatures. The solid lines are corresponding fits according to Equation 5.2.

The induction time is usually found from isothermal DSC experiments. For low degrees of supercooling, the crystallization rate can be extremely low and the associated latent heat flow can be below the equipment sensitivity. The heat of reaction associated with degradation also can deteriorate the measured crystallization heat. It is difficult to

overcome this limitation due to differential nature of the DSC analysis. The rheological parameters, meanwhile, are cumulative to crystallinity and can, therefore, be more convenient for detection of the onset of crystallization if a proper technique is implemented. We found that standardized residuals, r_i, are a convenient way to analyse the data:

$$r_i = \frac{e_i}{\sqrt{\hat{\sigma}^2}} = \frac{e_i}{\sqrt{\frac{1}{n-1}\sum_{i=1}^{i=n}\left(e_i - \bar{e}\right)^2}} \tag{5.4}$$

where e_i is the real residual (the difference between measured complex viscosity and corresponding value of the fit equation, here the exponential decay model) and the divider is the square root of the unbiased estimator. The standardized residuals can be used for evaluation of the adequacy of a model and the detection of outliers as they magnify any difference between the model and the data. Any sporadic standardized residuals out of the [-2, 2] range suggest outliers while a sustained occurrence of standardized residuals outside of this range indicate a lack of fit of the model in that region. Once crystallization begins, the exponential decay model no longer describes the evolution of the complex viscosity over time, and the standardized residuals increase monotonically. As the standardized residuals magnify the deviation with respect to the model, they are very useful for determining the induction time.

The time from which the standardized residuals show a monotonic increase is considered to be the onset of homogeneous crystallization (Figure 5.3). It was found that along with the complex viscosity, the storage modulus G´ and loss modulus G´´ can also be used for this analysis although complex viscosity and loss modulus were found to be more accurate in this particular study. We note that the first points are identified as outliers

likely because the temperature conditions have not reached isothermal for a short time after beginning the experiment. As expected, before induction, the residuals are pseudorandom and show small cyclic fluctuations of various periods, which are most likely related to small cycles in the temperature controller. We note that although the oscillations in Figure 5.3 appear large, this is only due to the amplification inherent to the standardized residuals and the temperature is actually controlled within 1 ºC.

There are obvious limitations to the proposed technique. The sample of polymer used in rotational rheometer is ~100 times bigger than that used in DSC experiments and the rheometer heating chamber itself has significant thermal inertia and, therefore, takes a longer time to equilibrate at the set point temperature. This limits the lowest induction time reliably detected by this technique to 800 – 900 s since sufficient amount of data must be available prior to the onset of crystallization to obtain a precise fit of the exponential decay model. By using low shear rate experiments, this limit can be reduced and induction times of 200–300 s can be successfully detected. We note that the technique can also be applied to any form of viscosity development, if its functional dependence on time is known. In particular, in the case that the viscosity is not changing prior to crystallization then the expected dependence on time is simply a constant, the mean, and the unbiased estimator, the variance.

The resolution, with which induction times are determined, depends on the sampling rate of the viscosity measurement which, in turn, depends on the oscillation frequency. For 1 Hz as used in our study, each data point requires at least 42 s to be measured. None of the samples demonstrated signs of significant heterogeneous nucleation which can be detected by a decrease or complete disappearance of the

induction time since polylactide has a very low induction time for heterogeneous nucleation [78, 87].

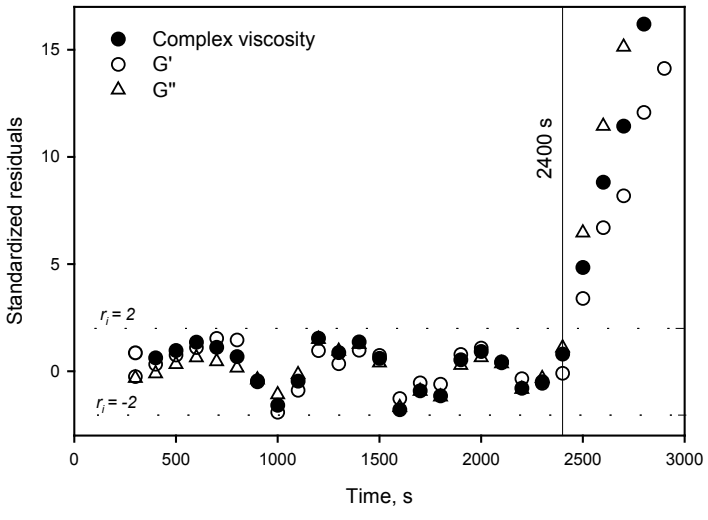

a)

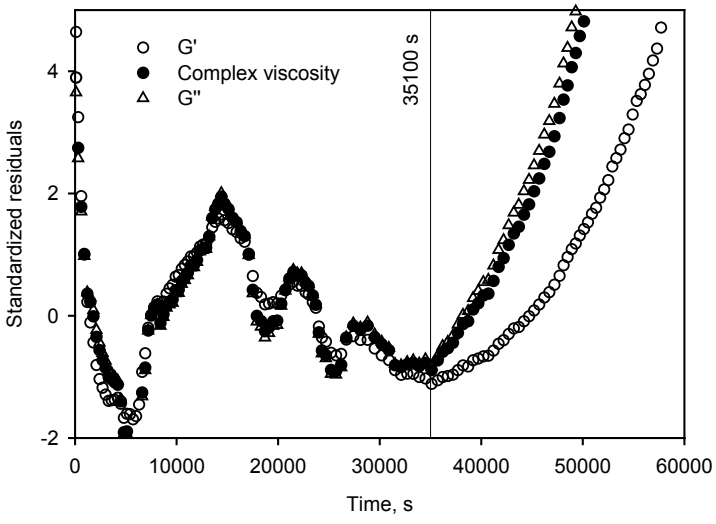

b)

Figure 5.3. The standardized residuals of complex viscosity, storage G´ and loss G´´ modulii at 1 Hz during homogeneous crystallization at (a) 140 °C and 155 °C (b). The vertical lines at 2400 s (140 °C) and 35100 s (150 °C) show the induction points.

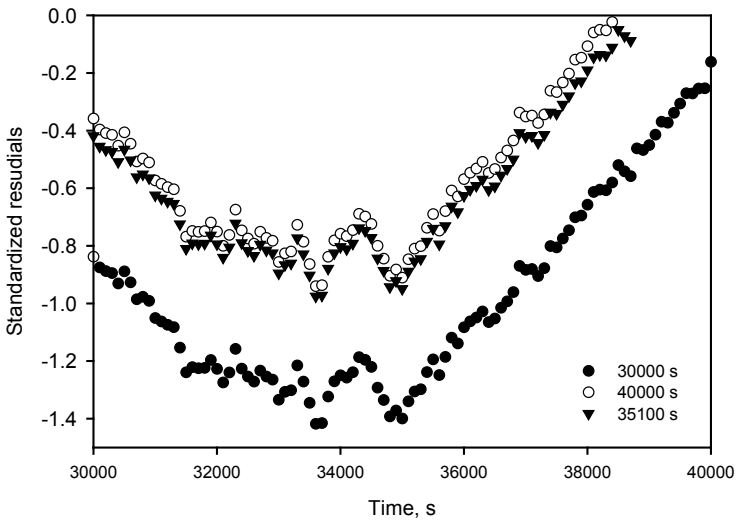

Figure 5.4. The standardized residuals for complex viscosity at 155 ºC based on model fits using various data sets: up to 30000 s: no crystallization; up to 35100 s: until onset of crystallization; and up to 40000 s: beyond onset of crystallization.

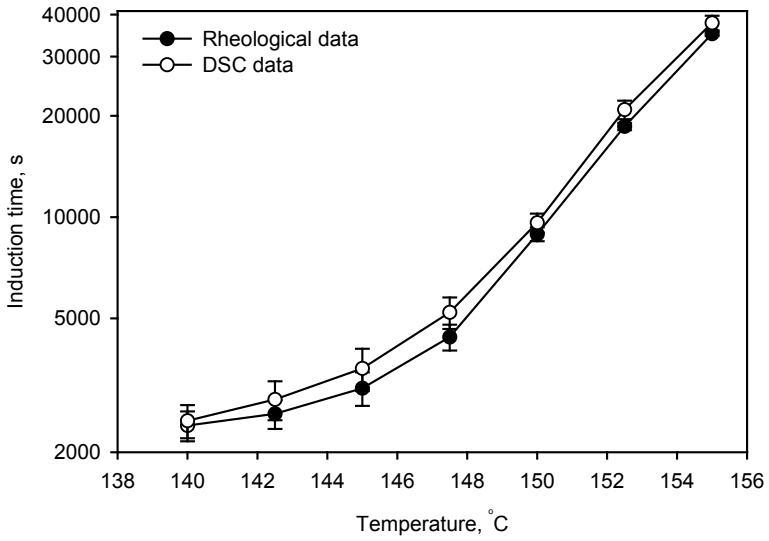

Figure 5.5. Comparison of induction times of homogeneous crystallization of polylactide determined from rheological data and DSC measurements. Error bars for rheological data represent 1 standard deviation from 3 measurements at each point. Error bars for DSC data were determined using the confidence band technique for scarce data.

Clearly, the exponential decay model parameters depend on the set of experimental data used for fitting the model. Nevertheless, we have found that the determined induction time is independent of the data set used for fitting (demonstrated in Figure 5.4).

The induction times of homogeneous crystallization at different temperatures determined from rheological data and DSC analysis showed close correlation (Figure 5.5). It should be noted that the rheological measurements gave lower values of induction time at all temperatures; however, the difference is similar to the uncertainty in the data.

5.3.3. Rheological Properties and Crystallization at the Initial Stages

The influence of crystallites on polymer melt viscosity cannot be completely described by equations suitable for suspensions because the interaction between the solid phase and the melt is complicated by the physical entanglement of partially crystalline polymer chains within the amorphous domain. This prevents such chains from relaxing stress by reptation resulting in much more complicated viscoelastic behavior referred to here as the crosslink effect. In this section we develop a phenomenological model to describe the viscosity of a crystallizing melt which is valid in the initial stages before impingement occurs. We consider separately the filler effect, due to the presence of solid particle, and the crosslink effect, due to the entanglement of partially crystalline chains in the amorphous domain. Our primary assumption is that the increase in viscosity due to crystallization can be modeled as the product of the filler effect and the crosslink effect. We begin with the development of the model for the filler effect.

The morphology of filler significantly affects the viscosity of a suspension [88,89]. For the polylactide under investigation, it was found that up to 155-160 °C crystalline structures are spherulitic and only at 160 °C and higher crystallization proceeds in form of axialites therefore here it can be considered that the melt is filled with crystalline structures of spherical shape [87].

The Maron-Pierce equation [90] is one of the simplest equations describing viscosity of filled melts over a relatively wide range of volume fraction of filler:

$$\frac{\eta_f}{\eta} = \frac{1}{\left[1-\left(\frac{\phi}{A}\right)\right]^2} \tag{5.5}$$

where ϕ is the volumetric fraction filler and A is a constant mostly depending on morphology and size distribution of the filler. It is known that A=0.68 [91] gives good approximation for viscosity of the melt filled with spheres of equal diameter. The first part of the proposed model for the effect of crystallinity on complex viscosity is based on Equation 5.5.

In order to relate the crystalline content to the volume fraction filler we make use of the Avrami equation [92]:

$$(1-\lambda(t)) = 1-\exp\left[-\frac{\rho_c}{\rho_l}\int_0^t \upsilon(t,\tau)N(\tau)d\tau\right] \tag{5.6}$$

where $\lambda(t)$ is a fraction of untransformed (i.e. amorphous) material, ρ_c and ρ_l are densities of crystalline phase and melt respectively, $\upsilon(t,\tau)$ is a volumetric growth rate of crystalline structure and $N(\tau)$ is a nucleation rate. Assuming that a steady-state nucleation rate is achieved at the onset point of crystallization at a time $t=t_0$ and that it remains invariant on volume fraction of crystallized material, then the nucleation rate $N(t)$ can be considered

constant. This assumption is not accurate for all cases of homogeneous nucleation; nevertheless, this approach can be accepted in some cases.

It should be noted that for most cases, the nucleation rate can significantly deviate from constant causing nucleation rate determined in this manner to deviate significantly from the above and a more general expression for the Avrami equation [93] is appropriate:

$$1 - \lambda(t) = 1 - \exp(-kt^n) \tag{5.7}$$

where k is a crystallization constant and a function of nucleation rate and growth rate and n is the Avrami exponent.

The observed Avrami exponents n determined from DSC data in our experiments ranged from 2.61 to 3.03. (Figure 5.6).

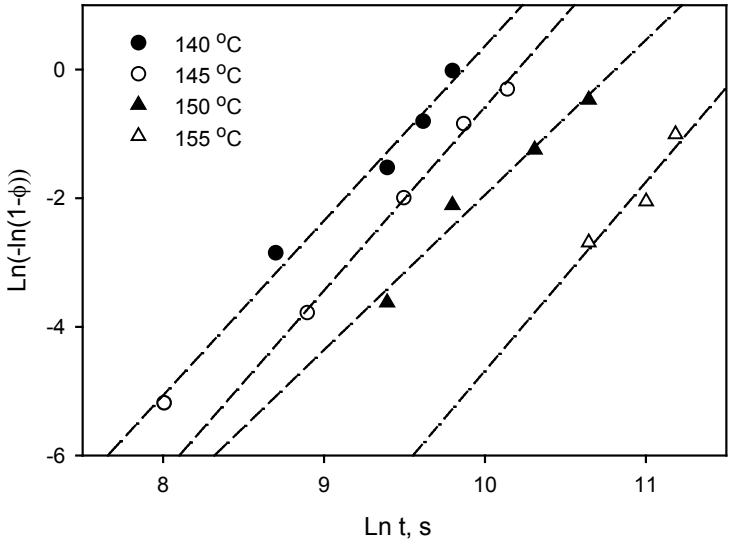

Figure 5.6. The Avrami fit for isothermal DSC data used in the determination of nucleation rate.

These values are significantly lower than the value for the case of ideal three-dimensional homogeneous nucleation (n=4) [93]. A number of factors affect an Avrami constant determined from DSC data including the presence of heterogeneities which were not removed during melting, spherulite impingement, physical limits of small volume samples, and the aforementioned non-constant rate of nucleation.

Considering $\phi=1-\lambda$ then Equation 5.7 and Equation 5.5 can be combined to give:

$$\frac{\eta_{filler}}{\eta_{melt}} = \frac{1}{\left[1-\frac{1}{A}\left(1-\exp\left(-kt^{n}\right)\right)\right]^{2}} \qquad (5.8)$$

Equation 5.8 only accounts for the filler effect and it will be used to evaluate the physical crosslink effect as explained in the following paragraphs.

We begin by looking at the viscosity enhancement due to the physical crosslink effect in Figure 5.7 by comparing the case of the experimental data (points) and the hypothetical filled system of the same crystalline content given by Equation 5.8 (curves). Note that we are plotting the ratio of the viscosity of the crystallizing melt to that of the pure melt. For the experimental data, the numerator is simply the measured viscosity and the denominator is given by the exponential decay model. As expected, the real viscosity of the crystallizing polylactide is significantly higher than that estimated when only the filler effect is taken into account. Clearly, the crosslink effect is significant and exceeds the filler effect especially during the initial stages of crystalization.

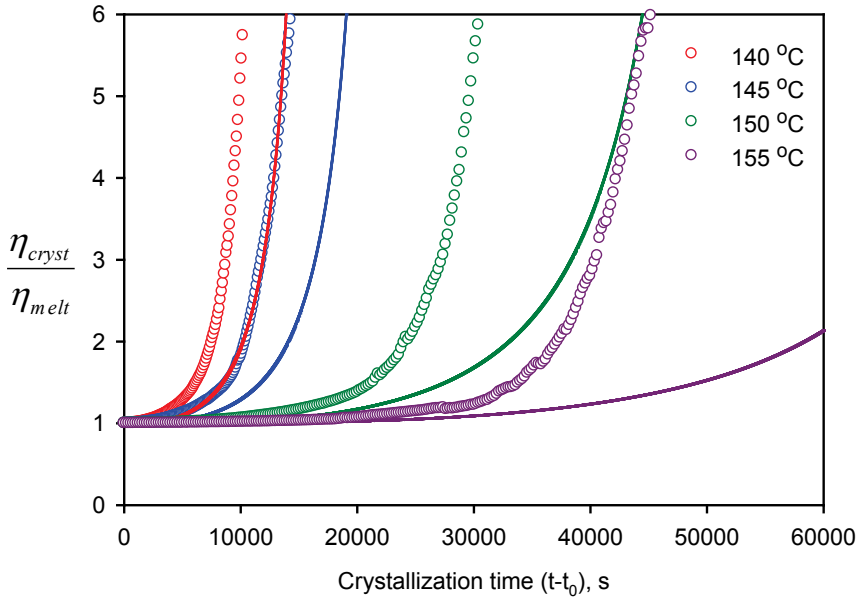

Figure 5.7. The enhancement of viscosity during homogeneous crystallization of polylactide at different temperatures. The curves represent the filler effect estimated using Equation 5.8.

Next we look at the evolution of $\frac{\eta_{cryst}}{\eta_{filler}}$ over crystallization time in Figure 5.8. The magnitude of the crosslink effect is expected to be related to the concentration of partially crystalline polymer chains participating in entanglements in the amorphous region per unit volume. This concentration, in turn, is dependent on the melt – crystallite interface area per unit volume or the specific interfacial area. Considering ideal homogeneous crystallization conditions, accepted for derivation of Equation 5.6, an evolution of interfacial area *S(t)* for any given volume of crystallizing polymer can be expressed in terms of the volume of transformed material *V(t)* as:

$$S(t) = \frac{4}{3Gt} V(t) \tag{5.9}$$

It can be expected that this relation would be true until significant impingement events start to occur. Considering Equation 5.9, and borrowing from molecular theories of the linear viscoelasticity of blends of star and linear polymers [94], the crosslink effect on the viscosity can be expressed as:

$$\frac{\eta_{cryst}}{\eta_{filler}} = \exp\left[\frac{4\delta\phi}{3Gt(1-\phi)}\right] \tag{5.10}$$

In this equation, the term within the exponential approximates the fraction of chains in the amorphous region that are partially crystalline or physically crosslinked and the parameter δ is empirical in nature (Figure 5.8).

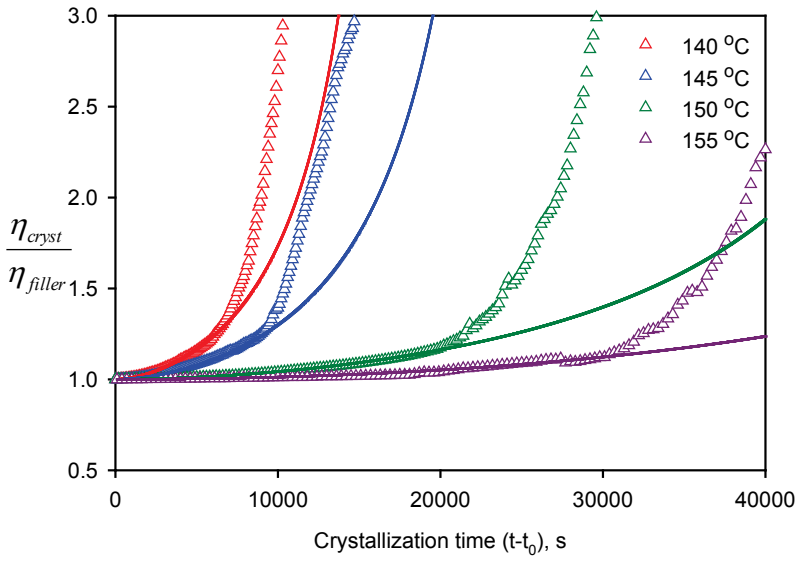

Figure 5.8. Effect of physical crosslinks on the viscosity of crystallizing polylactide at different temperatures. The *Y* axis is the ratio between real viscosity and the viscosity after taking into account only the filler effect using Equation 5.8. Curves represent the best fits of Equation 5.10.

The best fits of the δ parameter are shown in Figure 5.9 and the physical meaning of this model is discussed in more detail in section "The Physical Crosslink Model".

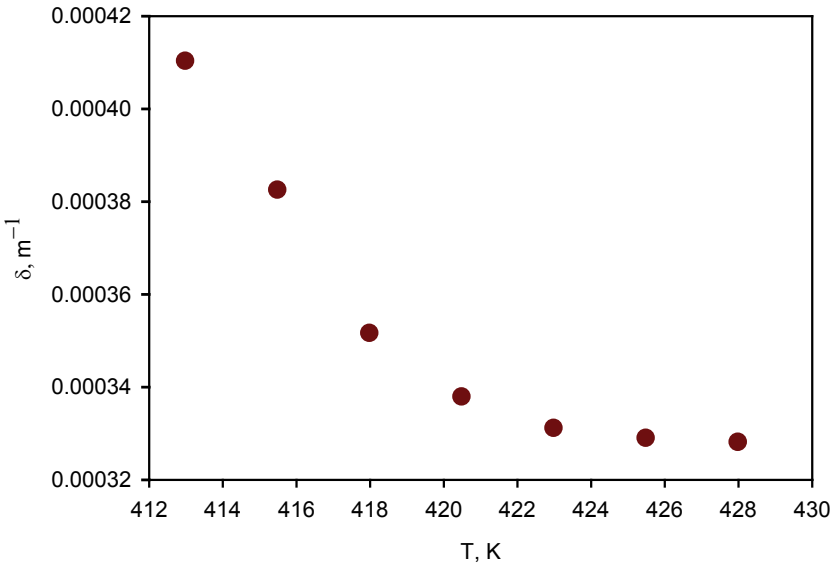

Figure 5.9. Physical entanglement factor δ at different temperatures.

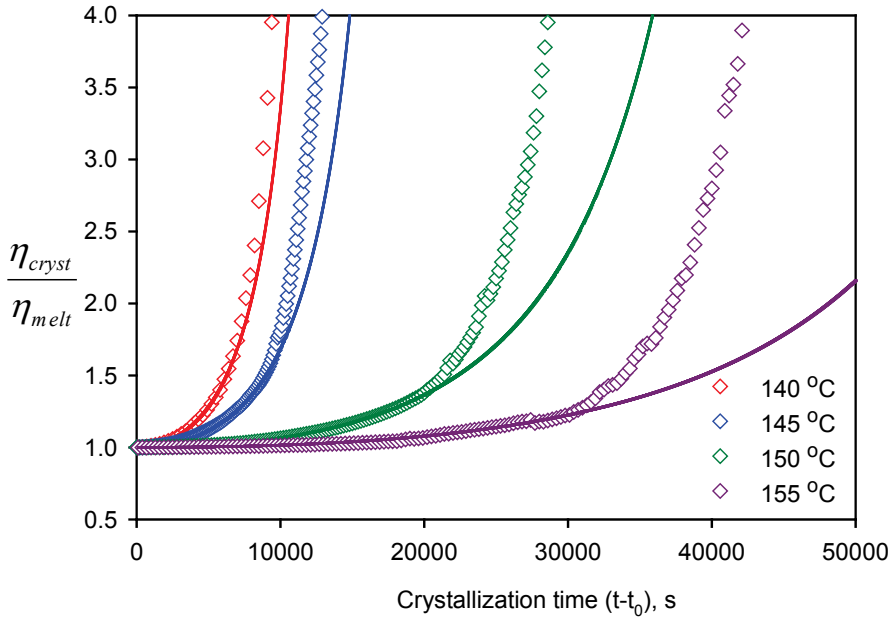

Figure 5.10. The fit of the proposed model (Equation 5.11).

Taking into account the filler effect and the crosslink effect together (Equations 5.8 and 5.10), the following equation can be derived:

$$\frac{\eta_{cryst}}{\eta_{melt}} = \frac{\eta_{filler}}{\eta_{melt}} \cdot \frac{\eta_{cryst}}{\eta_{filler}} = \frac{\exp\left[\frac{4\delta\phi}{3Gt(1-\phi)}\right]}{\left[1-\frac{\phi}{A}\right]^2} \qquad (5.11)$$

A comparison of the experimental data and Equation 5.11 are presented in Figure 5.10. The proposed model provides an accurate fit of complex viscosity of crystallizing melt in the range of crystallinity from 4.8 % (155 °C) to 7.4 % (140 °C).

5.3.4. The Physical Crosslink Model

The physical crosslink effect is caused by chains that take part in a crystallite but also extend into the amorphous region deep enough to be entangled, i.e. by at least $2M_e$ in length [Figure 5.11(a)]. These "dangling arms" relax stress by the contour length fluctuations process which is much slower than the reptation process exhibited by the completely amorphous chains.

The slower relaxation process of the arms has the effect of increasing the viscosity. To a first approximation we expect this increase in viscosity to depend on the volume fraction of dangling arms in the amorphous region (φ_{da}) and the average length of these arms, $\overline{M}_{da}$:

$$\frac{\eta_{cryst}}{\eta_{filler}} = f\left(\phi_{da}, \overline{M}_{da}\right) \approx \exp\left(k\phi_{da}\overline{M}_{da}\right) \qquad (5.12)$$

where k is a constant.

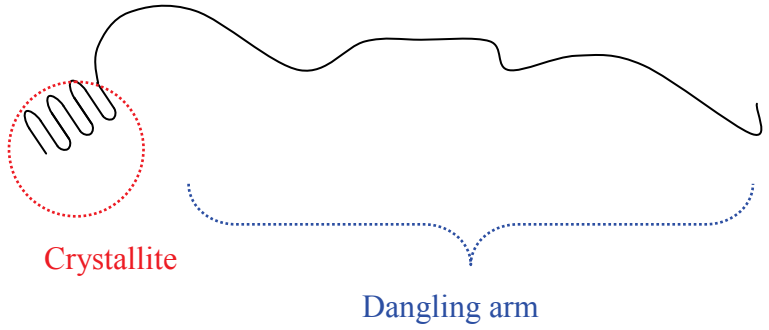

a)

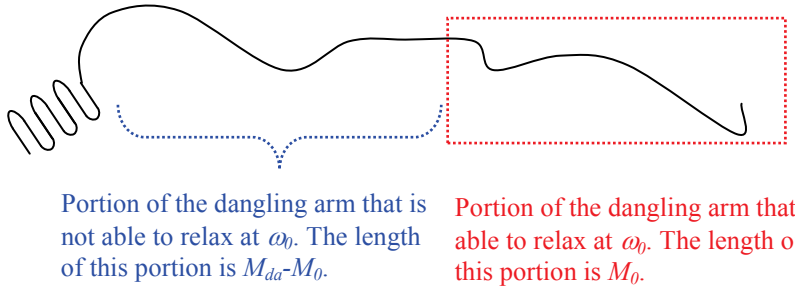

b)

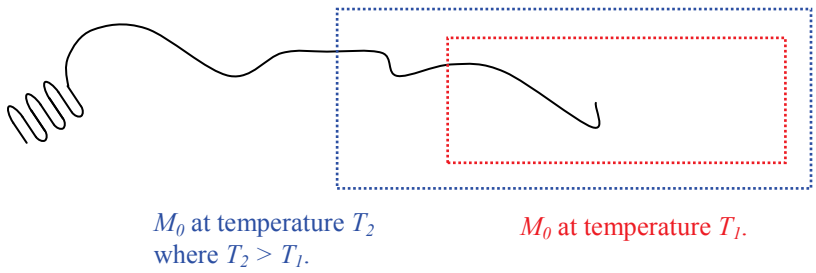

c)

Figure 5.11. A schematic illustration of physical crosslink effect.

If we excite the system at a frequency within the terminal zone, then the entire dangling arm has time to relax and contribute to the complex viscosity (i.e., the complex viscosity within the terminal zone is the highest value and is equal to the zero shear

viscosity). If we excite the system at a frequency outside of the terminal zone *(φ_0)* then only a part of the dangling arm will have time to relax and contribute to the complex viscosity Figure 5.11(b).

Now we have:

$$\left.\frac{\eta_{cryst}}{\eta_{filler}}\right|_{\omega_0} = f\left(\phi_{da}, \overline{M}_0\right) \approx \exp\left(k\phi_{da}\overline{M}_0\right) \tag{5.13}$$

As time passes, the crystallites grow due to both secondary nucleation events and the laying down of adjacent stems next to existing secondary nuclei. At the temperatures covered in this study we expect to be in Hoffman's regime II where these two processes are occurring at similar rates [87]. This is important because the two processes affect the parameters in the equation above differently. The volume fraction dangling arms increases with each secondary nucleation event, whereas the average molecular weight of the dangling arm decreases as additional stems lay down next to existing nuclei. The complex viscosity increases mainly because φ_{da} increases, following the above equation. The changing $\overline{M}_{da}$ has no effect on the complex viscosity as long as $\overline{M}_{da} > M_0$. When $\overline{M}_{da} \leq M_0$ then we have:

$$\left.\frac{\eta_{cryst}}{\eta_{filler}}\right|_{\omega_0} = f\left(\phi_{da}, \overline{M}_{da}\right) \approx \exp\left(k\phi_{da}\overline{M}_{da}\right) \tag{5.14}$$

In this case, as the crystallites grow, the complex viscosity increases because φ_{da} increases but at a slower rate than before because $\overline{M}_{da}$ is continually decreasing.

Our simple model with δ is able to describe the viscosity increase when $\overline{M}_{da} > M_0$ but does not account for the transition to $\overline{M}_{da} \leq M_0$. This becomes important when

we change the temperature because that effectively changes M_0 if we continue to excite at ω_0 as shown in Figure 5.11(c). For example, at T_2, because M_0 has been increased relative to a lower T_1, we expect that $\overline{M}_{da} = M_0$ at a lower φ_{da} than at T_1. Therefore the rate of increase in the complex viscosity will reduce at a lower φ_{da}. As the δ parameter essentially defines the rate of increase of complex viscosity, we expect this to cause a lower δ to be fitted at higher temperatures as we have observed in Figure 5.9. In Figure 5.9, we also note that δ reaches a constant value at 150 °C and above. This may indicate that at these temperatures, $\overline{M}_{da} \leq M_0$ during the entire early stage crystallization fitted by our model.

Finally, we note that our analyses in this section and the model proposed in the previous section are approximate in that we have neglected any effects of polydispersity in the length of the dangling arms. Any effects related to polydispersity are lumped into the empirical parameter δ along with the effects of temperature explained earlier.

5.3.5. Gelation and the Transition to Solid-like Behavior

Until this point we have been considering data at a single frequency, but it is important to also look at how the properties as a function of frequency are evolving over time, as this can provide added information about the microstructure. In Figure 5.12 we show the frequency dependence of the complex viscosity and the storage modulus. We can see evidence of solid-like behavior at longer times in both the complex viscosity (divergence of η^* as $\omega \rightarrow 0$) and storage modulus (presence of a nonzero equilibrium

modulus as $\omega \rightarrow 0$). Such behavior indicates the formation of a 3-dimensional percolating structure.

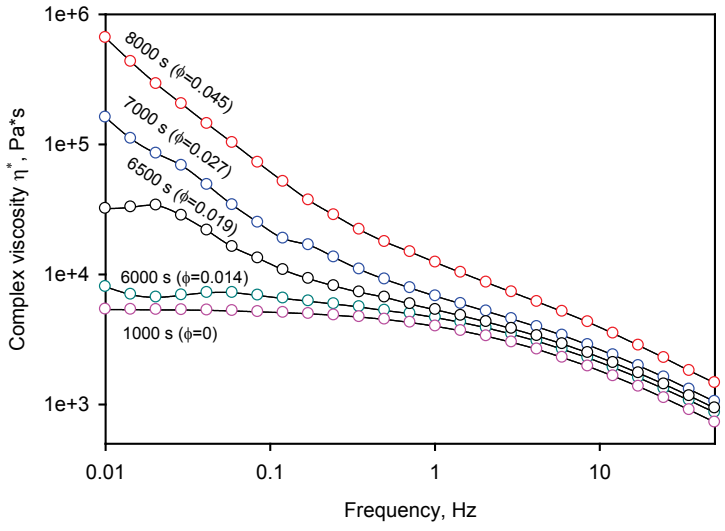

a)

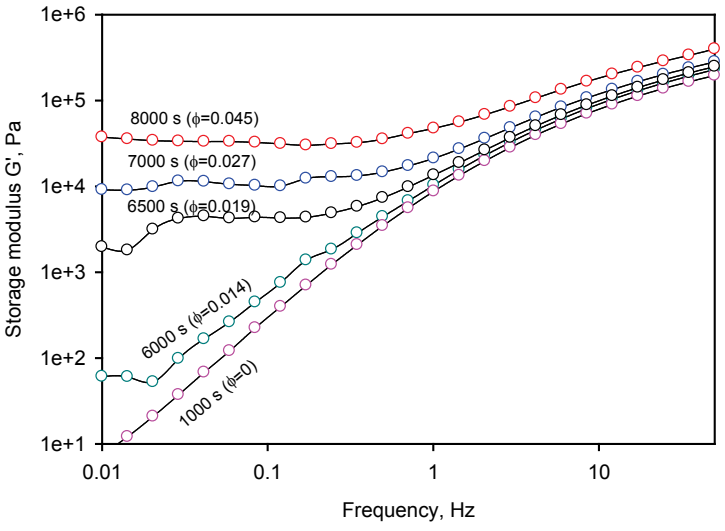

b)

Figure 5.12. A series of frequency sweeps of crystallizing polylactide at 140 °C interpolated to the same moment in time. (a) Complex viscosity η^* and (b) storage modulus G'. Note that induction takes place at 2400 s at this temperature and φ is the volume fraction crystallinity corresponding to the time of the sweep.

The early stages of this transition from a liquid to a solid can be considered to be a physical gelation [95], where the critical gel point is defined as the point when 3-dimensional connectivity first appears. After the gel point, the material behaves mechanically as a viscoelastic solid, exhibiting an equilibrium modulus, G_e. The gel point is often identified by looking at the shape of the tangent of the loss angle as a function of frequency [96].

For viscoelastic liquids the slope of this curve is negative at all frequencies, whereas it is positive at low frequencies for viscoelastic solids. At the gel point, the slope is exactly 0 at low frequencies (see for example Figure 8 in reference [96]). Using this criterion we have identified 6200 s (or 3800 s after induction) as the gel point, corresponding to $\varphi = 1.6\%$.

Horst and Winter [96] have proposed three possible mechanisms for gelation in crystallizing polymers: (i) contact between spherulites, (ii) a network of bridging molecules between and (iii) contact between immobilized amorphous chain segments on neighboring spherulites. These segments are immobilized due to their covalent connection with segments in a crystalline structure. As those authors have explained, case (i) is clearly not occurring at a crystallinity of less than 2%. Percolation of a suspension of monosized hard spheres occurs at $\varphi_{spheres} = 29.5\%$ [97] and we would have to accept that the sphereulites consist of 95% amorphous segments in order for a crystallinity of 1.6% to undergo gelation following this mechanism. Although spherulites are certainly composites of crystalline and amorphous segments, this seems unreasonable especially when considering that Gatos et al. [98] have shown that spherulites of isotactic polypropylene are ~40% crystalline. It is our opinion that above mechanism three is

similarly unlikely in that it would require a layer of immobilized chains around each spherulite that is larger than the radius of the spherulite itself. This leaves mechanism (ii) as the most likely scenario and we will now use our data in an attempt to provide evidence supporting this mechanism.

We consider the crosslinking of long linear precursor chains which is the appropriate model for mechanism (ii) above and use the ideas presented in sections 6.5.4 and 7.5 of Rubinstein and Colby [99]. The molecular weight of the long branched chains formed in this process follows Eq 5.15 in the vicinity of the gel point.

$$N^* \approx N_0 P_{gel}^{-2} \tag{5.15}$$

In this equation, N_0 is the molecular weight of the precursor and P_{gel} is the fraction of all chain segments that are attached to the gel. The equilibrium modulus of such crosslinking systems in the early stages of the gelation regime is given by

$$G_e = \frac{kT}{b^3}\frac{P_{gel}}{N^*} \tag{5.16}$$

where k is the Boltzmann constant, b is the Kuhn length, and T is the temperature. By combining the two above equations and assuming that in our crystallizing polymer $P_{gel} \propto \phi$ we find that the following proportionality should hold:

$$G_e \propto \phi^3 \tag{5.17}$$

In Figure 5.13, we plot the post gel point experimental (not interpolated) G' data at low frequencies against φ^3 showing that the data do follow the above proportionality. The inset shows $G'(t)$ for three frequencies illustrating the initially frequency dependant storage modulus which becomes frequency independent after the gel point. As measurements at different frequencies take different times, we have for each frequency sweep; data corresponding to 8 different times covering about 500 s. In all, we have data

covering 3000 s after the gel point and the data in Figure 5.13 span the range of 1.6–8% crystallinity. These results, while not offering direct proof, are clearly consistent with the proposed mechanism of gelation due to a network of tie chains between adjacent spherulites.

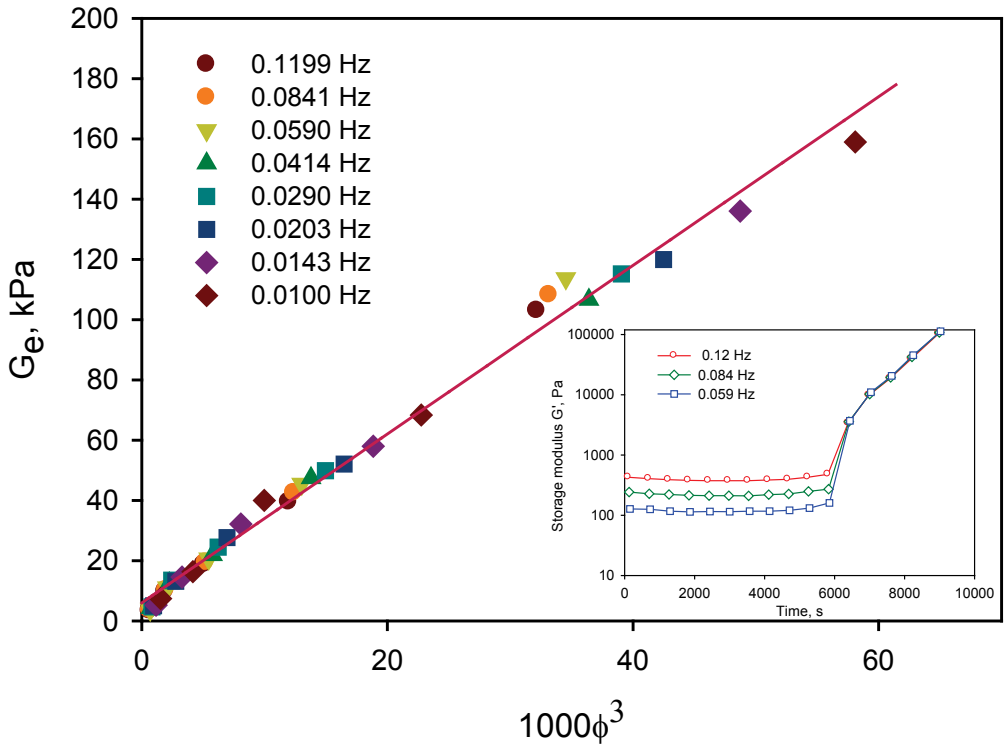

Figure 5.13. Relationship between equilibrium modulus and volume fraction crystallinity at 140°C. Symbols are raw experimental data, and the straight line emphasizes the proportionality between G_e and φ^3. Inset shows $G'(t)$ for 3 frequencies.

We now return briefly to the issue of selecting 1 Hz as out test frequency for most of our experimental studies. This frequency is convenient in terms of speed of measurement, sensitivity to crystallization, and applicability of the simple model developed in Section "Rheological Properties and Crystallization at the Initial Stages".

This model cannot adequately describe the low frequency solid-like behavior observed after the gel point but does work rather well in fitting the shorter time relaxation processes which are essentially governed by the relaxation of the dangling arms as explained previously. More precisely, the model is only consistent at the frequencies where the complex viscosity curves at different times are parallel. In the case of our sample and temperatures, 1 Hz is in this region for crystallinity up to between 5 and 7%.

5.4. Conclusions

It was found that the evolution of complex viscosity of polylactide during thermal degradation can be well described by a simple exponential decay over a wide range of temperatures and degradation times. By understanding this behaviour, we were able to then use viscosity measurements to study crystallization of this material. A precise determination of induction time was achieved using the decay model and its experimental standardized residuals during homogeneous crystallization. The measured induction times correlate well with and are more sensitive than traditional DSC measurements.

A phenomenological model describing the evolving viscosity of crystallizing polylactide was proposed and validated experimentally. The model accounts separately for the filler effect, due to the presence of solid particles, and the crosslink effect, due to the entanglement of partially crystalline chains in the amorphous domain. It was found that the influence of crystallites far exceeds the effect of a typical foreign solid phase due to the crosslink effect. The new model satisfactorily describes the evolution of viscosity over a wide range of crystallization temperatures at low crystallinity level. The model

also predicts the decrease of the crosslink effect at higher crystallinity where the specific interfacial area between the crystallites and the melt begins to decrease due to impingement. It was shown that the very large impact of the crosslink effect makes rheological measurements very sensitive to the onset of crystallization.

After the gel point, the sample exhibits an equilibrium modulus which increases as crystallinity increases. The equilibrium modulus was found to be proportional to φ^3 which is consistent with gelation due to a network of tie chains between neighbouring spherulites.

Acknowledgements

This work was supported by the NSERC Discovery grants program.

CHAPTER 6

The Surface Crystallization Phenomenon in Polymer Crystallization

It is accepted that polymer crystallization is a two-stage process. During the first stage, nucleation of the crystalline phase happens; during the second stage, crystallization continues with the growth of semi-crystalline entities originating from the nuclei.

It is generally admitted that homogeneous nucleation rarely happens in polymers. Unlike the homogeneous version, heterogeneous nucleation requires the presence of a foreign surface. A theoretical approach for this type of nucleation has been developed by Binsbergen [100]. When the foreign body initiating the crystallization is a macroscopic surface, a large number of spherulites appear at the contact region between this body and the polymer. Due to their proximity, these spherulites lead to what is usually called “transcrystalline regions", in which crystals preferentially grow normal to the surface [101]. Three different terms can be encountered in the literature regarding this phenomenon: “surface crystallization”, “transcrystallization”, and “epitaxial crystallization”. While all three terms describe the same phenomenon, “surface crystallization” is the most general term and “transcrystallization” is more visually descriptive. “Epitaxial crystallization” is seen more often in crystalligraphical descriptions of this phenomenon, where it relates to the growth plane’s orientation with regard to the surface [102].

While being widely observed and described in filled polymer systems, the surface crystallization phenomenon gets undeservingly little attention from researchers. Meanwhile, there are numerous indications that it is the surface crystallization that is to

blame for unpredictable thermal analysis results which are difficult to interpret from polymer crystallization kinetics point of view. Very little research on the kinetics of surface crystallization has been done previously and only fragmentary data exist regarding polymer-foreign surface pairs which facilitate surface crystallization. Essentially all research techniques used to study crystallization involve polymer foreign surface contact and it is extremely important to reveal the input of the surface crystallization to the overall crystallization kinetics. There is concern that the importance and effect of surface crystallization are overlooked in the vast majority of polymer crystallization studies using such popular techniques like DSC and rheometry. Especially dramatic effects of surface crystallization can be when smaller polymer samples are used for analysis which is becoming a growing trend of modern thermal analysis. This is why much effort was put into our research described in the article included in Chapter 7. In this article, the isothermal crystallization of polylactide films laminated between aluminium foils was studied. The relatively slow crystallizing polylactide with well characterized crystallization parameters used in our work was a perfect model for this study.

CHAPTER 7

Effect of Surface Nucleation on Isothermal Crystallization Kinetics: Theory, Simulation and Experiment

7.1. Introduction

Surface induced nucleation and the subsequent formation of transcrystallinity is a phenomenon occurring in many practical instances of polymer crystallization. The presence of virtually any foreign surface in intimate contact with a crystallizing polymer causes surface nucleation [101]. This phenomenon has been observed for wide range of polymer-surface pairs; in particular, intense surface nucleation has been observed in polymers in contact with other polymers [103-105] and glass fibers [106,107], carbon [108-110] and aluminum [111-114]. The nucleating ability of the later is often attributed to alumina which is always present in the form of a thin layer on an aluminium surface [115]. In some cases of surface induced nucleation, the nuclei concentration is very high and almost immediately upon the onset of crystallization, the growing crystallites coalesce in the lateral direction leading to the formation of a so-called transcrystallinity region propagating normal to the foreign surface as a unified front. Transcrystallinity is often observed during processing on tool contact, in reinforced polymers around inclusions and even in immiscible polymer blends along phase boundaries.

In order to evaluate the substrate activity, Chatterjee [115] followed by Ishida and Bussi [116] related the nucleation ability of the surface to the interfacial free energy difference, $\Delta\sigma$:

$$\Delta\sigma = \gamma_{cs} + \gamma_{cm} - \gamma_{ms} \tag{7.1}$$

where γ_{cs}, γ_{cm}, γ_{ms} are the crystal-substrate, crystal-melt and melt-substrate interfacial free energies respectively. A lower value of $\Delta\sigma$ indicates a more favorable nucleation condition. Therefore, when considering the nucleating ability of a foreign surface, one should compare $\Delta\sigma$ to $\Delta\sigma'$, which is interfacial free energy difference for homogeneously nucleated crystal-melt interface. A higher $\Delta\sigma'/\Delta\sigma$ ratio indicates a higher tendency for surface nucleation.

According to nucleation theory, an overall nucleation rate, *I(T)*, at temperature, *T*, is determined by the critical excess free energy due to the creation of a nucleus, ΔG^*:

$$\Delta G^* = \frac{16\sigma\sigma_e\Delta\sigma(T_m^0)^2}{\Delta T^2\Delta H_f^2} \qquad (7.2)$$

where σ and σ_e are the crystal surface energy and fold energy respectively, ΔT is the degree of supercooling, T_m^0 is equilibrium melting temperature, ΔH_f is crystal heat of fusion. Here we are considering surface nucleation and we have therefore incorporated $\Delta\sigma$ in Equation 7. 2. In the case of homogeneous nucleation $\Delta\sigma'$ would be incorporated instead.

Since the formation of transcrystallinity requires a high surface nucleation rate, whether or not it is observed depends on a number of *parameters* other than the nature of the interface alone. Therefore transcrystallinity, while very common, is not the only pattern of surface induced crystallization development. Considering the significant dependence of ΔG^* on the degree of supercooling (Equation 7.2), it can be assumed that even for those surface-polymer pairs exhibiting strong transcrystallinity under some conditions, there will be always a temperature range of rather limited surface nucleation concentration. Additionally, surface nucleation cannot be considered as a standalone

process as it will normally be accompanied by bulk nucleation which must also be considered if one tries to understand the overall crystallization kinetics. The relative effect of surface and bulk nucleation on the overall crystallization kinetics is determined by the $\Delta\sigma$ to $\Delta\sigma'$ ratio, the crystallization temperature and the interfacial area to volume ratio. As the degree of supercooling decreases, surface nucleation will also decrease and the pattern of crystalline formation will transform from transcrystallinity to the growth of relatively sparse surface induced crystallites. Simultaneously, the relative contributions of surface and bulk crystallization to the overall kinetics will change.

A related issue is the induction time of nucleation which can significantly affect observed crystallization kinetics. It is commonly accepted that induction time t_i is an inverse function of nucleation rate but a recent study indicates a more complex and indirect relation between these two parameters [117]. It can be expected that crystallization kinetics of a polymer-substrate system will be affected by both a changing nucleation concentration and a changing induction time.

One reason that surface nucleation is a topic of importance is that it may inadvertently enter into experimental studies using instrumental techniques such as differential scanning calorimetry (DSC) which involve samples of 0.3 – 30 mg of polymer. Such small samples have high surface to volume ratios, leading to situations were surface nucleation can significantly affect the overall crystallization pattern [118] and can in fact mask the bulk crystallization processes which may be the primary focus of the experiment. The results of DSC studies can therefore be significantly different from the crystallization behaviour of the bulk material and demonstrate pronounced thickness dependence [113]. Surface nucleation could also be a serious issue during polymer

crystallization studies using new DSC techniques where extremely small samples, sometimes less than 0.1 mg are used [119]. The obvious solution is to increase the thickness of the sample reducing the relative impact of surface nucleation but unfortunately increasing temperature non-uniformity across the sample thickness. This temperature non-uniformity is caused by the crystallization heat [120,121] and the low thermal conductivity of the polymer [122] for which the instrument cannot compensate quickly enough. Such temperature disturbances, of course, also affect the crystallization kinetics [123].

A number of studies have been dedicated to revealing the influence of sample thickness on shape and magnitude of DSC traces [111, 113, 124]. Many of these studies neglect the possibility of surface nucleation, which can lead to erroneous conclusions. The deficiency of this approach is clearly seen in the extensive study of Hargis and Grady [124] who looked at the crystallization of polyethylene samples of varying thickness via DSC. The authors attribute the observed thickness-dependant crystallization kinetics solely to the heat transfer issue. However, the DSC samples were encased in aluminium pans and there are numerous observations of transcrystallinity initiated at the polyethylene-aluminium interface [115]. Polyethylene crystallizes very quickly, making the exact determination of kinetics data from DSC results problematic and the separation of surface nucleation and heat transfer effects nearly impossible. Additionally, the thickness dependency of the crystallinity rate as a function of time curves in reference [124] can be substantially explained by surface induced nucleation as we will show in this work. Altogether significant doubt remains as to the interpretation of such data.

Hence it is necessary to create experimental conditions when surface nucleation can be unmistakably detected and its effect on crystallization kinetics can be correctly measured. The simplest way to separate crystallization heat, apparatus thermal stabilization effects and crystallization kinetics itself is to choose a polymer crystallizing at a significantly slower rate than polyethylene or polypropylene which are usually used in these experiments and whose crystallization times are comparable to many DSC apparatus thermal stabilization times [120, 125]. In this work, we chose to study poly(L/D-lactide) for this reason. This and other considerations for our choice of polymer will be addressed in detail.

The few existing studies of the dependence of surface nucleation concentration on temperature are focused on reinforced polymer systems. While transcrystallinity is very common in reinforced systems and can be easily observed, the complex shape of reinforcement-polymer interface and difficulties in correct determination of interfacial area make these systems extremely difficult for quantitative studies. This necessitates the studies of relatively simple systems having uniform shape and predictable interface area, e.g. flat discs or plates. Billon et al. [126] presented studies of transcrystallization in flat, disk-like, polyamide samples in contact with an aluminum surface during non-isothermal crystallization. These authors also performed a theoretical analysis of crystallization kinetics of systems having different thickness in the presence of surface nucleation. They also proposed a technique for determining surface nucleation concentration from crystallization kinetics [114]. This technique is based on a modified Kolmogoroff-Avrami-Evans theory that accounts for surface nucleation and requires the availability of heterogeneous bulk nucleation concentration and growth rate data. This model also

simplifies surface crystallization kinetics to the case of pure transcrystalline growth making it increasingly inaccurate as the thickness of the specimen decreases.

Little is written in the literature about the effect of surface crystallization on overall crystallization kinetics. While epitaxial growth is characterized by a significantly lower Avrami exponent than that of 3-dimensional growth, it should be noted that this applies only for a completely formed growth front. Before such a front is formed, the kinetics of surface crystallization maintains its three-dimensional nature but with a planar arrangement of nuclei. This leads to crystallization kinetics that follows the Avrami equation with an exponent that is lower than that for bulk nucleation but higher than that for pure 1-dimensional growth. Therefore it is possible that surface nucleation is the cause of lower than expected Avrami exponents obtained in many DSC studies especially for slower crystallizing polymers such as polylactide.

The kinetics of crystallization in the presence of surface nucleation depends on many factors: growth rate, induction time, surface nucleation concentration, bulk nucleation rate, sample thickness, the slope of the growth rate vs. temperature curve in the vicinity of crystallization temperature and the heat transfer parameters of the DSC apparatus and the polymer. Many researchers tend to use thin samples to accommodate heat transfer and thermal inertia issues. While decreasing the sample thickness reduces these problems, the possible presence of surface nucleation could significantly affect experimental results especially for very thin samples. This makes us believe that the proper evaluation of the relative importance of these factors on crystallization kinetics would be an important input to understanding and interpretation of experimental data. Here we attempt to do just that. While most studies of surface crystallization are

dedicated to fibre or particle reinforced systems, we have chosen to study the simpler planar polymer-substrate interface. This allows us to generalize the theoretical aspects and provides a convenient experimental variable, sample thickness, for control over the relative importance of surface and bulk nucleation at each temperature. In this way we can observe separately the effect of each of these phenomena on the overall kinetics allowing us to validate our theoretical and numerical results.

7.2. Experimental Methods

This research was intended to reveal the effects of surface induced nucleation on the crystallization kinetics of poly(L/D-lactide) specimens having different thicknesses. This polymer was chosen over PE or PP which are commonly used for fundamental crystallization studies for several reasons. The crystallization rate of poly(L/D-lactide) is moderate and approximately 10 to 40 times slower than that of fast crystallizing polymers such as HDPE and PP. This extended crystallization time allows us to dramatically decrease the impact of the initial temperature transient (when cooling to the crystallization temperature) on the results. This also allows for a decreased crystallization heat flow rate, leading to a more uniform temperature field across the sample. Additionally, poly(L/D-lactide) has a lower crystallization heat as compared to HDPE or PP (~39 J/g as compared to. ~156 J/g and ~105 J/g [127] respectively) also contributing to a lower heat flow during crystallization. Poly(L/D-lactide) also has rather broad crystallization temperature range as compared to fast crystallizing polymers ~ 70 °C as compared to ~15 °C for HDPE. As well as providing more room for experiments, this

means that the magnitude of the derivative of crystallization rate with respect to temperature for poly(L/D-lactide) is significantly lower than for fast crystallizing polymers making it less sensitive to temperature non-uniformity. On the other hand, polymers that undergo extremely slow crystallization (such as polystyrene) challenge the DSC sensitivity limits. Finally, poly(L/D-lactide) has a rather low bulk nucleation rate allowing us to unambiguously detect surface induced crystallization. For these reasons as well as its current practical significance and its above room temperature glass transition, poly(L/D-lactide) is a particularly good model material for these studies.

The poly(L/D-lactide) sample used here was supplied by Biomer (Germany). It is a commercially available poly(L/D-lactide) copolymer containing 2% of D-lactide (L 9000). It was found via gel permeation chromatography measurements that this polymer has a number average molecular weight of 50,000 and a polydispersity index of 2.0. The glass transition of this polymer is 59.1°C and its melting point is 171.2 °C (5°C/min heating/cooling). The thermal transitions and spherulitic growth rates of this polymer have previously been described [78].

The presence of oxygen and humidity leads to noticeable degradation of poly(L/D-lactide) even at temperatures below its melting point and sample preparation is therefore extremely important. The pellets were thoroughly dried at 80°C in a vacuum oven for 24 hours immediately prior to pressing into disks of 1.25 mm thickness at 185°C in a Carver hydraulic press. This drying procedure reduced the adsorbed water content in the polymer from 0.26 wt% to 0.03 wt% significantly suppressing the influence of hydrolysis during the experiments. Samples with controlled thickness were prepared by further pressing the disks between the hot plates of a rotational rheometer (MCR 500

model of Anton Paar) at 180°C under a nitrogen atmosphere (oxygen content of less than 2.5 ppm). The precise control of the plate alignment afforded by the rheometer allowed us to produce samples of controlled thickness with ±0.002 mm tolerance. The use of liquefied nitrogen as source of the protective medium also assures the absence of humidity in the nitrogen.

The choice of the substrate material was based on the numerous observations of surface nucleation on contact with aluminium. Also, aluminium is commonly used to encase polymer samples for thermal analysis, thus the study of its nucleating abilities has a practical importance. During the preliminary experiments using DSC aluminium pans as the substrate, it was found that while the crystallization kinetics showed a clear thickness dependency, the experimental results had significant variation. This large variation was caused by non-uniform contact between the sample and aluminium pan leading to variation of interfacial area from experiment to experiment. The cold pressing of sealed DSC pans does not provide for a complete wetting the aluminium surface during subsequent melting, making the spatial distribution of surface nucleation sites unpredictable. In order to reduce this uncertainty, the samples were melt laminated between layers of thin aluminium foil (12 μm thickness) ensuring reliable contact between polymer and the substrate over a defined area. The laminated sample was then hermetically pressure-sealed in a DSC pan to ensure good thermal contact between surfaces and to retain the shape and dimensions of the sample during the premelting stage. The foil thickness was 8 times less than that of the pan providing a negligibly small thermal resistance. The differential scanning calorimetry (DSC) measurements were performed using a ThermalAnalyst Q10 system calibrated using an indium standard. The

DSC data sampling rate was 2 acquisitions per second which ensured highly precise crystallization curves. The surface area of the samples ranged from 16.4 to 25.2 mm^2 and the polymer weight was in the range of 1.4 to 22.6 mg depending on the thickness which ranged from 58 μm to 1.2 mm. The temperature protocol was designed to ensure conditions as close as possible to isothermal crystallization (Figure 7.1).

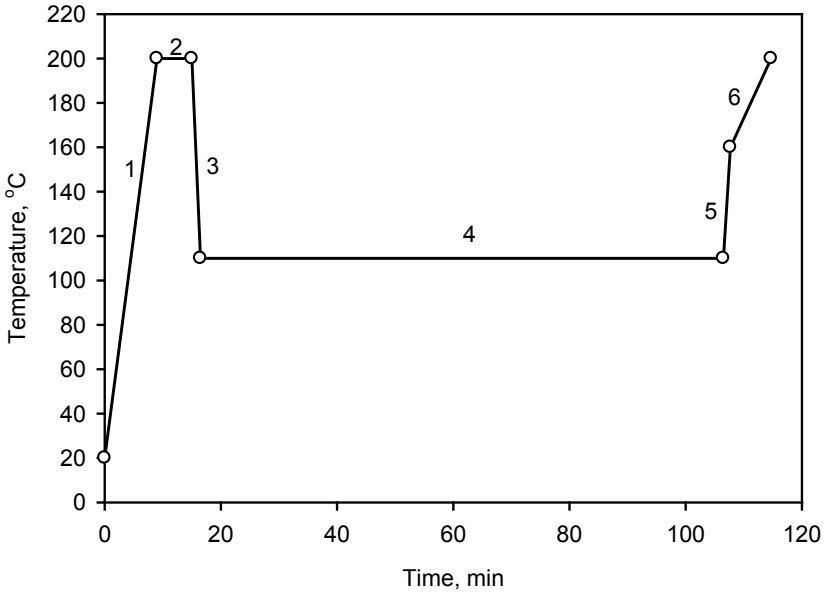

Figure 7.1. Temperature protocol for DSC experiments. The sample was first heated to 200°C (30°C above the melting point) at 20°C/min (1) then held at 200°C for 5 minutes to erase the thermal history (2). Next, the sample was rapidly cooled at 50°C/min (3) to the isothermal crystallization temperature (4) and held for a predetermined time. Next, the sample was rapidly heated at 50°C/min to 150°C to avoid secondary crystallization (5) and finally heated to 200°C at 5°C/min (6).

The baseline references were individually determined for each experimental temperature. In this regard, an empty sample pan was used to measure the thermal response of the DSC apparatus when subjected to rapid cooling before reaching the crystallization temperature. This method produces baseline curves which are specific to each combination of high temperature soak (interval 2 in Figure 7.1), rapid cooling rate (interval 3) and crystallization temperature (interval 4). The overall melting heat obtained in interval 6 of the temperature protocol for each particular experiment was used for the determination of the baseline offset and to ensure that the dwell time in interval 4 was sufficient for the crystallization process to complete (Figure 7.2).

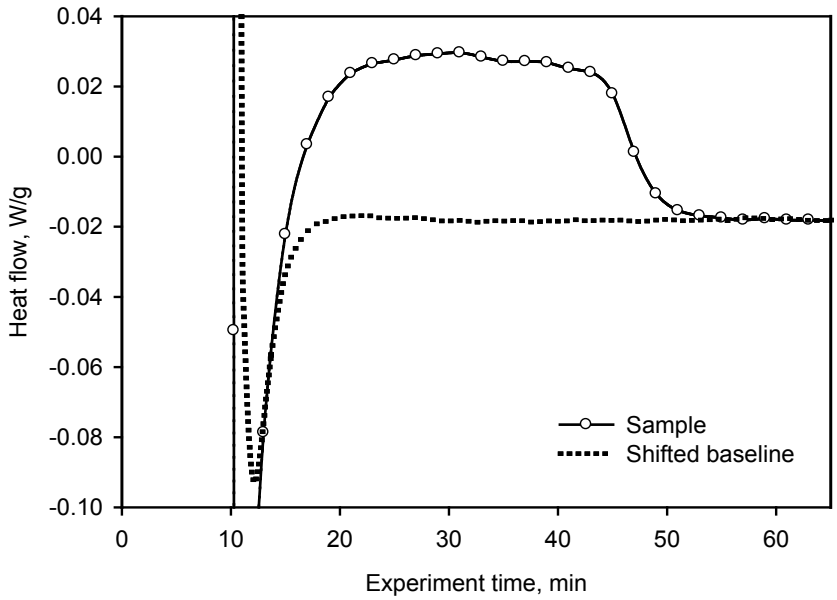

Figure 7.2. An example of shifted baseline and crystallization heat curve (a 77 μm sample at 130°C is shown). The sharp endotherm at about 10 minutes, present in the baseline and in the experimental data, is due to the thermal response of the apparatus.

The DSC data were converted into crystallinity as a function of time curves as follows. The ultimate heat of crystallization ΔH_∞ is the area between heat flow from the sample and the shifted baseline curve:

$$\Delta H_\infty = \int_0^{t=\infty} \left(\frac{\partial Q}{\partial \tau} \right) d\tau \tag{7.3}$$

where Q is the heat flow of crystallization. Then the heat evolved until time *t* is:

$$\Delta H_t = \int_0^{t} \left(\frac{\partial Q}{\partial \tau} \right) d\tau \tag{7.4}$$

and the fraction of transformed material is found from the following.

$$\alpha(t) = \frac{\Delta H_t}{\Delta H_\infty} \tag{7.5}$$

Note that the fraction transformed material here is not the same as the true fraction crystallinity which would be evaluated using the heat of fusion of poly(L/D-lactide).

7.3.Numerical Methods

A Monte Carlo simulation has been employed to study the combined and individual effects of surface and bulk nucleation on overall crystallization kinetics. This simulation is a useful tool for a broad parametric study which is experimentally impossible but is required for the validation of our theoretical analysis presented in the following section. Additionally, since the simulation does not include heat transfer effects, the divergence of experimental data and the simulation results under certain

conditions can be used to evaluate the relative importance of surface nucleation and thermal effects.

The Monte-Carlo simulation presented here was intended to mimic heterogeneous surface crystallization occurring simultaneously with bulk crystallization. The simulated volume represents a rectangular plate of thickness d. The numerical simulation program used in this study was a modified version of a previously described simulation of homogeneous crystallization [128]. The homogeneous crystallization algorithm was adapted for mixed-type crystallization in the presence of surface nucleation. The major components of the algorithm were left intact, however the need to track a significant number of crystallizing entities required a simplification of the algorithm as a trade-off between precision and computation time. In particular, the determination of the crystallinity of the bordering elements was performed by a simple randomized switch following Raabe [129,130] instead of the more accurate approach that we have previously described [128].

The bulk nuclei were randomly seeded during the crystallization process in the manner previously described [128] based upon the bulk nucleation frequency, N, throughout a predetermined three-dimensional space. The algorithm assumed equal probability of nucleation throughout all untransformed material and that nucleation could occur only in the untransformed phase. The surface nucleation centres were seeded independently on both opposing surfaces with a density corresponding to the surface nucleation concentration N_s.

For a typical simulation the total number of crystallizing entities can exceed 10^5 making the tracking of a realistic sample volume time-consuming. Thus only a fraction of

a DSC sample with a lateral dimension in the range of 500 - 1500 μm was simulated and the crystallization kinetics of that fraction was considered to be representative of the overall kinetics. Thus, the simulated space can be represented as a right rectangular cuboid with dimensions $a_x=a_y >> a_z$. The *x* and *y* dimension size was chosen individually for each simulation such that further expansion of these dimensions did not result in noticeable changes in crystallization behaviour for a particular set of simulation parameters.

Right rectangular cuboid elements were used to evaluate the volume fraction crystallinity. (Note that the nucleation process is not affected by the element shape or size as the nuclei are placed randomly at any *x, y, z* coordinate within the untransformed simulation volume). The number of elements, *m*, for each simulation was in the range of 8×10^6 to 6.4×10^7 and was chosen to balance computational time and accuracy.

The probability of the formation of a crystallization site (nuclei) was considered to be equal throughout the volume of untransformed matter (bulk nucleation) and surfaces (surface nucleation). The nucleation rate N [$s^{-1}m^{-3}$] and concentration N_s [m^{-2}] were set to be constant in each particular simulation. The growth rate G also considered to be constant and equal in all three dimensions ($G_x= G_y =G_z$) and diffusion-independent. This is applicable for most isothermal crystallization cases and justified in many studies [93]. The ratio of densities of crystalline and amorphous phases ρ_c/ρ_l was accepted to be equal to 1 to avoid polymer-specific simulation bias. In practice, the density ratio for poly(L/D-lactide) can reach ρ_c/ρ_l =1.034 for the fully transformed phase and does not have a significant impact on this particular simulation. It should be noted that degree of crystallinity we are referring in this study is the degree of phase transformation and not

true crystallinity *per se*. Therefore, the crystallization parameters (N, N_s, G) and the sample thickness, d, are inputs to the simulation and the crystallinity as a function of time, $\alpha(t)$, is the output. The half-time of crystallization was determined as the moment of time when $\alpha = 0.5$.

The Avrami exponent n was calculated as the slope from the linear regression of as $ln\ t$ vs. $ln(-ln(1-\alpha))$. It is well known that due to impingement phenomena an Avrami plot can deviate from linearity at higher degree of transformation. To maintain the uniformity of approach, the Avrami fit was performed within the data range of $\alpha = 0.001 - 0.3$. The lower limit was chosen in order to take into account the limited resolution of the simulation. The upper limit of crystallinity of $\alpha = 0.3$ used for the Avrami exponent evaluation was chosen in compliance with recommendations of Lorenzo et al. [131].

7.4. Kinetics of Surface Crystallization: Theory and Simulation

We begin by considering the case when only surface induced nucleation occurs in an infinite plate with thickness d. When the surface nucleation concentration is very high, $N_s=\infty$, crystallinity builds up in the form of a uniform layer of transformed phase of thickness Gt and the crystal-amorphous interface can be represented by a plane. Considering two-sided crystallization, the fraction of transformed phase for this case can be expressed as:

$$\alpha_{N_s=\infty} = \frac{2Gt}{d} \tag{7.6}$$

In many cases the surface nucleation concentration is limited, which causes significant deviation from Equation 7.6. Three stages of pure surface induced

crystallization can be identified when $N_s \neq \infty$ (Figure 7.3) corresponding to the growth geometry. In the first stage, the surface induced crystallites are growing without any impingement. This stage ends when impingement occurs at the surface. In stage 2 the crystallites are growing without confinement in the transverse direction but with increasing confinement in the lateral direction. Stage 2 ends when impingement occurs in the transverse direction. In the final stage growth occurs only in the small interstices. We refer to these three stages as: (1) impingement-free growth, (2) increasingly laterally-constrained transverse growth, and (3) intersticial growth.

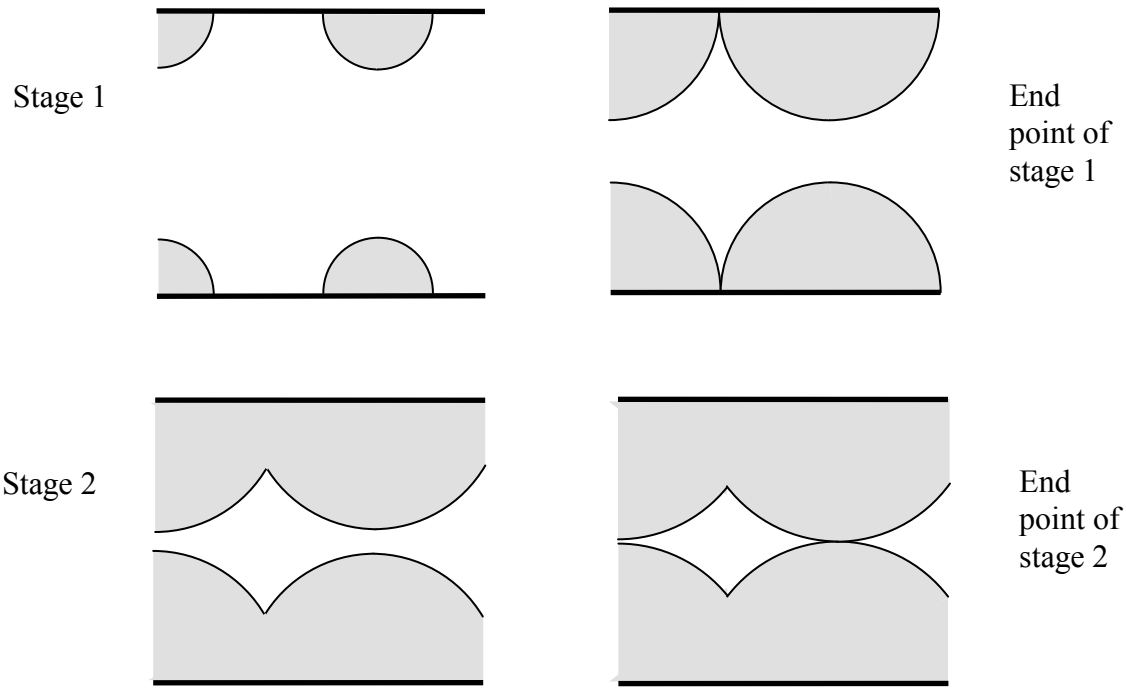

Figure 7.3. Illustration of the first 2 stages of surface induced crystallization.

The first stage of surface crystallization represents a particular case of heterogeneous bulk crystallization where the nuclei are distributed randomly on a plane and can be well described by Avrami-Evans equation:

$$\alpha_I = 1 - \exp(-kt^n) \qquad (7.7)$$

where k is a crystallization constant and n is the Avrami exponent.

In order to illustrate this, we performed a series of Monte Carlo simulations with varying surface nucleation concentration in which the bulk nucleation rate was set to 0 (Figure 7.4).

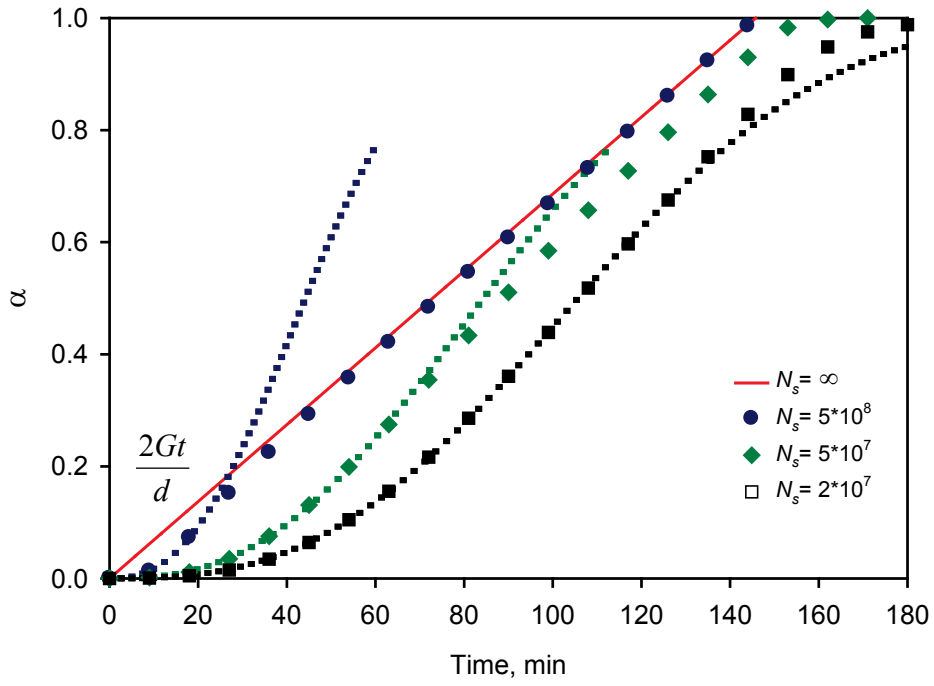

Figure 7.4. Kinetics of surface crystallization for different surface nucleation concentration. Data points are the simulation results for d=500 μm and G=1.715 μm/min. Doted lines are fits of simulated crystallization data for the first stage of crystallization using Equation (7.7).

We then fit Equation (7.7) to the initial portions of the $\alpha(t)$ results from each simulation. The fitting parameters are given in Table 7.1 and the quality of fit is illustrated in Figure 7.4. We note that the Avrami exponent decreases as N_s increases due to an increasing number of lateral impingements. The kinetics approach pure transcrystalline growth as N_s increases and pure heterogeneous bulk crystallization kinetics as N_s decreases.

Table 7.1. The effect of surface nucleation concentration on the Avrami parameters for the initial stage of surface induced crystallization.

N_s, m^{-2}	k	n	R_{adj}^2
2×10^7	2.699×10^{-11}	2.738	0.999963
5×10^7	2.177×10^{-10}	2.566	0.999717
1×10^8	5.441×10^{-10}	2.514	0.999588
5×10^8	2.576×10^{-9}	2.465	0.999423

The initial stage of surface induced crystallization ends with complete lateral confinement of individual crystallites at the surface and the second stage of crystallization begins where primarily transverse growth occurs (Figure 7.3). This leads to significant changes in crystallization kinetics. While for $N_s=\infty$, crystallinity increases linearly with time, for $N_s<\infty$, $\alpha(t)$ becomes a nonlinear function. The nonlinearity is caused by an increasing of radius of curvature of the growth front of each crystallizing entity. To accommodate an increasing radius of curvature, the confinement interface propagates with velocity υ_c higher than the growth rate G:

$$\vartheta_c = \frac{G^2 t}{\sqrt{G^2 t^2 - \frac{1}{\pi f N_s}}} > G \tag{7.8}$$

where f is an equivalency coefficient which accounts for the fact that the confinement interface is polyhedral rather than circular. The concept and geometry of the confinement interface is shown in Figure 7.5.

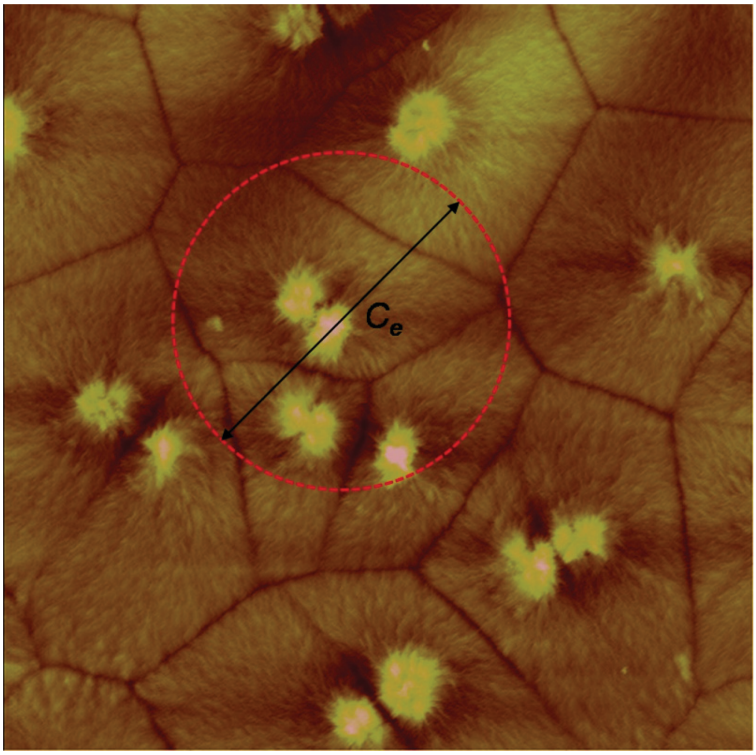

Figure 7.5. An illustration of the concept of equivalent spherical segment. Image is a 100 μm by 100 μm AFM height image of a poly(L/D-lactide) film, surface crystallized at 120°C on a glass surface and having local nucleation density of 1.3×10^9 m^{-2}. The dashed circle represents an equivalent diameter c_e corresponding to this nucleation concentration. The confinement interfaces show up as the dark lines bordering the crystallites.

In order to derive an analytical expression for the evolution of crystallinity during the second stage of crystallization, it is necessary to use a simplified model of the shape of a typical crystallite. Due to the random placement of nuclei on the surface, the shape of a particular confined entity can be complex. In our model, we consider the equivalent crystallite to be a vertical cylinder capped with a segment of a sphere. The radius of curvature of the cap is *Gt*, the height of the cap is *h*, the height of the cylinder is *(Gt-h)* and the diameter of the cylinder is given by the equivalent diameter, c_e.

The average surface area occupied by single crystallizing entity is:

$$A_c = \frac{1}{N_s} \tag{7.9}$$

Then the equivalent diameter c_e can be expressed as:

$$c_e = \sqrt{\frac{4}{\pi f N_s}} = 2\sqrt{h(2Gt-h)} \tag{7.10}$$

and the volume of the equivalent crystallite, V_e, is:

$$V_e = \pi h\left[\frac{c_e^{\,2}}{8} + \frac{h^2}{6}\right] + \frac{\pi}{4}\left(Gt-h\right)c_e^{\,2} \tag{7.11}$$

By combining Equations 7.10 and 7.11 we find:

$$V_e(t) = \frac{1}{fN_s}\sqrt{G^2t^2 - \frac{1}{\pi fN_s}} + \left[Gt - \sqrt{G^2t^2 - \frac{1}{\pi fN_s}}\right]\left[\frac{1}{2fN_s} + \frac{\pi}{6}\left[Gt - \sqrt{G^2t^2 - \frac{1}{\pi fN_s}}\right]^2\right] \tag{7.12}$$

and

$$\alpha_{II} = \frac{2fV_e(t)N_s}{d} \tag{7.13}$$

We make use of our Monte Carlo simulation to evaluate the analytical model and determine the best value for our equivalency coefficient, *f=0.48* (Figure 7.6). It should be noted that Equation 7.12 provides real values for the crystallite volume only for the second stage of crystallization. The onset of the second stage is:

$$t_{II} = \frac{1}{G\sqrt{\pi f N_s}} \tag{7.14}$$

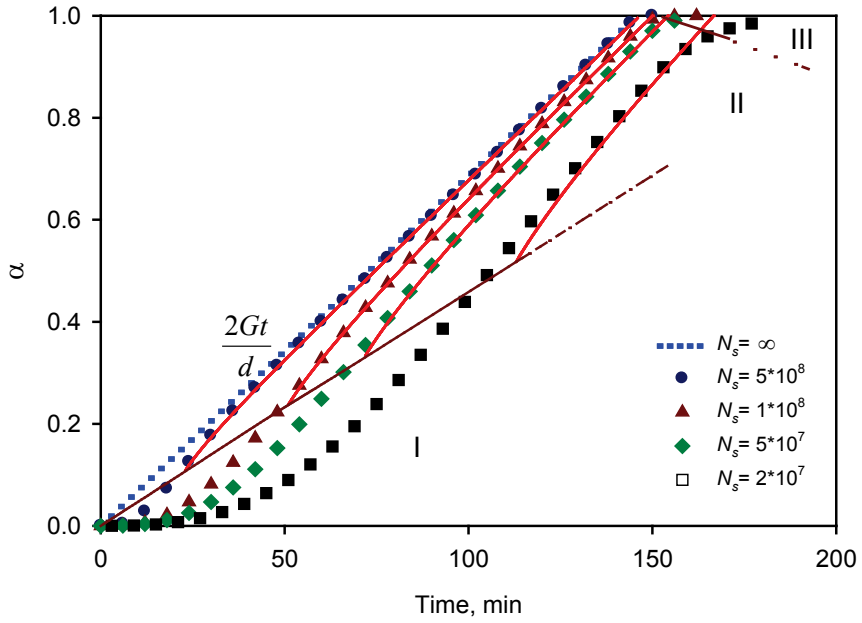

Figure 7.6. The simulated crystallization kinetics (symbols) and corresponding analytical functions Equations 7.12 and 7.13 (solid lines). The three crystallization stages are denoted in roman numerals. Data for d=500 μm and G=1.715 μm/min are shown. The best fit value of f is 0.48.

The final stage of crystallization begins when mutual impingement of the two crystallizing fronts occurs. At this moment, the transverse growth stops and the remaining untransformed phase in the small interstices is converted via an increase of radius of curvature of the equivalent spherical segment.

It is also interesting to look at the crystallization rate curves, $d\alpha/dt$, as these curves have a characteristic shape in the case of surface induced crystallization. Using the Monte Carlo simulation we have generated bulk crystallization curve to compare with our simulation results for pure surface induced crystallization and mixed crystallization when both types of crystallization are present (Figure 7.7).

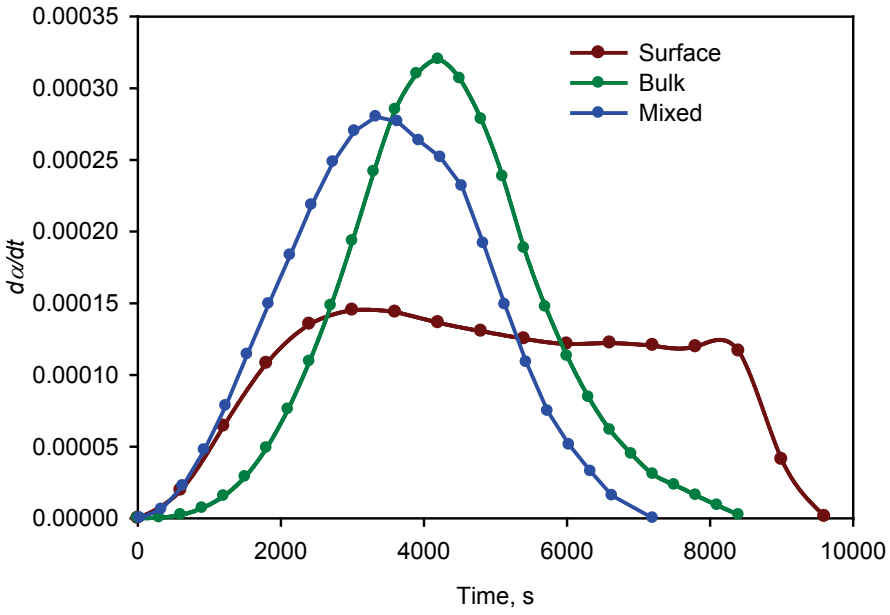

Figure 7.7. Simulated crystallization rate curves showing 3 different types of crystallization: pure surface nucleation (N_s= 10^8 m^{-2}, $\tau_{½}$=4874 s), pure bulk nucleation (N=10^8 $s^{-1}m^{-3}$, $\tau_{½}$=4242 s), and mixed nucleation (N_s= 10^8 m^{-2} and N=10^8 $s^{-1}m^{-3}$, $\tau_{½}$=3533 s $\tau_{1/2} = 3533\ s$). Data are the simulation results for d=500 μm and G=1.715 μm/min.

As it can be seen, not the only shape of the curve but also the half-times of crystallization are significantly affected by spatial restrictions in the case of surface crystallization. Also, the three stages of growth are clearly visible in the case of pure

surface crystallization which exhibits a characteristic flattened, broad peak. Note that the mixed crystallization curve can be more or less distorted from the classical bulk crystallization shape depending on the two nucleation constants, the growth rate and the sample thickness.

7.5. Results and Discussion

7.5.1 Experimental Results

We begin by considering the experimentally determined half-times of crystallization which were extracted from the DSC traces as shown in Figure 7.2 and Equations (7.3) through (7.5). The results for laminated aluminium-polylactide-alumunium samples of varying thicknesses are summarized in Figure 7.8 showing pronounced thickness dependence.

In particular, the half-times of crystallization are much smaller for the very thin samples as compared to the thick samples, due, likely, to the increased impact of surface nucleation. The effect of specimen thickness on half-time decreases as specimen thickness increases and ultimately, the half-time essentially plateaus for specimens thicker than 500 μm. This is consistent with surface nucleation, the impact of which is expected to diminish as the ratio of contact area to volume decreases. It should be noted that we also expect the half-time of bulk crystallization to be affected by specimen thickness due to spatial constraints imposed by crystallizing volume dimensions [128] diminishing the effect of the bulk crystallization on the overall kinetics. However, for the nucleation and growth rates observed in our experiments the spatial constraint effect is

very small. The surface crystallization kinetics, on the other hand, is dramatically affected by the specimen thickness as given by Equation (7.13).

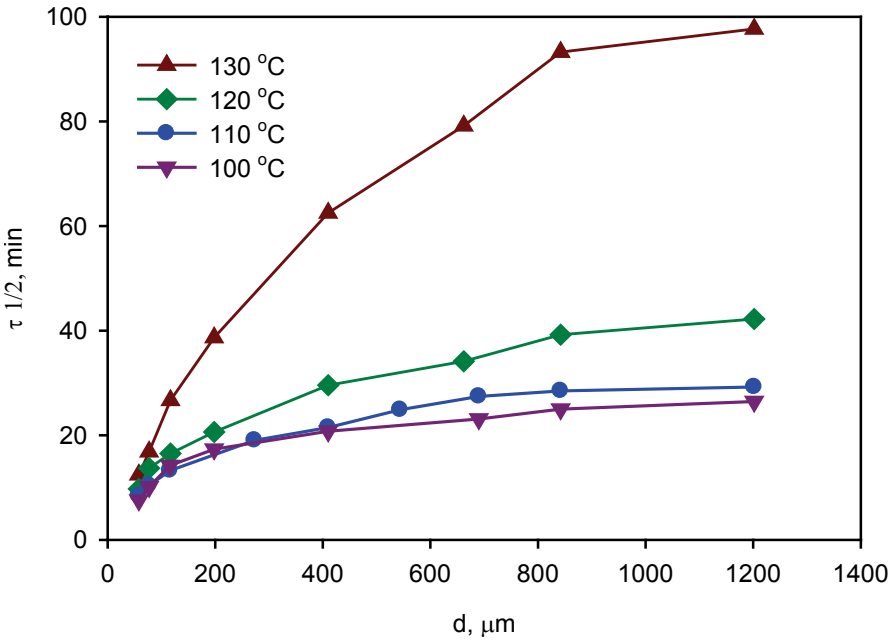

Figure 7.8. Experimental half-times of crystallization of poly(L-lactide) sandwiched between aluminium surfaces.

The other important aspect to these data is the temperature dependence. Although the experimental window was limited to 100°C to 130°C, we can still make some interesting inferences from the results. Firstly we see that $\tau_{1/2}$ is rather insensitive to temperature for thin samples indicating that it is primarily determined by the concentration of surface nuclei, which is expected to be athermal, and is less influenced by the growth rate, which is temperature dependant. It is important to note that for the thinnest samples, there is a small $\tau_{1/2}$ temperature dependency that is not consistent with the temperature dependency of the growth rate (Figure 7.9) indicating that the surface

nuclei concentration is somewhat affected by temperature. For the thicker samples, we see a much stronger and highly nonlinear influence of temperature on $\tau_{1/2}$. This is because the crystallization kinetics of the thicker samples is affected by both the bulk nucleation rate and the growth rate (Figure 7.9) which are temperature dependant. It can be seen that most dramatic changes in half-time of crystallization happens at temperatures above 120°C.

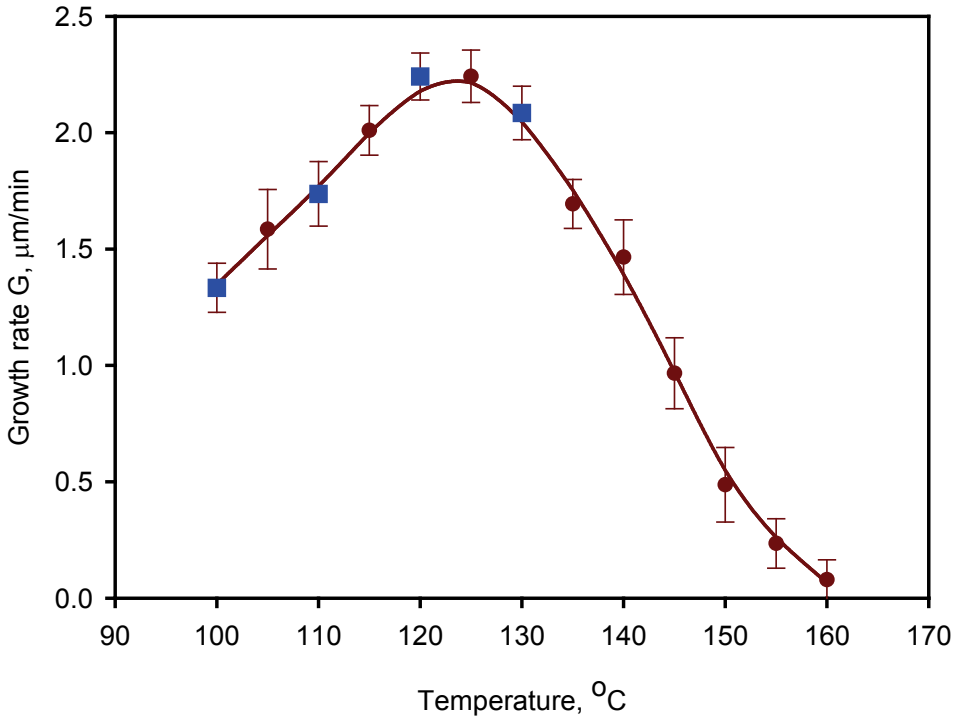

Figure 7.9. The experimental spherulitic growth rate of the poly(L/D-lactide) used in thist study. Data are taken from Yuryev et al. [78]. The square symbols highlight the experimental conditions of this study.

The spherulitic growth rate is particularly important in this specific example because while both the surface and bulk nucleation concentration decrease with temperature at these conditions, the growth rate of poly(L/D-lactide) is noticeably higher at 120°C as compared to 110°C. At 130°C the nucleation concentration is the lowest and the growth rate is also lower than that at 120°C which causes a dramatic increase in $\tau_{1/2}$. It can be noticed that there is little difference between 100°C and 110°C curves. At the lower temperatures, the effect of the increasing bulk and surface nucleation concentrations is offset by the steadily decreasing growth rate resulting in only a minor half-time decrease.

While no explanation is needed as to nature of the effect of growth rate on the half-time of crystallization, it is very important to establish its magnitude. The growth rate, along with other parameters, is a component of the constant *k* in the Evans-Avrami Equation (Equation (7.7)). The exact functional form of this dependency can be expressed directly only for some simple cases and for this reason the Monte-Carlo simulation is an obvious tool to study the effect of this factor on crystallization kinetics. The results of these simulations are shown in Figure 7.10 where bulk crystallization rates of hypothetical systems having the same nucleation rate but different growth rates (equal to our experimental rates for poly(L/D-lactide)) are shown. We can see that even relatively small variations of growth rate significantly affect the crystallization kinetics.

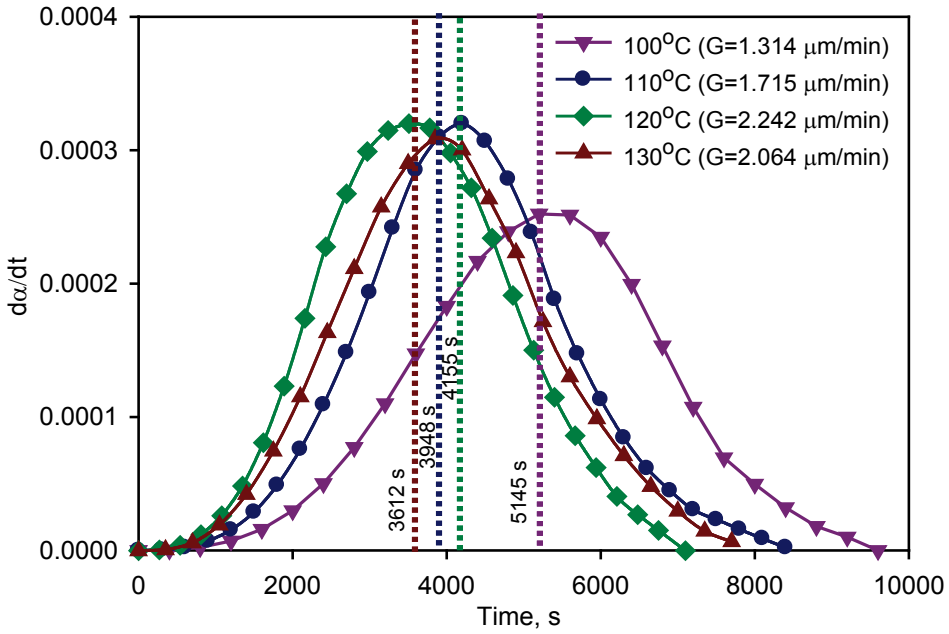

Figure 7.10. The simulation of bulk crystallization kinetics of the system having $N=1\times10^{8}$ $s^{-1}m^{-3}$ with different growth rates. The dashed lines represent the half-time $\tau_{½}$ of crystallization.

Next we consider the kinetics in more detail by examining the experimental crystallization rate curves (Figure 7.11). As expected [132], there is a distinctive induction time required for bulk nucleation to start and this induction time rapidly increases with temperature. This effect is most visible in Figure 7.11d (130°C) for the thickest sample. In this case, as surface nucleation has essentially no effect on the overall crystallinity, we can see a clear zero rate of crystallization in the first 500 s. The induction time of bulk nucleation is also visible in Figure 7.11c (120°C) for the 77 and 116 μm thick samples where we see a skewing of the top of the peak at induction. The ultimate enthalpy of crystallization gradually increased with the increasing isothermal

crystallization temperature (Table 7.2). This observation was in accordance with a previous study of isothermal poly(L/D-lactide) crystallization [133].

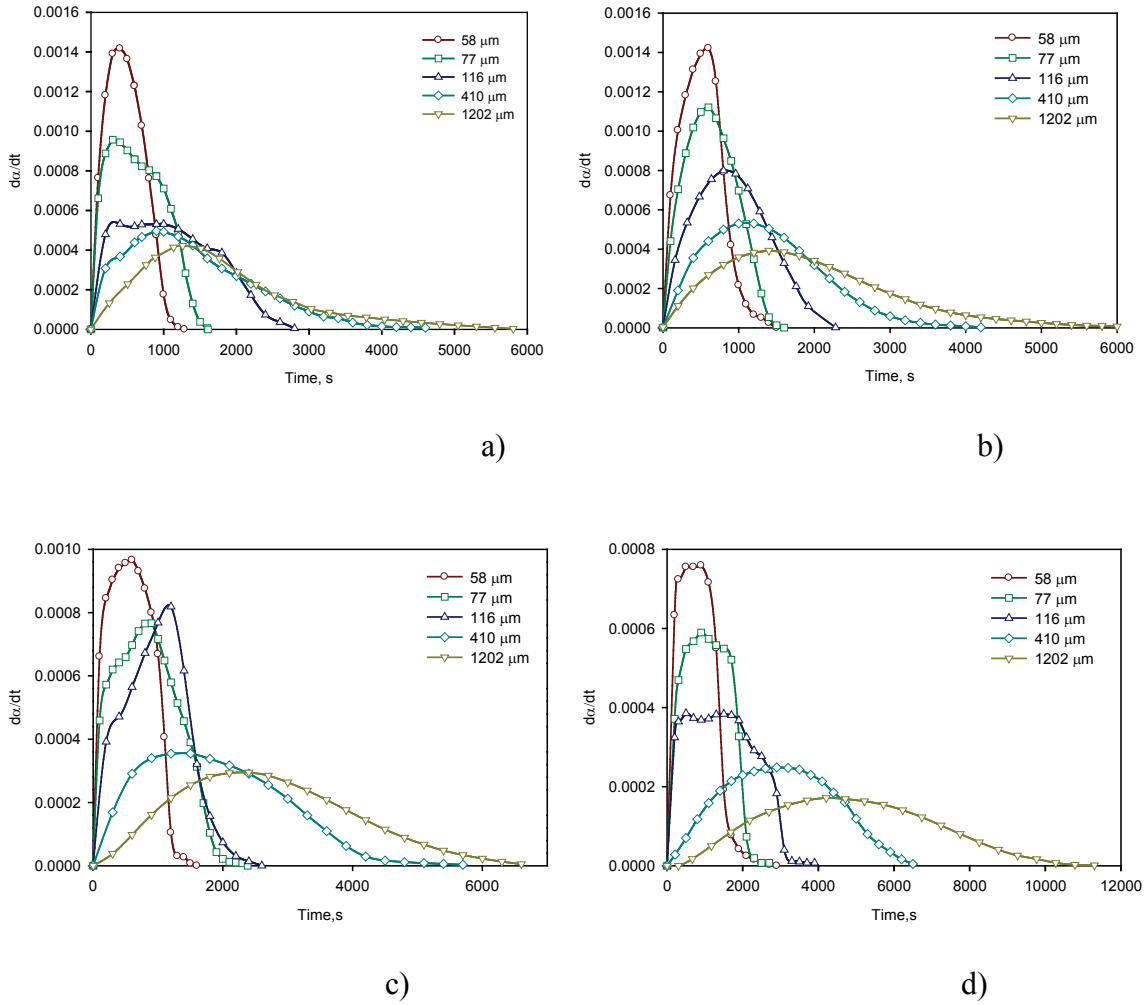

Figure 7.11. The experimental crystallization kinetics data of the poly(L/D-lactide) samples of different thickness in contact with aluminum surface at a) 100°C b) 110°C; c) 120°C; d) 130°C. These curves were calculated from the DSC traces as explained in the Experimental Methods section. Points have been thinned by a factor of 3000 to 24000 to allow for clear viewing of the behaviour.

The shape of the crystallization rate curves undergoes an evolution depending on the relative importance of surface and bulk nucleation, which is affected by both specimen thickness and temperature. For thicker samples, at all temperatures, the shape of the curve is symmetric as is typical of bulk crystallization. The same is true for thin samples at low temperatures. For thin samples, as the temperature increases, the shape of the curve transforms, showing a shoulder at short times, and under some conditions becoming the flattened peak characteristic of surface induced crystallization (Figure 7.7). From this we can infer that while both surface and bulk nucleation concentration decrease as temperature increases, the bulk nucleation concentration decreases much more steeply.

7.5.2. Monte-Carlo simulation of Crystallization Kinetics of the Samples of Different Thickness.

Next we attempt to combine the experimental results with Monte Carlo simulations in order extract nucleation density and rate from the results as well as to comment on the effect of heat transfer issues. To do this, we selected values of N_s and N that gave the best fits to the experimental $\tau_{1/2}$ data for the 4 thinnest samples at each temperature (Figure 7.12 and Table 7.2). As expected, we found that while N_s decreases as temperature increases, it is much less sensitive to temperature than N (Table 7.2). This is consistent with the evolution of the experimental rate curves in Figure 7.11 to a surface crystallization characteristic shape at higher temperatures. Accepting the idea that both types of nucleation are governed by a free energy difference ($\Delta\sigma$ or $\Delta\sigma'$) and all other parameters in Equation (7.2) are the same, it can be concluded that the free energy

difference function is the reason for the different temperature sensitivities of N and N_s. In fact, it can be shown with Equation (7.2) that in all cases where surface nucleation is favourable (i.e. $\Delta\sigma' > \Delta\sigma$) we expect N to be more temperature sensitive than N_s.

The Monte-Carlo results exhibit the expected increase of $\tau_{1/2}$ with increasing thickness that gradually slows down reaching the limit of $\tau_{1/2}(d=\infty)$. Since the influence of surface nucleation decreases as the thickness increases, this limit was determined from the simulation as the half-time of crystallization at N_s=0 (dashed lines in Figure 7.12). At $d=0$ the simulated system transforms to a two-dimensional case having surface nucleation concentration of $N_{surf}=2N_s$. The half-time of crystallization for this case $\tau_{1/2}(2D)$ is the time when half of the area is covered by crystallizing entities.

As explained previously, there are factors other than growth rate, geometry, nucleation pattern and concentration that contribute to the crystallization behaviour of polymers and are not included in our Monte Carlo simulation. It appears that induction time and mixed nucleation are the most influential amongst them. While there is very little delay for onset of heterogeneous surface crystallization of poly(L/D-lactide), the bulk crystallization is characterized by an induction time. We have shown previously with a different experimental study, that for the poly(L/D-lactide) under investigation the induction time dramatically increases with the crystallization temperature from 2100 s at 140°C to 35100 s at 155°C [134]. For temperatures less than 140°C we expect shorter but still significant induction times. We recall that the onset of bulk crystallization is clearly visible in several of the experimental crystallization rate curves (Figure 7.11).

In this study we attempted to eliminate effects of thermal inertia and crystallization heat on isothermal crystallization kinetics by choosing a specific model

polymer having moderate crystallization rate. We expect a temperature gradient due to crystallization heat to be approximately $\frac{\Delta T}{d} \propto \Delta H \frac{d\alpha}{dt}$. As explained in the Experimental Methods scetion, the RHS of this proportionality for polyethylene is up to 160 times that of polylactide. Therefore, while temperature gradients are significant in such isothermal crystallization studies with PE they are much less so for polylactide. Nevertheless, we cannot completely neglect their impact and we expect that temperature disturbances are part of the reason for the increasing deviation of the experimental kinetics from the simulated kinetics with increasing sample thickness as temperature increases (Figure 7.12). There are number of other reasons for the difference between simulation and experiment. First, the simulations presented in this study are based homogeneous nucleation in the bulk while in reality a significant portion is expected to be athermal nucleation. Athermal bulk nucleation is characterized by a lower Avrami exponent and our simulation would tend to overestimate the crystallization rate at final stages of crystallization for thick samples. Another possible contributing factor is nuclei clasterization. While the nucleation distribution in the simulation is perfectly random, in real studies nucleation centers often tend to aggregate into rather extended areas of elevated nucleation concentrations leaving significant areas free from crystallite growth. This contributes to both overall increase of observed crystallization time and asymmetry of crystallization curve. Our previous studies of thin film polylactide crystallization [78] showed that the nuclei clasterization is also typical for surface nucleation but it has less effect on overall crystallization kinetics due to lower dimensionality of surface crystallization.

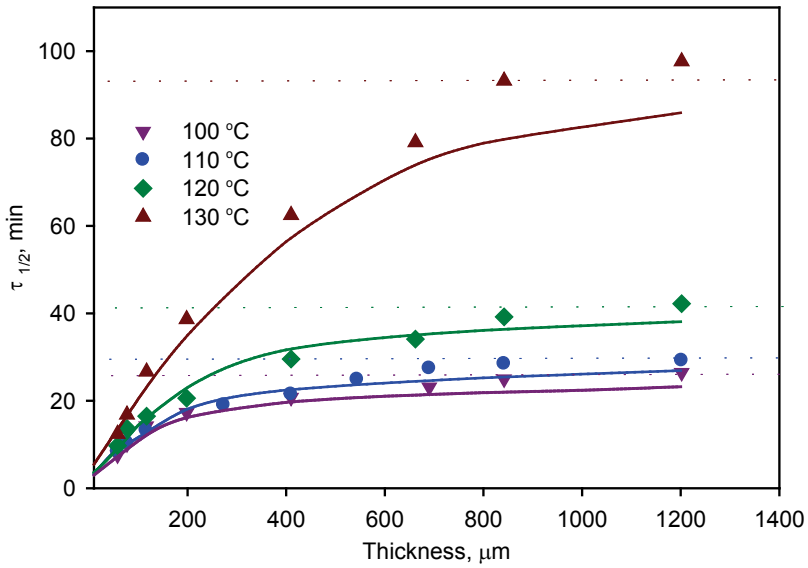

Figure 7.12. The experimental data (symbols) and Monte-Carlo simulation results (solid lines). The dashed lines represent corresponding $\tau_{1/2}(d=\infty)$ lines.

Table 7.2. The surface crystallization of poly(L/D-lactide) simulation results at different temperatures.

T, °C	N_s, m^{-2}	N, m^{-3} s^{-1}	$\tau_{1/2}(2D)$, min	$\tau_{1/2}(d=\infty)$, min	G, μm/min*	ΔH_∞, J/g*
100	2.49×10^{10}	3.11×10^{10}	1.89	26.76	1.314	38.21±0.77
110	9.27×10^{9}	4.87×10^{9}	2.11	29.37	1.715	38.83±0.53
120	2.05×10^{9}	4.17×10^{8}	2.76	41.48	2.242	40.32±0.49
130	3.23×10^{8}	2.24×10^{7}	3.77	92.91	2.064	42.02±0.68

*Experimental data

7.6 Conclusions

In this study we revealed the crystallization kinetics of poly(L/D-lactide) in the presence of surface nucleation caused by intimate contact with aluminum surface. It was found that surface crystallization dramatically affects the crystallization kinetics of poly(L/D-lactide) changing both crystallization rate and the very shape of the crystallization curve. Because of the specific spatial arrangement of surface nuclei, crystallization kinetics in the presence of surface crystallization demonstrated a distinctive dependence on sample thickness. It was found that the half time of crystallization can change up to an order of magnitude depending on sample thickness. For certain conditions, the crystallization rate curve exhibited a distinctive shape typical of surface nucleation. Theoretical aspects of surface nucleation were considered and three distinctive stages of surface crystallization were identified. Governing equations for the first two stages were suggested. These equations were verified using a Monte-Carlo simulation of pure surface crystallization. The experimental conditions were also simulated with the Monte Carlo framework allowing the estimation of surface nucleation concentrations and bulk nucleation rates, revealing their temperature dependence. It was found that both nucleation parameters decrease with increasing temperature while that of bulk nucleation is much more temperature sensitive in a highly nonlinear manner.

Acknowledgments

This work was supported by Auto 21; an NSERC funded Centre of Excellence.

CHAPTER 8

Overview of Polymer Crystallization Induced by Electric Field

8.1. Thermodynamics of Polymer Crystallization

Below the melting point, the nonequilibrium state of the system forces the transportation of the polymer chains from the liquid melt or solution to the solid crystalline phase. The driving forces of polymer crystallization are generated by the surplus of free energy in the homogeneous system. The crystallization process increases the level of order in the system and drives it to a new more stable state.

Turnbull and Fisher [135] further developed the Gibbs equation for nucleation in polymers. According to Turnbull and Fisher, when the free energy of the system becomes negative, the energy barrier of transformation can be overcome and this triggers the phase transformation. This transformation begins with the formation of nuclei which will grow to the size corresponding to its free energy. If no chemical changes are present and the volume constraints are neglected, the Gibbs free energy of the system, G, is given by:

$$G=H-TS \tag{8.1}$$

In this case, the temperature change and the resulting change in Gibbs free energy drive the crystallization process:

$$\Delta G=\Delta H-T\Delta S \tag{8.2}$$

where ΔH is the change in enthalpy equal to the heat of melting and ΔS is change of the entropy between the crystalline state and the melt or solution. In order to understand crystallization in polymers, nucleation and crystal growth should be considered as two independent phenomena.

8.2. Nucleation and Crystal Growth in Homogeneous Polymer Systems

Above the equilibrium melting temperature the value of ΔG, defined in equation (8.2), increases monotonically with increasing temperature. Below the equilibrium melting temperature this function has a maximum at:

$$\frac{d(\Delta G)}{dr} = 0 \qquad (8.3)$$

where r is the radius of the nucleus.

This maximum value of Gibbs free energy, denoted as ΔG^*, is the activation energy barrier which has to be overcome in order to form a stable nucleus. On the crystal surface, a new layer can only be grown after secondary nucleation, a process similar to primary nucleation, but having a somewhat lower free energy barrier because the surface area that must be created anew is smaller. The change in free energy of the growing crystal is [136]:

$$\Delta G'' = \Delta G_c + \sum \gamma A \qquad (8.4)$$

where ΔG_c is the change of the free energy of phase change and γ is the specific surface energy, A is the corresponding surface area and the summation is carried out over all crystal surfaces.

There are three physical mechanisms for polymer nucleation: 1) spontaneous homogeneous nucleation that occurs in a supercooled homogeneous melt; 2) orientation induced nucleation caused by alignment of macromolecules and spontaneous crystallization and 3) heterogeneous nucleation on the surface of a foreign phase.

Heterogeneous nucleation always occurs at lower supercooling than does homogeneous nucleation. Thus the heterogeneities with whose surfaces the nucleation is

concerned are frequently referred to as nucleation catalysts or nucleating agents. Solvent residue, impurities and intentionally introduced phases can all act as nucleating agents for most polymer systems.

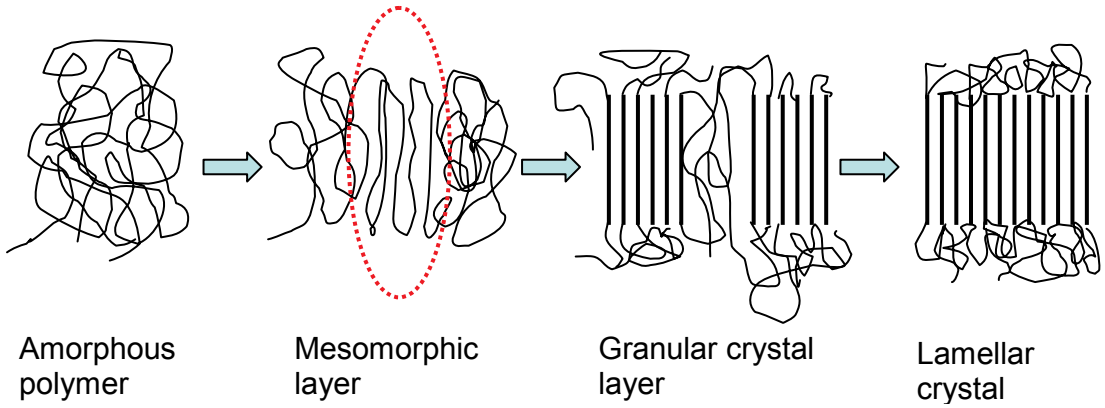

Figure 8.1. Steps in polymer crystallite growth. The orientation of polymer chains is critical for homogeneous nucleation. Sketch was adapted from Hoffman et al. [137].

Orientation, which also induces nucleation, can be caused by external factors such as shear, pressure, electric and magnetic fields. The search for understanding of this effect leads to a crystallization model which is based on statistically induced mesomorphic-crystalline transformation. According to this model the process starts with an attachment of chain sequences from the melt onto a growth face of a mesomorphic layer of minimum thickness, which then spontaneously thickens. After reaching a critical thickness the layer forms block-like crystallites and, finally, the crystallite stabilizes by block merging thus decreasing the Gibbs free energy. Schematic representation of this process is given in Figure 8.1. For homogeneous nucleation the formation of mesomorphic layer is assumed to be formation of nucleus. It can be expected from this

model that any external influence leading to orientation of polymer chain segments should dramatically increase the probability of homogeneous nucleation.

Modification of materials using external forces, such as shear, electric, magnetic, thermal, and photonic, have received much attention for tailoring structures for specific demands. Among them, electric fields have often been employed to create anisotropic structures and to attain desirable actuation in response to a stimulus with ferroelectrics, nonlinear optics, liquid crystals, and electrorheological fluids.

8.3. Effect of the Electric Field on Polymer Nucleation

It is critical for our studies to estimate impact of electrical field on nucleation in polymer melts. As discussed earlier, this would depend on changes in free energy of the nuclei when the electric field is applied.

For a nucleus consisting of N strands of length L to be stable the free energy of formation of the nucleus in the absence of an electric field can be expressed as [138]:

$$\Delta F_0 = -NFA\Delta f + 2NA\sigma_e + 2L\sqrt{NA\pi\sigma} \tag{8.5}$$

where A is cross-sectional area, σ_e, σ are the end-surface and side-surface free energies of the nucleus and Δf is the free energy of melting of an unbounded unit volume of crystal.

When an electric field E is applied this equation can be represented as [138]:

$$\Delta F_0 = -NFA(\Delta f + \vec{p}\cdot\vec{E}) + 2NA\sigma_e + 2L\sqrt{NA\pi\sigma} \tag{8.6}$$

Polarization, p, and electric field have the same direction and their product is always positive. Thus the presence of electric field decreases the free energy of

nucleation which facilitates nucleation. Schematic illustration of this orientation effect is shown in Figure 8.2.

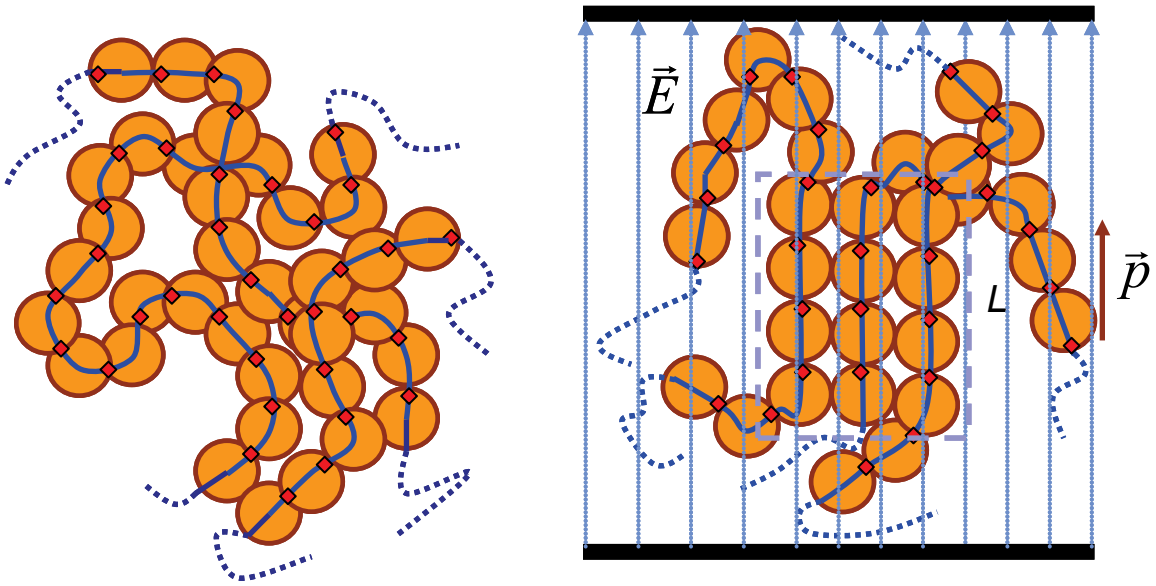

a) b)

Figure 8.2. Schematic illustration of electric field effect on mesomorphic layer formation. The polymer chains conformation in absence of electric field (a) and local orientation of chains in electric field (b).

8.4. Effect of Electric Field on Morphology and Growth Rate of Polymer Crystalline Structures

The electric field influence on crystallization of polymers is not restricted to increasing homogeneous nucleation. Due to orientation effect of electric field, different effects on crystalline morphology can be observed including spherulite alignment for polymer blends, lamellar orientation and changes in growth rate.

The alignment of spherulites into groups happens with their long axis parallel to the field. A driving force for this alignment of under an electric field is a mismatch between the two phases in dielectric constant when AC field is applied or conductivity for DC electric field. The misalignment from Brownian motion or thermal agitation act against this and to achieve alignment, the aligning force must be larger. This is one of the reasons for studying polymer chain's dipole properties and its dielectric relaxation parameters.

The lamellar crystals within the spherulites also become aligned with the electric field. Studies showed that even lamellae whose growth was perpendicular to the field direction tend to orient with their planes parallel to the field. This alignment takes place because the induced polarization of the lamellae by the electric field is the highest along the longest plane axis, even when the material is dielectrically isotropic by itself.

In addition to the alignment of the spherulites and crystal lamellae, elongation of the individual spherulites can also take place. Even when field-induced polarization has a negligible effect on crystal nucleation and growth in the initial stage of crystallization, it becomes increasingly important as the crystals grow. Polarization increases with the cube of the lamellar size and this effect may be further increased by the platelet shape of the lamellae. As result, the polarization forces may become large enough compared with the interfacial energy of the lamellar surfaces to lower the secondary nucleation barrier for crystal growth. All this would accelerate crystal growth in the field direction in contrast to that in all other directions and would generate elongated spherulites [139].

8.5. Dipoles in A1-type Polymers and Dynamic Properties of Polymer Chains

It is known that flexible polymer chains exhibit a wide variety of conformations because of a large number of degrees of freedom in the spatial configurations of their statistical units. These conformations are in some degree of dynamic equilibrium, which results in the chain motion over a wide range of spatial scales covering from the length of chemical bonds to the global chain size (end-to-end distance). Obviously the characteristic time of the motion increases with an increase in the length scale and the local motion occurs much more rapidly than the global motion. Thus the equilibrium chain motion always has a wide spectrum in its time scales. This equilibrium motion determines the relaxation of various dynamic properties in the linear stimulus-response regime, e. g., linear viscoelastic and dielectric properties.

In fact, the chain dynamics at various length scales has been most extensively studied for these properties. Obviously the sensitivity of a polymer chain to an external electric field would depend on orientation and magnitude of dipole moment of its repeat units. Some other factors like chain rigidity also would contribute to sensitivity. In polymers this orientation also facilitates crystallization and thus increases growth rate. In this sense effect of polymer chain orientation in electric field is similar to shear induced crystallization.

Stockmayer classified the dipoles of flexible chains into three basic types, the type-A and type-B where dipoles attached to the chain backbone and type-C where dipoles attached to the side chain groups. The type-A and type-B dipoles are parallel and perpendicular to the chain backbone, respectively. For the type-C polymers, it is the

motion of side chain groups that induces the dielectric relaxation (Figure 8.3). These two types of local relaxation processes have characteristic times that are dependent on the chemical structure of the chain but not on molecular weight M of the chain (unless effects of the chain ends influence for small *M*). In contrast, the slow relaxation due to the global chain motion, observed when the chains have the type-A dipoles, has the characteristic time depending on molecular weight of polymer chain.

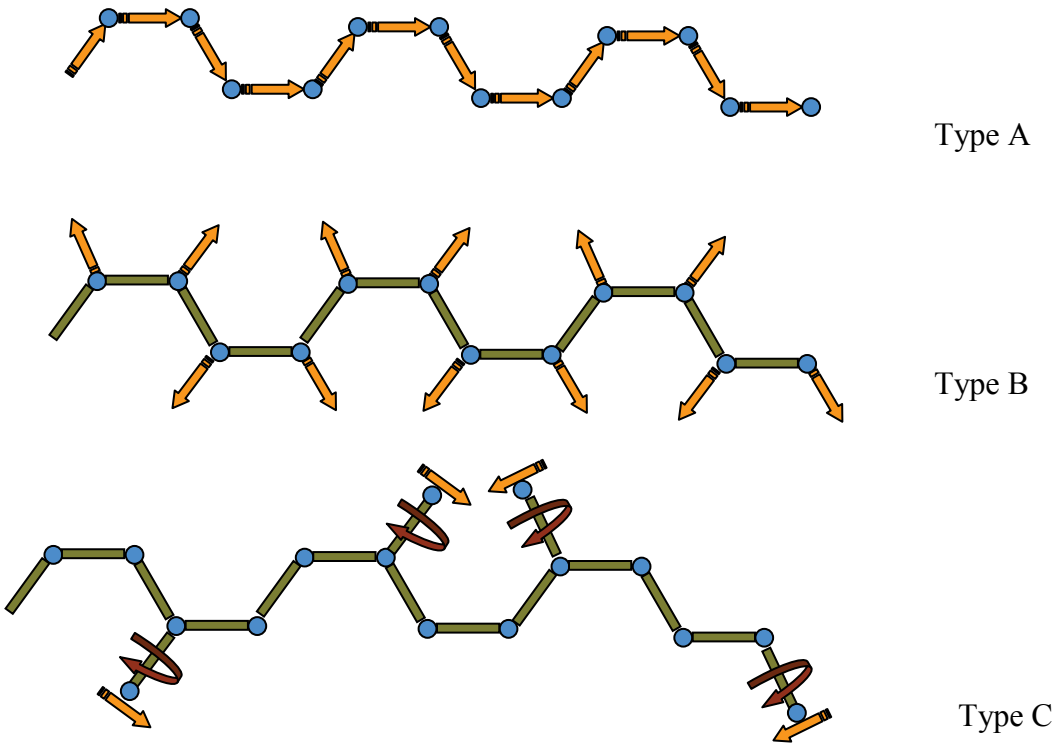

Figure 8.3. Schematic illustration classifying the dipoles of polymer chains. The circles indicate atoms in the chain backbone. Type-A and type-B dipoles, both attached to the chain backbone, are parallel and perpendicular to the backbone. The type-C dipole is attached to the side group.

Polymers having dipoles aligned in the direction parallel to the chain contour are classified by Stockmayer as type A and exhibit the *dielectric normal mode relaxation* due to fluctuation of the end-to-end vector. Dielectric spectroscopy on the normal mode relaxation provides fruitful information on global chain dynamics. The global chain dynamics is one of the main factors affecting crystallite growth and its growth rate. This is the main reason for studying of dielectric relaxation properties of polymers since these studies provide valuable information on factors affecting crystallization.

Most typical representatives of A-type polymers are aliphatic polyesters having structures given by - $(R_m\text{-COO})_n$ -. Here R_m represents an aliphatic hydrocarbon composed of *m* backbone atoms. Jones et al. [140] first reported the dielectric normal mode relaxation in dilute solutions of poly(-caprolactone). Later Urakawa et al. [141] reported the dielectric normal mode relaxations of solutions of poly(-caprolactone) and poly(varelolactone) with a narrow distribution of molecular weight. The dielectric normal mode relaxation of undiluted polymers was also extensively studied for polyisoprene.

Poly(lactic acid) (PLA) is an aliphatic polyester where the backbone atoms of the first repeat unit numbered from 1 to 4. C4 is the carbon atom of the next repeat unit. Because of the resonance effect, the C2-O3 bond has a double bond character and thus the internal rotation around C2-O3 is extremely constrained. Therefore, the backbone atoms C1, C2, O3, and C4 are located in the same plane. Considering this, the whole repeat unit can be regarded as a virtual bond, as pointed out by Jones et al. [27] The virtual bond possesses parallel (type A) and transverse (type B) components of the dipole moment *p*A and *p*B.

When an electric field is applied, dipoles of the chain adopt the orientation of the electric field *E* through chain motions. As a result, certain dielectric responses can be observed which contains information on the chain motion.

The polarization *P(t)* can be represented as a sum of all dipoles μ in a unit volume:

$$P(t) = \sum_j \mu_j(t) \tag{8.7}$$

At equilibrium state, a normalized dielectric relaxation function $\Phi(t)$ is defined as an auto-correlation of *P*:

$$\Phi(t) = \frac{\langle P_E(t) P_E(0) \rangle}{\langle P_E^2 \rangle} \tag{8.8}$$

where P_E is the component of polarization *P* in the direction of electric field *E*.

For an isotropic and homogeneous system the equation can be rewritten:

$$\Phi(t) = \frac{\langle P(t) P(0) \rangle}{\langle P^2 \rangle} \tag{8.9}$$

Here $\Phi(t)$ specifies all dielectric features and many important parameters like the complex dielectric constant ε^* can be expressed in terms of this function:

$$\varepsilon^*(\omega) \equiv \varepsilon'(\omega) - i\varepsilon''(\omega) = \varepsilon_\infty - \Delta\varepsilon \int_0^\infty \frac{d\Phi(t')}{dt'} \exp\left[-i\omega t'\right] dt' \tag{8.10}$$

where $\varepsilon'(\omega)$ and $\varepsilon''(\omega)$ are the dynamic dielectric constant and dielectric loss, respectively and ε_∞ is the high-frequency dielectric constant, and $\Delta\varepsilon$ is the dielectric relaxation intensity.

While effects of flow on polymer crystallization are studied by many researchers, those produced by electric field remain largely unexplored. Unlike flow induced crystallization, electric fields can affect only the crystallization of polymers having non-zero dipole moment. It can be expected also that those effects would be relatively weak as compared to flow effects. The electric field also far more uniform and is not affected by various surface fracture effects unavoidable in flow induced crystallization studies. This provides very interesting opportunities for better understanding of the nature of nucleation, crystallization and crystal growth in polymer melts.

CHAPTER 9

Crystallization of Poly(L-/D-lactide) in the Presence of Electric Fields

9.1 Introduction

The first attempts to study the influence of electric fields on crystallization phenomena were in early 1980's by Tynenska et al.[142] Sterzynski and Garbarczyk[143] found that electrocrystallization of blends of polymers in the presence of a strong electric field caused a noticeable increase in nucleating density, dissipate the larger domains of PEO into smaller circular ones and formed PEO spherulites which retained the domain's circular shape. Further studies confirmed that the crystallization behaviour of polymers having a permanent dipole moment or a high dielectric constant, such as poly(vinylidene fluoride), poly(ethylene oxide) (PEO), and polyamides exhibit sensitivity to electric fields.[144-146]

Electric fields affect not only nucleation and crystallization rates but in some cases can have a dramatic effect on the resulting crystal structure and morphology. For example, aligned PEO phases in diblock copolymers[147] and a fibrillar, thread-like PEO structure in a blend of poly(styrene-*b*-ethylene oxide) and poly(styrene) with a ternary solvent mixture[148] were observed when solvent-cast under an electric field. Hsu and Lu [144] investigated isothermal crystallization of poly(vinylidene fluoride) upon cooling from the melt in the presence of weak electric fields. The helical α phase is the favourable configuration under zero-field conditions while fields having strengths on the order of 70 kV/cm induced a solid-solid phase transformation from the α-form to the γ-form.

B. K. Hong et al. [146] studied the crystallization of the polyamide 6,6 under electric field using rheological measurements. It was found that crystallization rate of polyamide 6,6 which has antiparallel orientation of the dipoles formed by amide groups, significantly decreases with increasing electric field intensity. Researchers attributed this phenomenon to disturbance of the of dipole's orientation under electric field which resulted in retardation of crystallization. Kawai and Lee [149] performed an extensive studies of crystallization of poly(ethyleneglycol) under electric field. They suggested possibility of certain changes in molecular dynamics of polymer chains during crystallization when electric field was applied which resulted in lamellar thickening. As result, a noticeable increase of the polymer's melting point was observed.

These phenomena have been studied using different approaches and the effect of electric field on behaviour of larger domains was investigated. The alignment of cylindrical microdomains of a poly(styrene-*b*-methyl methacrylate) diblock copolymer under an electric field was also observed using transmission electron microscopy and small angle neutron scattering.[150,151] At that time the behaviour of liquid crystalline polymers, having rod-like, plank-like, or disk-like structures in electric fields were studied most extensively.[152] Electric field-induced alignment of rod-like structures and platelets in some composites was studied by Park and Robinson.[153] It was found that platelets align more efficiently than rod-like structures. The important conclusion drawn from these studies is that since crystalline lamellae have a platelet shape; they may also align readily in an applied electric field of sufficient strength. A study of the lamellar surface orientation of poly(styrene-*b*-methyl methacrylate) parallel to an electric field was reported by Amundson et al.[154,155] They found that lamellar orientation degree is

dependant on intensity of electric field. It should be noted that most studies have been done in two-dimensional systems i.e. films.

A careful study of the effect of electric fields on crystallization of PLA is relevant to the important area of electrospinning[156,157]. In the solution[156] and especially the melt-based[157] versions of this process, the resulting fibers of PLA tend to have very low crystallinity due to the rapid quenching below the glass transition that does not allow sufficient time for this slow crystallizer. It has been found however that upon annealing at around 100°C the fibers very quickly crystallize reaching over 40% crystallinity in a matter of minutes[156,157]. This is clearly related to a "frozen in" ordering which facilitates nucleation once the temperature is raised. The ordering of the amorphous chains is imparted by both the mechanical drawing down of the fiber transmitted via entanglements between chains and the presence of an electric field which aligns the dipoles parallel to the electric field.[158] Here we characterize the aspect related to the electric field.

Marand et al. [145] proposed a modification of the classical theory of homogeneous nucleation of a crystalline phase which accounted for external electric field. According to their approach, an electrostatic interaction between the total polarization of the nucleus and the electric field contributes to the free energy of nucleation. This contribution is expected to increase at lower undercooling and the nucleation rate of the polar phase should increase while the nucleation rate of the nonpolar phase should decrease. They supported their theoretical predictions with experimental observations of the crystallization of highly polar poly(vinylidene fluoride) in the presence of electric field. Another theoretical approach to homogeneous nucleation

in presence of electric field was proposed by Ziabiki and Jareki.[159] Their analysis is based on the extended nucleation theory taking into account the orientation of polymer chain elements. According to the Ziabiki and Jareki model, the presence of an electric field introduces an orientation dependent free energy which affects both thermodynamic and kinetic crystallization characteristics, i.e. nucleation rate. It should be noted that, sinces polylactide, has a polar repeat unit with dipoles parallel to the chain backbone we expect susceptibility of its crystallization behaviour to the presence of an electric field.

9.2 Experimental Section

The polylactide was supplied by Biomer (Germany). It is a commercially available poly(L/D-lactide) copolymer containing 2% of D-lactide (L 9000), with a number average molecular weight of 50,000 and a polydispersity index of 2.0. The glass transition of this polymer is 60 °C, and its melting point is 170 °C. Its thermal transitions and spherulitic growth rates have previously been described. [78] The pellets were thoroughly dried at 80 °C in a vacuum oven for 24 hours prior to pressing at 185 °C in a Carver hydraulic press. This procedure allowed the decrease of adsorbed water content in the polymer from 0.26 wt% to 0.03 wt%, significantly suppressing the influence of hydrolysis during the rheological measurements. Subsequent experiments showed no noticeable decrease in water content with increase of drying temperatures and times.

The rheological measurements were performed under a nitrogen atmosphere with oxygen content of less than 2.5 ppm in a modular compact rheometer (MCR 500 model of Anton Paar). The small amplitude oscillatory shear experiments were performed using plate-plate configuration (25 mm diameter) with a 0.5 mm gap at 3% strain and 1 Hz

oscillation frequency. The experimental procedure used for studying the rheological properties of crystallizing polylactide has been described in detail previously.[134]

Residual crystallinity was eliminated by the heating of each sample to a temperature exceeding the melting point inside the rheometer prior to testing. The sample was held at 190 °C for 3 minutes and then cooled to the set point at the rate obtainable by the rheometer. Due to the thermal inertia of the sample and setup the cooling rates were relatively slow, on average 3.4 °C/min. This polylactide has very long crystallization induction times at the high temperatures considered here thereby minimizing the effect of the slow cooling. Additionally an identical cooling pattern as used previously[134] was followed allowing us to use the previously developed model. The SAOS complex viscosity measurement was started and the electric field was applied simultaneously upon reaching the set point temperature.

A custom, low-friction, tungsten attachment was used for supplying the voltage to the moving upper plate of the rheometer. The average friction associated with this attachment was determined in terms of free rotation viscosity to be 62±8.5 Pa·s (Averaged from 5 independent experiments). Thus, the relative viscosity measurement error introduced by the attachment ranged from 2.4 to 0.5% depending on the experimental temperature. A gap of 0.5 mm was chosen in order to accommodate an acceptably low voltage and minimize surface crystallization effects. A static electric field was applied using an Agilent stabilized power supply E3612A and an in-house developed system for achieving an electrical connection to the rheometer plates with a minimal effect on measured viscosity. The rheometer plates were used as electrodes to apply an electric field across the sample thickness allowing for the *in situ* measurement of

complex viscosity during the crystallization under electric fields of varying strength. We note that in this geometry, the flow is in the θ-direction and the velocity gradient is in the z-direction with the r-direction neutral. The electric field was applied in the z-direction, parallel to the gradient and perpendicular to the flow. Since all measurements were performed within the linear viscoelastic regime the flow has no effect on the crystallization and is simply acting as a route for observing the crystallization which is affected by the electric field. Induction times for crystallization were determined from the complex viscosity data using our previously described technique. [134]

The XRD analysis was performed with poly(L-/D-lactide) samples laminated between two layers of 12μm aluminium foil and having an overall thickness of 0.432 mm. The laminating was necessary because of the polylactide's high adhesion to the rheometer plate surface making it almost impossible to detach the polymer layer from the plate undamaged. The lamination procedure has been previously described[160]. The samples were crystallized in the same setup used for the viscosity measurements in the absence of shearing deformation. The thin samples allowed the use of our superfast heating/cooling technique previously described [78]. This technique allows us to efficiently "freeze" the polymer crystalline structure after a predetermined crystallization time.

The optical microscopy studies were done with 0.3 mm samples sandwiched between thin preparation glasses having 0.15 mm thickness and crystallized in the same setup using the same heating/cooling procedure as that used for the XRD specimens. The electric field was applied across the sample thickness which is perpendicular to the surface viewed in the micrograph images.

9.3 Results and Discussion

The polylactic acid repeat unit has a pronounced dipole moment parallel to the polymer backbone, characteristic of a type-A1 polymer (Figure 9.1). [161] Polylactide has been shown to switch from the random coil to a uniaxially drawn configuration upon the application of an electric field on the order of 1 MV/m at 190°C[158]. Therefore we expect various physical effects related to chain orientation in the presence of electric fields.

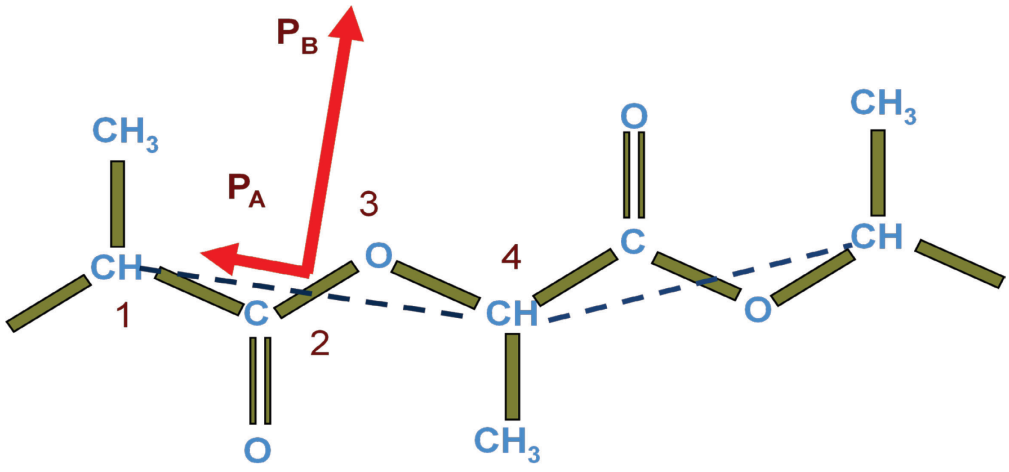

Figure 9.1. The polylactic acid chain representation showing the directions of dipole moment of the repeat unit. P_A and P_B are the parallel and transverse dipole vectors respectively and the dashed line represents the virtual backbone. Schematic illustration from work by Ren et al. [161]

While the dielectric relaxation properties of the polylactides over a wide range of temperatures are well studied; [161, 162] the consequences of electric field induced chain

orientation on other aspects of the behavior of polylactide is still not known. Since crystallization of polymers is dramatically affected by chain stretching and orientation, the effect of the electric field on the crystallization of type-A1 polymers represents a particular interest.

9.3.1 Effect of the Electric Field on Induction Time for Crystallization

The induction times determined from the rheological measurements are shown in Table 9.1.

Table 9.1. Effect of applied electric field on induction time t_i (s) of the polylactide crystallization. The induction time determined from rheological measurements using 0.5 mm gap. The induction times for the 1 mm gap are also shown to demonstrate the effect of heterogeneous surface crystallization on induction time.

T, °C	Applied electric field intensity, kV/m					
	0	60	120	180	240	0 (1mm gap)
140.0	2280	-	-	2240	2220	2460
142.5	2460	-	-	2340	2480	2600
145.0	2820	2740	2940	3080	2880	3120
147.5	4060	4180	4080	4140	4120	4440
150	8080	8220	7880	8120	8060	8960

We found that the presence of the electric field had no discernable effect on the observed induction time of polylactide crystallization. We did note that the all of the induction times were slightly lower than observed previously [134] most likely due to surface nucleation and working with a smaller sample thickness (0.5 mm here compared to 1 mm previously). [134] The decrease in induction time with reduced sample thickness varied from 4.4% at 140 °C to 9.3 % at 150 °C. With decreasing sample thickness, the relative impact of surface crystallization on overall crystallinity increases, causing the reduction in observed induction time. We have shown previously, using DSC studies that the relative impact of surface crystallization on the overall crystallization kinetics of this polymer increases with increasing crystallization temperature consistent with our results here. [160]

9.3.2 Effect of Electric Field on the Complex Viscosity of Crystallizing Polylactide

It was found that the evolution of complex viscosity of the crystallizing polylactide is noticeably affected by the presence of an electric field (Figure 9.2). From these results, we conclude that the presence of an electric field increases the rate of crystallization of polylactide and that this effect is more pronounced at higher crystallization temperatures. We also note that there appears to be a threshold of electric field intensity below which there is no effect on the crystallization rate. The threshold is higher at lower temperatures; at 145 °C it requires between 60 and 120 kV/m to influence the crystallization.

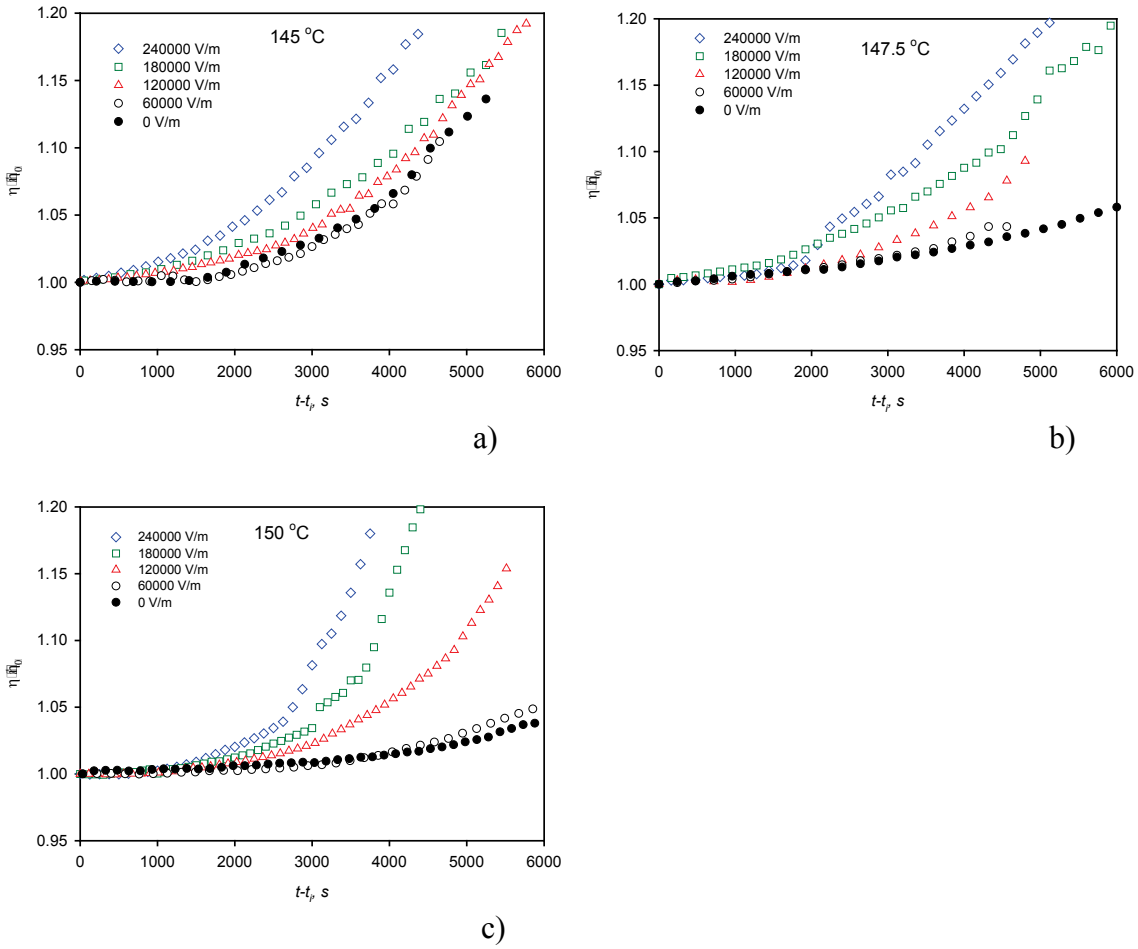

Figure 9.2. The effect of static electric fields of different intensity on relative complex viscosity of the polylactide melt at: a) 145 °C, b) 147.5 °C, c) 150 °C.

It is possible to measure the complex viscosity of crystallizing polylactide to much higher levels of crystallinity reflected orders of magnitude changes in the complex viscosity. Here we have limited our studies to lower values of crystallinity, primarily in order to avoid effects of gelation which occurs at about ϕ=1.6%.[134] We have shown previously that the functional dependence of the complex viscosity on the crystallinity changes at about ϕ=5% due to the increasingly solid-like behaviour of the gelled system.

We will use our model relating low levels of crystallinity and complex viscosity to interpret our electric field results and therefore have limited our experiments to about ϕ=5% which corresponds to a reduced complex viscosity of less than 1.2.

From the rheological studies, we know that electrical fields increase the rate of crystallization of polylactide but that they have no measurable effect on the induction time. Since electric fields induce chain orientation and stretch of type-A1 polymers[163] which is known to increase nucleation, we expect to find an increased nucleation rate.[164] This is consistent with the observed increase in crystallization rate but is apparently inconsistent with the lack of effect on induction time which is generally accepted to be inversely proportional to nucleation rate. Nevertheless, the limited sensitivity of the techniques for determining of the induction time allows for significant uncertainty in this regard. In order to further elucidate the effect of electric field on the fundamental processes of crystallization we have performed an XRD study of the crystal structure and an optical microscopic study of the spherulitic morphology.

9.3.3 The Crystal Structure as Determined by XRD Analysis

The XRD spectra (Figure 9.3) show that crystalline structure of polylactide is not affected by the electric field. Our XRD spectra were consistent with those observed by Shen et al. [165] for polylactide crystallized at high temperatures (T>110 °C); the peak observed at 2θ~16.5° corresponds to the spacing of the α-crystals typical for polylactide crystals formed at high temperature. The magnitudes of this peak in the two spectra

suggest a significantly higher crystallinity for the sample crystallized under the electric field, in agreement with the rheological data and an increased crystallization rate.

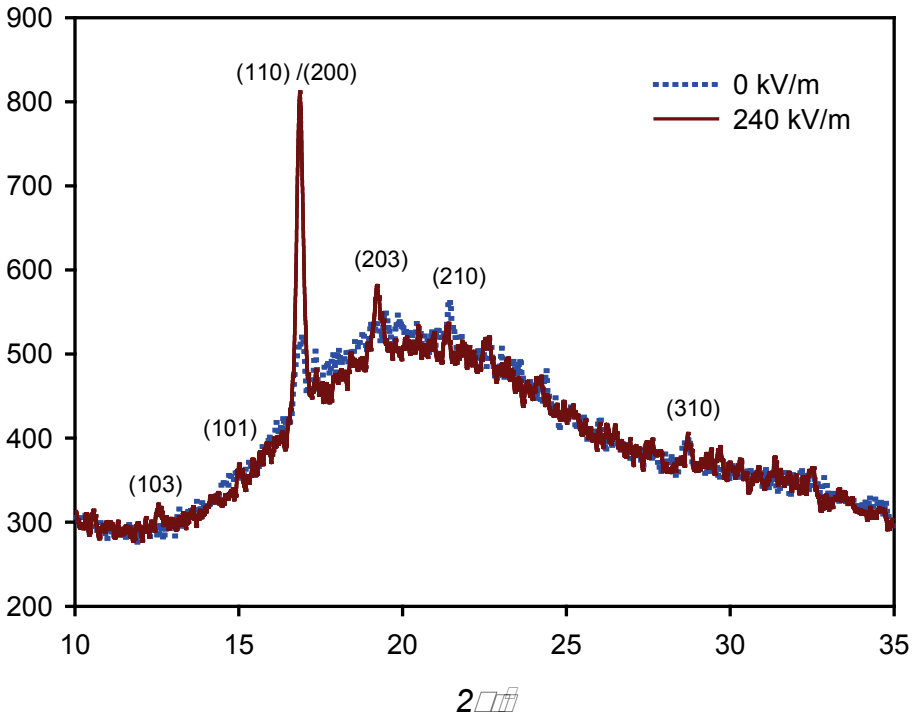

Figure 9.3. An overlap of the XRD profiles of the polylactide samples subjected to crystallization for 9000 s at 147.5 °C without applied electric field (dotted blue line) and under the influence of 240 kV/m electric field (solid red line).

9.3.4 The Crystalline Morphology as Observed Using Optical Microscopy

The crystalline morphology of polylactide sandwiched between thin layers of glass was also studied using optical microscopy under 10 fold magnification (Figure 9.4). It should be noted that the crystallization of polylactide is significantly affected by the presence and nature of a foreign surface. In our observations, glass [78] and especially

aluminium [160] induce intense but different degrees of surface nucleation and steel is expected to have yet another nucleating ability. Thus, it is not possible to relate the nucleation density observed in polylactide samples crystallized in contact with a glass surface to that of a sample crystallized between steel plates during the viscosity measurements, however both are expected to exhibit the typical heterogeneous behaviour of inducing all of the nuclei simultaneously.

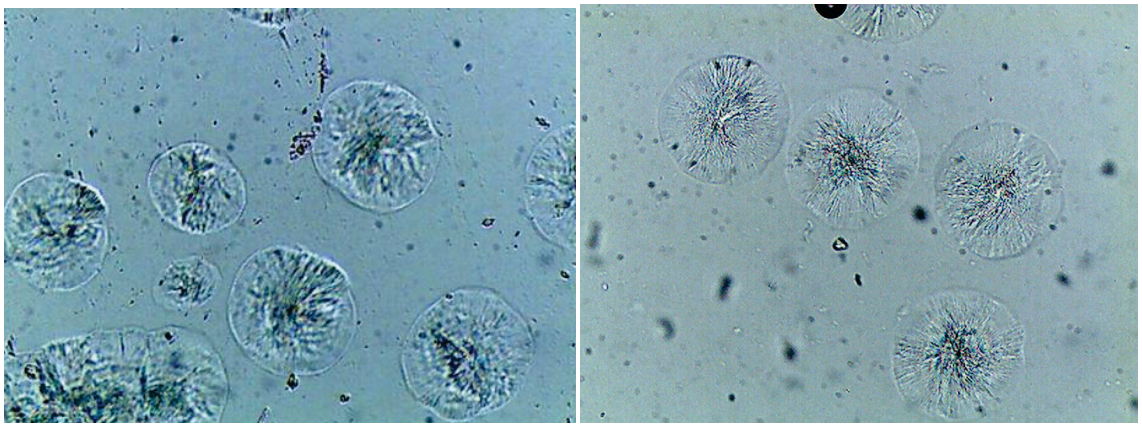

a) b)

Figure 9.4. Optical micrographs of polylactide crystallized at 147.5 °C for 60 minutes: a) 240 kV/m electric field applied; b) no electric field (10X magnification).

The optical micrographs presented in Figure 9.4 are a representative of many images which were taken during our studies. Glass induces surface nucleation which starts instantaneously and results in the spherulites all having the same size at each time. Our previous studies of polylactide crystallization on glass[78] showed that the spherulites all have the same size, determined only by the growth rate, G, and the crystallization time. This clearly indicates heterogeneous nucleation. In our previous studies of polylactide crystallization on glass [160] and in the current work,

homogeneous nucleation events were never observed in the absence of an electric field at these high temperatures as long as only one heating/cooling cycle was applied with sufficiently high heating/cooling rate. Of course, this observation does not mean that homogeneous nucleation is absent when no electric field is applied, it is just hidden by the overwhelming concentration of heterogeneous nuclei and almost negligible because of the short overall time of crystallization needed for heterogeneous crystallization to complete. The optical microscopy provides valuable information regarding the nucleation pattern (instantaneous versus continuous) and the spherulitic growth rate.

The optical micrographs showed that when crystallized in the presence of the electric field, the nucleation pattern differs from that of the polylactide crystallized in the absence of electric field. All of the spherulites are the same size in the sample crystallized in the absence of an electric field as is typical of instantaneous, heterogeneous surface nucleation. In comparison we observe a range of spherulite sizes in the sample crystallized under an electric field, indicating continuous, homogeneous nucleation in addition to the simultaneous surface nucleation which also occurs. This electric field induced homogeneous nucleation causes the number of crystallizing entities to be approximately doubled after 60 minutes of crystallization at 147.5ºC. The presence of an electric field accelerates homogeneous nucleation and its effect is noticeable by direct observations using optical microscopy. As explained previously, in the absence of an electric field, homogeneous nucleation is not observed in our experiments.

Note that the largest spherulites in Figure 9.4a, which are likely surface nucleated, are the same size as the spherulites in Figure 9.4b. This indicates that the spherulitic growth rate is not affected by the electric field. These images and others taken during this

study allow us to conclude that only the nucleation is affected by the electric field at least within the limits of our experimental uncertainty.

9.3.5 Estimation of ϕ from Viscosity

We have previously described the dependence of viscosity of polylactide on low levels of crystallinity in the form of a semi-empirical model. [134] The model employs the spherulitic growth rate G, to relate crystallinity $\phi(t)$ and reduced viscosity ηR:

$$\frac{\eta_{cryst}}{\eta_{melt}} = \eta_R = \frac{\exp\left[\frac{4\delta\phi}{3Gt(1-\phi)}\right]}{\left[1-\frac{\phi}{A}\right]^2} \tag{9.1}$$

where A=0.68 is a constant, δ is a physical crosslink coefficient, t is the crystallization time, $\eta cryst$ is the complex viscosity of the crystallizing polymer and $\eta melt$ is the complex viscosity of the completely molten polymer which is decreasing over time due to degradation as expressed by the exponential decay model. [134] We will make use of Equation 9.1 to infer the crystallinity content over time from our complex viscosity data. This approach is justified by the following arguments. Since the optical microscopy studies revealed the that the growth rate, G, is independent of electric field we can assume that this parameter is a function of temperature only and make use of our previous measurements of this property.[78] The crystal structure and the morphology of spherulitic formation also remained unchanged in the presence of electric fields and it is therefore safe to assume that the physical crosslink coefficient δ, is also a function of temperature only and once again make use of previously measured values for this

parameter.[134] Therefore, Equation 1 can be used unambiguously to infer $\phi(t)$ from ηR using the following numerical procedure which is applied at each time, t:

First, the model is linearized:

$$\mathrm{Ln}(\eta_R) = \frac{4\delta\phi}{3\mathrm{Gt}(1-\phi)} - 2\mathrm{Ln}\left(1-\frac{\phi}{\mathrm{A}}\right) \tag{9.2}$$

then an initial guess for ϕ is obtained from:

$$\phi_0 = \frac{3Gt \cdot Ln(\eta_R)}{3Gt \cdot Ln(\eta_R) + 4\delta} \tag{9.3}$$

In deriving Equation 9.3, we have noted that at low ϕ, the magnitude of the second term in Equation 9.2 is much smaller than that of the first term. We therefore truncate the second term and rearrange to solve for ϕ. This provides a rather accurate initial guess that is corrected using an iterative procedure.

At each iteration, a new value of crystallinity, ϕi, is calculated from the value obtained in the previous iteration, $\phi i\text{-}1$, using Equation 9.4.

$$\phi_i = \frac{3Gt \cdot [Ln(\eta_R) + 2Ln(1-\phi_{i-1}/A)]}{3Gt \cdot [Ln(\eta_R) + 2Ln(1-\phi_{i-1}/A)] + 4\delta} \tag{9.4}$$

Equation 9.4 is derived by replacing $Ln(\eta R)$ in Equation 3 with $[Ln(\eta_R) + 2Ln(1 - \phi_{i-1}/A)]$. This effectively corrects for having truncated the second term in Equation 9.2. This procedure is continued until convergence is obtained which is taken to be $|\phi_i - \phi_{i-1}| < 10^{-6}$.

This approach is validated in Figure 9.5, by comparing the $\phi(t)$ determined from rheological measurements (in the absence of an electric field) to that determined from the Avrami parameters from previous DSC measurements.[134] Since we do not have DSC

data for crystallization under an electric field, we can use this approach to infer $\phi(t)$ assuming as previously explained that G, and δ are independent of electric field strength.

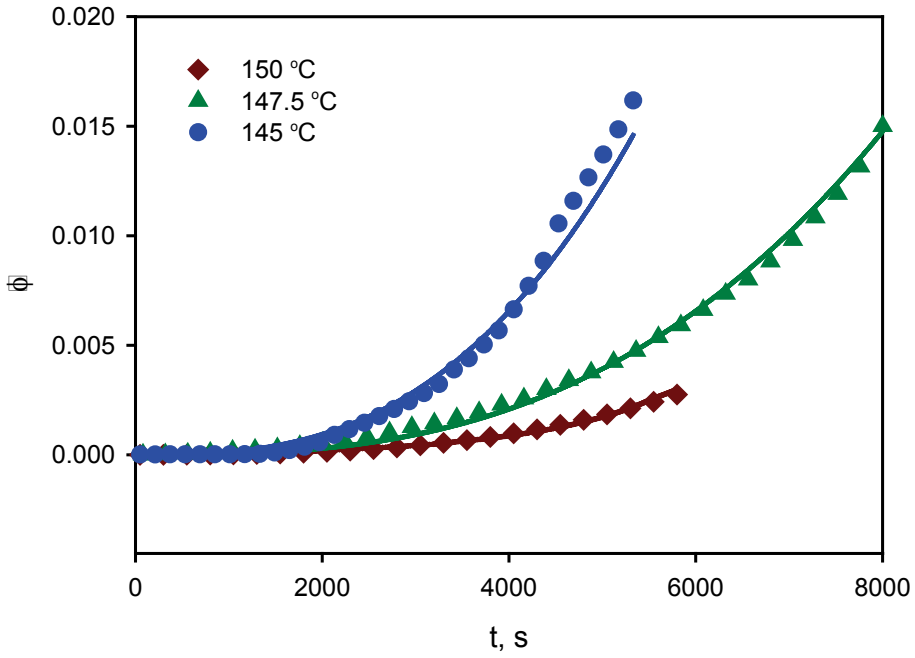

Figure 9.5. Crystallinity, $\phi(t)$, in the absence of electric field. Symbols represent values estimated from complex viscosity $\eta^*(t)$ and curves represent crystallinity determined from DSC experiments using Avrami equation.

9.3.6 Estimation of Nucleation Rate from Viscosity

Previous studies [143,145,149] suggest that electric fields are expected to facilitate primarily homogeneous nucleation. Therefore, assuming a homogeneous nature of nucleation in the presence of an electric field, it is possible to estimate the nucleation rate induced by the electric field from $\phi(t)$ using an Avrami approach. The assumption of the homogeneous nature of the nucleation in presence of electric field is easily verified

with a plot of *ln(1/(1-ϕ))* vs. *t4* which is linear with a slope of *NG3π/3* in the case of homogeneous nucleation. In Figure 9.6 we demonstrate that our data for crystallization under an electric field are consistent with homogeneous nucleation. For comparison purposes we have also included the data for crystallization in the absence of electric field in Figure 6 indicating that they are not consistent with homogeneous nucleation. Nucleation rates, *N*, determined from the slopes of such plots for crystallization under an electric field are presented in Figure 9.7. The results of this analysis agree with the theory proposed by Marand et al.[145] in that crystallization is more sensitive to the magnitude of electric field at lower supercooling. It suggests that the primary effect of the electric field is the local orientation of the polymer chains which induces additional nucleation.

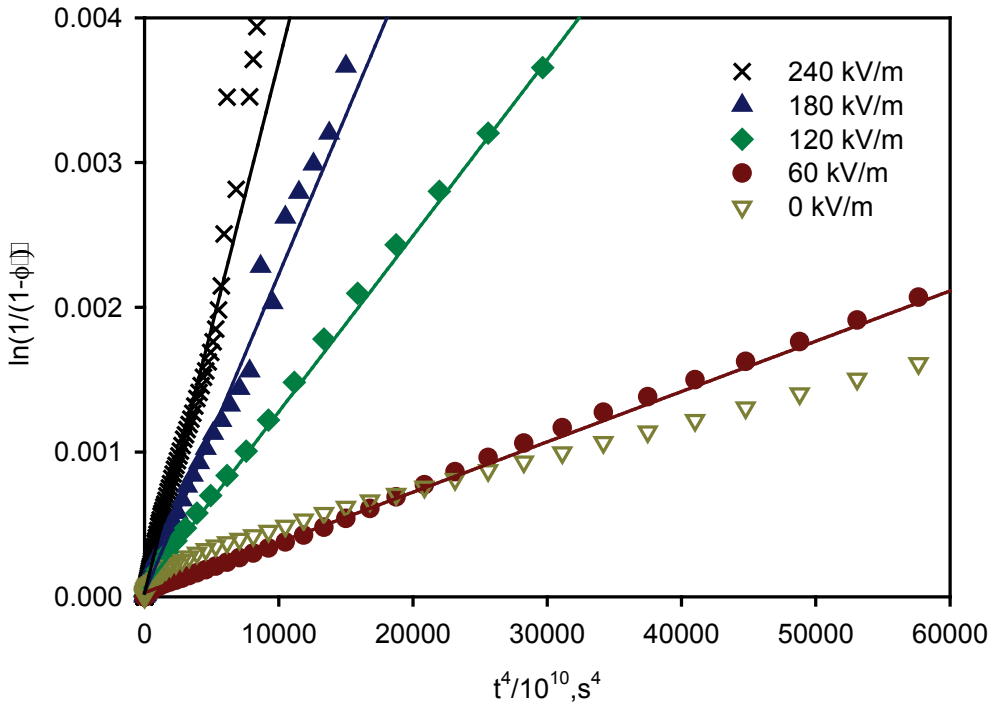

Figure 9.6. Example of linear relation between *ln(1/(1-ϕ))* and t^4 at 150°C.

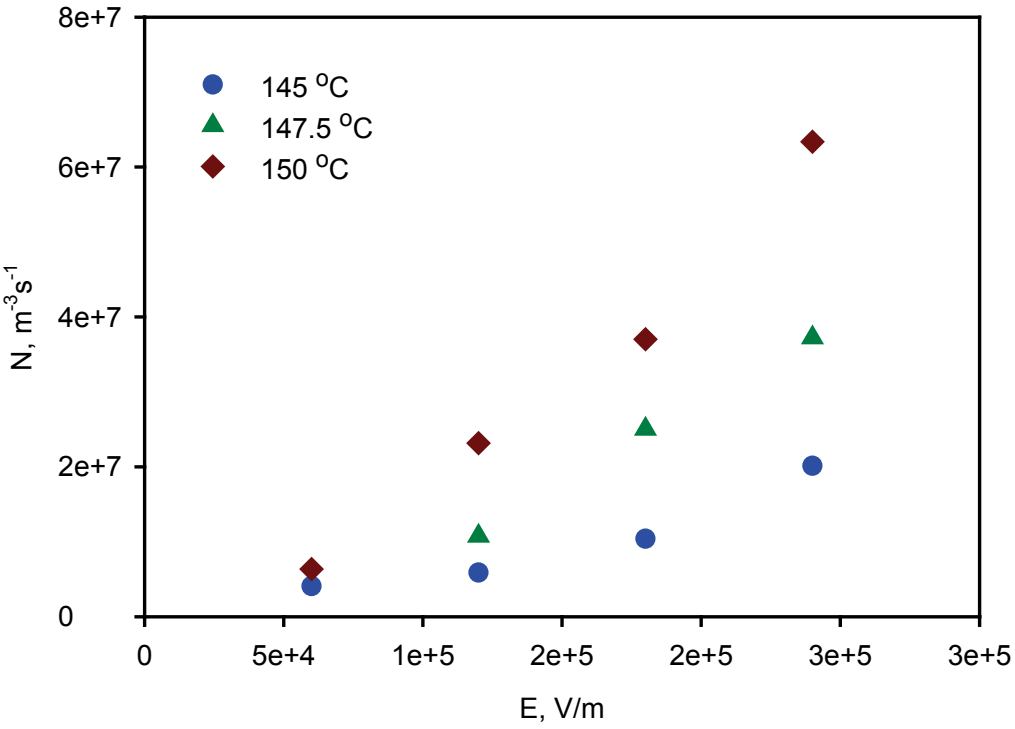

Figure 9.7. Nucleation rates N ($m^{-3} \cdot s^{-1}$) as a function of electric field intensity E.

We return briefly to the surprising finding that the increased nucleation rate had no effect on induction time in contradiction to the typical understanding that induction time is considered to be inversely proportional to nucleation rate. There are two likely explanations for this: (1) the change in induction time was smaller than our experimental uncertainty and/or (2) the observed induction time is affected by factors other than nucleation rate alone. Since the observed induction time is simply the time when our experimental technique can detect crystallinity, there are almost certainly other factors playing a role. It is therefore surprising that the shifting of the timescale in Figure 9.6 results in a picture that is consistent with the rest of our results and pointing towards increased homogeneous nucleation since we would have expected a distortion due to the

nonlinear time dependency. We believe that this lies in the current weak understanding of the relationship between an observed induction time and a nucleation rate. This relationship certainly depends on the measurement technique, the nature of the nucleation and perhaps even our understanding of the meaning of a nucleus and the mesaphase transition which is especially complex for polylactide [166].

9.4 Conclusion

Enhanced crystallization rate is observed for polylactide in the presence of an electric field. This can be attributed to electric field induced orientation of the polylactide chains leading to an increased nucleation rate in the melt. This conclusion is supported by the observation that the magnitude of the increase in crystallization rate increases with increasing crystallization temperature suggesting a close relation to the effect of electric fields on crystallization and chain mobility. XRD indicates that the crystallization rate increase is not accompanied by a change in the crystalline structure. Optical microscopy provides direct evidence of the changing nucleation pattern of polylactide in the presence of an electric field while supporting the assumption that the spherulitic growth rate is not affected by the electric field. An analysis based on a model relating crystallinity to complex viscosity shows that nucleation rate increases with electric field intensity and this effect is becomes more pronounced at lower supercooling.

Acknowledgements: This work was supported by the NSERC Discovery Grant Program.

CHAPTER 10

Flow-induced Crystallization of Linear Polylactide Observed by Rheological Measurements

10.1 Introduction

The flow-induced crystallization (FIC) phenomenon is often observed during processing of crystallisable polymers. Due to flow, crystalline polymer chains become highly oriented and crystallize with different nucleation and growth from those under quiescent conditions. This phenomenon can significantly affect crystallization kinetics and morphology, resulting in, for example, shish-kebab structures. Numerous studies have been done to reveal the nature of FIC. Keller et al.[167] demonstrated a distinctively sharp coil-stretch transition in elongational flow at some specific strain rate. The further studies showed that certain critical strain is necessary to attain steady-state extension of polymer chains. While during polymer processing melt experiences both elongation and shear, it was assumed that later is less influential in developing FIC than elongation of melt. Nevertheless, it was shown in numerous studies that shear flow also can significantly affect crystallization. No wonder why this phenomena continues to attract researchers since the fundamental understanding FIC implies possibility of control over industrial product morphology and properties. Kumaraswamy et al.[168], Pogodina et al.[169,170], Janeschitz-Kriegl et al.[171,172] and many others discussed the fundamental processes controlling flow-induced crystallization in details. It was found that massive disentanglement of polymer chains, subsequent creation of long sequences

of aligned chains and convective transport mechanism is among main factors promoting accelerated nucleation and specific crystallization morphology.

A number of theories have been proposed to describe flow induced crystallization. Among the most significant are those proposed by Graham and Olmsted [173], Tanner and Qi [174], Eder and Janeschitz-Kriegl [175,176], flow-induced dumbbell free energy theory by Zheng and Kennedy [177] and recoverable strain theory by Zuidema et al. [178]

Coppola et al. [179,180] proposed a FIC model based on the theory of Doi and Edwards [181] based on a micro-rheological model. This model describes the combined effect of temperature and flow effects on the early stages of polymer isothermal crystallization. The model describes an evolution of dimensionless induction time of crystallization Θ from the point of change of flow-induced free energy of the melt ΔG_f relative to the quiescent crystallization free energy change ΔG_q according to equation:

$$\Theta(T_c,\dot{\gamma}) \cong \frac{\dot{N}_q}{\dot{N}_f} = \frac{1}{1+\frac{\Delta G_f}{\Delta G_q}} \exp\left\{ \frac{K_n}{T(\Delta G_q)^n} \left[\frac{1}{\left(1+\frac{\Delta G_f}{\Delta G_q}\right)^n} - 1 \right] \right\} \tag{10.1}$$

where $\dot{N}_q$ and $\dot{N}_f$ are the nucleation rates under flow and quiescent conditions respectively, K is a constant taking into account energetic and geometrical factors of nuclei, n is a coefficient specific to crystallization temperature having values of 1 or 2. The most crucial parameter of FIC used in this and many other models is a dimensionless induction time of crystallization:

$$\Theta = \frac{t_{if}}{t_{iq}} \tag{10.2}$$

where t_{if} and t_{iq} are the induction times under flow and quiescent conditions, respectively.

A number of different techniques are used for studying of flow-induced crystallization including optical microscopy, XRD and rheometry. The use of a rheometer is a very convenient technique for application of precise shear rate to polymer melt and simultaneous observation of the development of crystallinity by means of viscosity or loss modulus. Due to the simplicity of the use and high accuracy of measurements, the rotational rheometers are the most popular. Both plate-plate [179, 182-185] and cone-plate [186,187,188,189] geometries are used in FIC studies.

While the application of precise shear rate in experimental studies is not an issue for modern equipment, the determination of precise induction time from rheological data seemed to be problematic. The most popular method involves defining two tangents to the viscosity (or storage modulus) vs. time curves and then taking their intersection as the induction time [180,184,190]. Nobile et al. [186] determined the induction time as the moment when the viscosity of the melt increased by a specified value. Another approach to determine induction time is to define it as a moment of time when a sudden upturn of viscosity curves is observed [179,188]. Chen et al. [191] defined in their study induction time as the moment of time when normal force increases twice as compared to initial value. They found that in some cases the normal force is a parameter which is more sensitive to onset of crystallization than viscosity. Nevertheless it should be noted, that for cone-plate geometry the measurements of correct normal force represents a difficult and non-trivial problem demanding high temperature and instrument accuracy [192]. Often the induction time values obtained using these techniques are referred as "instrumental" [193], "rheological" [187] or "viscosity" induction time. The use of these

techniques results in enormous variation in reported induction times, as the determination of the location of the tangent points and/or the cut-off value of viscosity are somewhat arbitrary. Moreover, the induction times determined using these techniques are dependent on the rheology of non-crystallizing melt which is not related to flow-induced crystallization in any way.

In this research we studying the flow induced crystallization of polylactide using induction time determined using the technique proposed in our previous study [134]. Very few studies have been done on shear induced crystallization of polylactides despite its increasing field of applications. It will be shown later that the use proposed standardized residuals technique allows to determine induction time with much higher precision than previously used techniques.

10.2 Experimental

The polylactide sample used was supplied by Biomer (Germany). It is a commercially available poly(L/D-lactide) copolymer containing 2 % of D-lactide (L 9000). It was found via gel permeation chromatography measurements that this polymer has a number average molecular weight of 50,000 and a polydispersity index of 2.0. The pellets were thoroughly dried at 80 °C in a vacuum oven for 24 hours prior to pressing at 185 °C in a Carver hydraulic press. This procedure allowed the decrease of adsorbed water content in the polymer from 0.26 wt% to 0.03 wt% significantly suppressing influence of hydrolysis during the rheological measurements. Subsequent experiments

showed no significant decrease in water content with increase of drying temperatures and times.

The rheological measurements were performed under a nitrogen atmosphere with oxygen content of less than 2.5 ppm in a modular compact rheometer (MCR 500 model) supplied by Anton Paar. The use of liquefied nitrogen as source of protective media during experiments allowed avoiding influence of humidity in nitrogen. All SAOS experiments used to determine the quiescent crystallization induction time were done using CP25-1 cone-plate configuration with 1.007 degree cone angle and 43 μm truncation and PP25-1 plate-plate configuration with 1 mm gap in linear viscoelastic regime at 5% strain and 1 Hz. The small strain value and allowed us to avoid shear induced crystallization. It was found that this strain-frequency combination is located in linear viscoelastic zone over our temperature range The homogeneous crystallization conditions were ensured by a brief heating of each sample to 190 °C directly inside rheometer to eliminate any residual crystallinity prior to dropping the temperature to within the crystallization regime and starting the rheological measurement.

10.3 Results and Discussion

10.3.1 Specifics of the Geometry of the Measuring System in Context of the Shear-induced Crystallization Experiments

Though both cone-plate and plate-plate geometries are equally popular for viscosity measurements there are significant differences in the results when these two different geometries are used for shear-induced crystallization studies. This difference

comes from the very nature of the measuring systems and thus cannot be ignored. The main difference between cone-plate and plate-plate geometries lies in radial strain rate distribution applied to the polymer melt. While in cone-plate geometry the strain rate is uniform and depends only on rotational speed (with the exception of the negligibly small truncated area), the polymer melt in parallel plate geometry is subjected to variable strain rate increasing from the plate's axis to the edges. This makes it impossible to apply a uniform strain rate to a polymer melt in the plate-plate geometry. In stress-induced crystallization studies this results in non-uniform crystallization of polymer melt where crystallization starts from the sample's edges where strain rate is the highest and gradually propagates to the centre of the sample. This phenomenon is illustrated in Figure 10.1.

Figure 10.1 Photograph of polylactide sample subjected to shear-induced crystallization in plate-plate geometry. The crystallization starts at sample's edges (white area) and propagates to the centre over the time. The sample's central area that was subjected to lower shear remains amorphous and transparent for a significantly longer time.

Also, note the nonuniform thickness of the outer crystalline ring in Figure 10.1. The crystallizing layer of polymer is significantly less compliant compared to the amorphous melt and continued shear deformation breaks this layer forcing it to mechanically propagate towards the centre of the disk.

Thus the viscosity measured by plate-plate in stress-induced crystallization is a result of a complex system with non-uniform crystallinity across the sample. All this makes rheological data used in stress induced crystallization studies obtained using plate-plate geometry unsuitable for crystallization process evaluation. It should be noted that the evolution of the complex viscosity in an experiment using plate-plate geometry can be successfully monitored for quiescent crystallization from melt.

The dramatic difference between these two systems can be readily seen from Figure 10.2. Clearly, the complex viscosity data obtained from the plate-plate geometry are not representative of crystallization of the melt after the onset of crystallization. Certainly, the induction time, determined from these two curves using any fixed change in viscosity or using the intersection of tangent lines applied to any arbitrary points would be significantly different and clearly not reflect real value of induction time at all. These approaches lead not only to significantly increased measured induction times but also to a very common opinion that rheological measurements are insensitive to the onset of polymer melt crystallization [193,194,195,196].

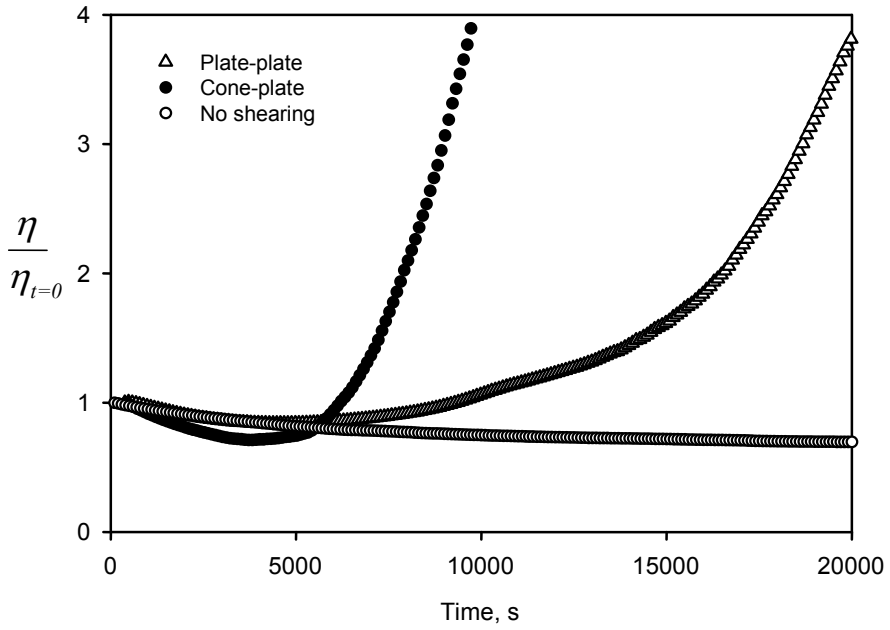

Figure 10.2 The comparison of development of the reduced zero shear complex viscosity of L 9000 polylactide previously subjected to 1 s^{-1} shear for 120 s at 155 °C measured using different measuring system geometries. The SAOS frequency is 1 Hz and strain is 5%. The viscosity of not previously sheared polylactide had been obtained using plate-plate geometry and is given for reference.

It should be noted that the use cone-plate geometry in FIC experiments can have significant limitations. The most unavoidable source of errors is the flow irregularity (sometimes referred to as edge fracture) [197,198]. It is accompanied by a significant distortion of melt's free surface during steady shear. The melt distortions grow rapidly inward in the sample leading to a decrease of effective radius of the sample [199]. As a result, viscosity data obtained using cone-plate geometry at higher shear rates reflects the viscosity of a sample of unknown shape rather than the real rheology of polymer melt. This can be seen from Figure 10.2; the viscosity measured by the cone-plate setup drops

significantly faster than that measured in the plate-plate configuration during the first 5000s. This also contributes to the necessity to develop a technique capable of handling flawed rheological data and reliably allowing for the determination of induction time.

10.3.2. The Effect of the Surface Crystallization on Rheology of the Crystallizing melt

Another important factor contributing to viscosity measurements is the surface nucleation phenomenon which is mostly overlooked in rheological studies. Surface crystallization is heterogeneously nucleated crystallite growth occurring on contact of polymer melt with many foreign phases. In extreme cases the surface crystallization can form transcrystallinity – a layer of crystalline polymer propagating from the contact surface. While being quite a common phenomenon, surface crystallization was never considered in scope of its effect on the rheology of a crystallizing melt before, even though its effect can be quite dramatic. Surface crystallization of polylactide was thoroughly studied by Yuryev and Wood-Adams for the polylactide – aluminum interface [160]. Since the surface crystallization is localized on the interface, its effect has a pronounced thickness dependency, becoming more significant with decreasing of gap in the measuring system geometry. Since the impact of surface crystallization on measured viscosity depends on the distance from the measuring system axis it is the effective gap which should be considered rather than just an average gap. An effective gap is a measure of equivalent distance between the plates in terms of local rheological input. As a result, the geometry having a higher effective gap is less susceptible to surface crystallization.

Surface crystallization, if present, leads to suppression of the observed induction time. The relative influence of the surface crystallization is inversely proportional to the effective gap. Therefore, it could be expected that data generated at lower gaps would be more affected by surface crystallization and there will be a minimum gap only above which viscosity data are representative of homogeneous crystallization. It should be noted that the surface crystallization phenomenon itself also demonstrates a small but noticeable temperature dependency and the effect of the surface crystallization decreases with decreasing temperature [160].

Surface crystallization is a factor which is very difficult to avoid. As result, we have an impressive list of factors which affect an observed induction time of crystallization: an effective gap, temperature dependant surface nucleation concentration, spherulitic growth rate, shear rate, bulk nucleation rate among others. Thus, it is very difficult to be very certain in the determination of induction time, nevertheless it is possible to suppress the affecting factors to acceptable level if certain precautions are made.

Typically, the plate-plate geometry is better suited for induction time measurements in FIC experiments. The shear rate is not constant across the sheared area in plate-plate geometry and the preset shear rate is achieved only at the plate's edge. It results in weaker overall increase of measured viscosity. Nevertheless, it will be shown later that our approach allows us to precisely identify the crystallization onset. When the cone-plate geometry is used, surface crystallization effects must be taken into account. Low cone angles result in very small effective gap and the heterogeneous surface crystallization significantly affects the measurements. For example, for the CP-25-1

cone-plate system the gap ranges from 22 μm in the middle of the disk to 273 μm at the edge which is not enough to exclude the effects of surface crystallization. Higher cone angles provide wider gap which may be sufficient to diminish effects of surface crystallization.

10.3.3 The Standardized Residuals Approach to Crystallization Onset Determination: Practice and Rheological Data Evaluations

All of the aforementioned complexities lead to the necessity to develop a more consistent approach for rheological data analysis which would be based on real effects of crystallinity on polymer melt properties. This approach was introduced and described in detail by Yuryev and Wood-Adams [134]. In the current FIC study we used the standardized residuals approach which was previously successfully implemented in quiescent polylactide crystallization studies using small amplitude oscillatory shear (SAOS).

This technique is based on the detection of deviations from an empirical fit of viscosity curves of non-crystallizing polymer melt using standardized residuals according to the equation:

$$r_i = \frac{e_i}{\sqrt{\hat{\sigma}^2}} = \frac{e_i}{\sqrt{\frac{1}{n-1}\sum_{i=1}^{i=n}\left(e_i - \bar{e}\right)^2}} \qquad (10.3)$$

where e_i is the real residual, i.e. the difference between measured viscosity and corresponding value of the fit equation and the divider is the square root of the unbiased estimator. The onset of crystallization causes increasing deviation from the model

resulting in a steady growth of residuals. Typically the onset of crystallization can be easily recognized by sharp change of the behaviour of the residuals from random variation inside the adequacy band to continuous steady growth (Figure 10.3).

Three basic scenarios are possible while a polymer melt is kept above the crystallization temperature. First, the polymer can exhibit little or no change in viscosity over an extended period of time, in other words, be rheologically thermally stable; second, the viscosity can decrease over the time due to thermal degradation, hydrolysis or oxidation, and, third, viscosity can increase due to repolymerization or cross-linking. Regardless of its pattern, the viscosity data of a non-crystallizing melt can be fitted using relatively simple empirical equations. It should be noted that in most cases there is no need to relate fitting coefficients to real reaction constants describing reactions undergoing in the polymer melt. The series of viscosity measurements at higher temperature range when no crystallization occurs give a clear idea of the functional relation between viscosity and time. Of course, the possibility exists that some reactions occur at elevated temperatures which do not occur at lower crystallization temperatures; this should be considered on a case to case basis.

The thermal degradation is observed for many polymers and mechanisms of this degradation are determined by the chemical structure of the polymer chain. The presence of oxygen and water can both significantly increase degradation rate and complicate the mechanisms of degradation. In this study we attempted to limit degradation processes to thermal degradation only.

For this particular case, the zero shear viscosity of polylactide melts can be well described by the exponential decay equation:

$$\eta^*_{0,t} = \eta^*_{0,t=\infty} + C\exp(-\frac{t}{\tau}) \qquad (10.4)$$

where $\eta^*_{0,\ t=\infty}$ is a limiting zero shear viscosity at long times, C is the viscosity decay coefficient, and τ is the thermal degradation exponential term. It was established that Equation (10.4) which well describes viscosity evolution at elevated temperatures is also applicable at whole range of polylactide crystallization at least to 140 °C [134].

Typically, the standardized residual remains within the ±2 limits if only degradation is occurring. Upon reaching the onset of crystallization the residual begins to grow steadily and rapidly exceeds 2 (Figure 10.3). The moment of time when the residual begins steady growth is considered to be the crystallization onset.

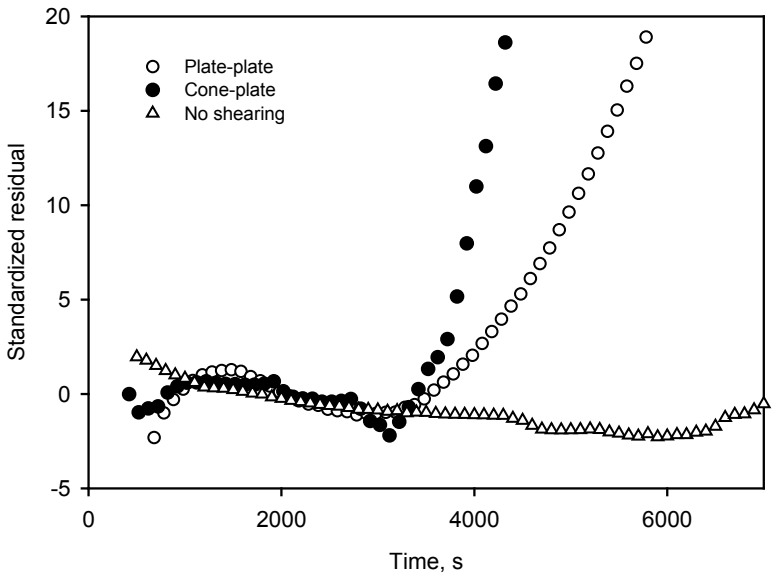

Figure 10.3. The standardized residuals of viscosity curves from Figure 10.2 derived from the exponential decay fits. The induction time of quiescent crystallization of polylactide at 155 °C is 35100 s.

From Figure 10.3 it is clear that the application of the correct technique to determine the onset of crystallization allows using even data obtained from the plate-plate geometry. The transition point for the case of plate-plate geometry is not as well defined as it is for cone-plate geometry; nevertheless it allows for the identification of the crystallization onset.

10.3.4 An Induction Time of the Polylactide Crystallization Under Continuous Constant Shear

As was already pointed out, it is very important to establish the correct functional dependency of induction time regarding the crystallization temperature. The studies done previously [134] (Figure 10.4) showed that rheological data could provide reliable data on induction time.

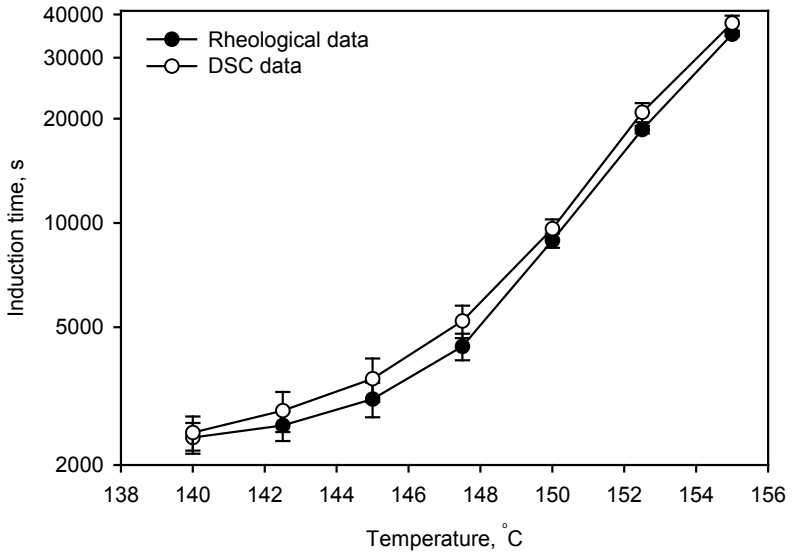

Figure 10.4 Induction time of the quiscent polylactide crystallization observed by rheology and DSC. Data are taken from reference [134] (also Chapter 5 of this thesis).

SAOS measurements are not applicable when steady constant shear is applied to polymer melt. As it was shown before [134] rheological parameters other than the complex viscosity can be used for induction time determination. In our continuous shear experiments, viscosity was used to monitor polylactide crystallization. Continuous shear experiments were done in the range of shear rates of 0.01 s^{-1} – 1 s^{-1}. The shear rate of predetermined amplitude was imposed on polymer melt upon reaching the set point temperature and maintained throughout the entire experiment. The lower limit was determined when it was not possible to experimentally detect changes of induction time as compared to quiescent crystallization. Though the experimental setup was capable of producing shear rates exceeding 1 s^{-1} the upper limit was determined by edge fracture which made the correct measurements of viscosity impossible. The melt fracture phenomenon is an ejection of the polymer melt from rheometer setup after certain level of shear rate is exceeded which in turn is the result of the melt flow instability (See Chapter 10.1). The experimental results for three different temperatures are shown in Figure 10.5.

From Figure 10.5 it can be concluded that while maintaining similar functional dependency on shear rate observed in many studies, the temperature dependency is significantly different from that observed in previous studies [180, 186, 188, 193]. The most probable cause of this peculiar behaviour is the technique used to determine the induction time. As it was mentioned before, the techniques typically used to determine the induction time tend to overestimate it and elimination of this overestimation has a different effect at different temperatures. The shorter induction time becomes significantly more affected by this overestimation than longer induction time, and as

result; the temperature dependency becomes reversed relative to the majority of previous observations. Eventually, other reasons related to experimental setup and conditions also cannot be excluded.

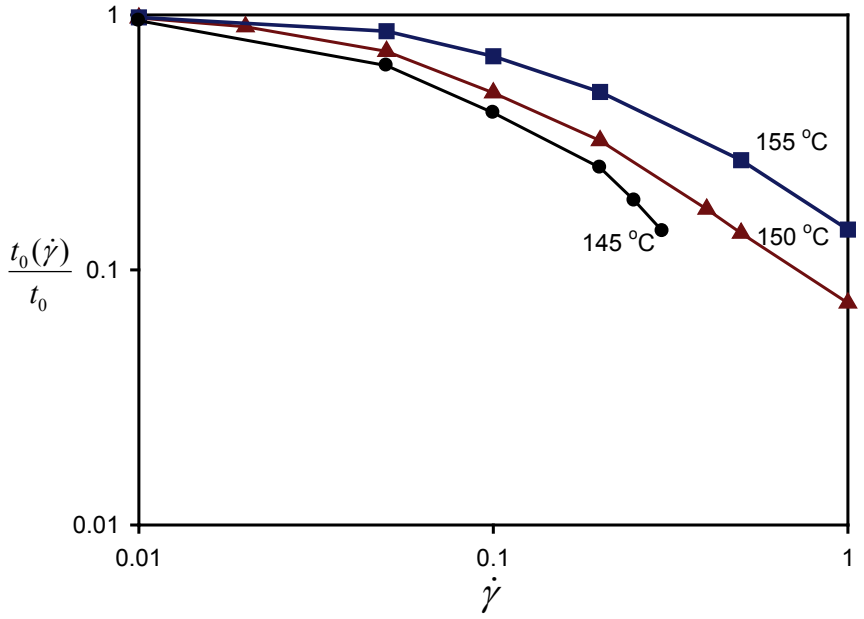

Figure 10.5 The relative induction time of polylactide crystallization depending on continuous shear rate at different temperatures. The *Y* axis represents the relative suppression of the induction time under continuous shear expressed as ratio of the induction time under shear to quiescent induction time and the *X* axis is the shear rate.

It could be concluded that this behaviour is not specific to poly(lactide) and reflect more general behaviour of crystallisable polymers. Unfortunately, there is no theory at this moment which successfully explains the observed induction time evolutions therefore; more studies are necessary to reveal such functional dependence. It is widely accepted that product of induction time t_i and the nucleation rate I is a constant [200]:

$$t_i(T)I(T) = K \tag{10.5}$$

This assumption based on the Zeldovich-Becker-Doering nucleation theory [201,202]. While Equation 10.5 has not been proven to be correct experimentally most studies do not contradict to it directly. Nevertheless, it cannot be excluded that the relation between nucleation rate and induction time is more complex than it is believed at least for some crystallizing polymers. Eventually, there are more hidden obstacles to deeper understanding of flow induced crystallization that need to be revealed.

10.3.5 An Induction Time of the Polylactide Crystallization under Step Shear

The step shear experiment allows observation of polymer melt crystallization subjected to constant shear rate for predetermined period of time followed by crystallization in the absence of shear. Continuous shear crystallization is a special case of crystallization under the step shear having shearing time of $t_s=\infty$. Therefore, the step shear experiments potentially could provide a valuable knowledge regarding the shear induced crystallization.

It should be noted that the step shear experiment is more demanding for the rheometer regarding start-up time and shear rate stability control. For our experiments we conducted a separate study to determine the optimal rheometer control parameters for step shear experiments. Using the customized set of control parameters the shear start-up and cessation times were reduced to less than 3 *s* which was more than an order of magnitude less than shearing time even for the shortest shear steps.

The induction time in step-shear experiments were also determined using the standardized residuals technique (Figure 10.6). It's interesting to note that the induction

time decrease reaches to the constant shear induction times at approximately the same $t_s\dot{\gamma}$ values for the shear rates in the range of 0.05 s^{-1} – 0.5 s^{-1}. For low rate step-shear there is an initial plateau where short time shearing has no visible effect on the induction time. From the other side, for higher shear rates the effect of step-shear on induction time is noticeable even at short shearing times.

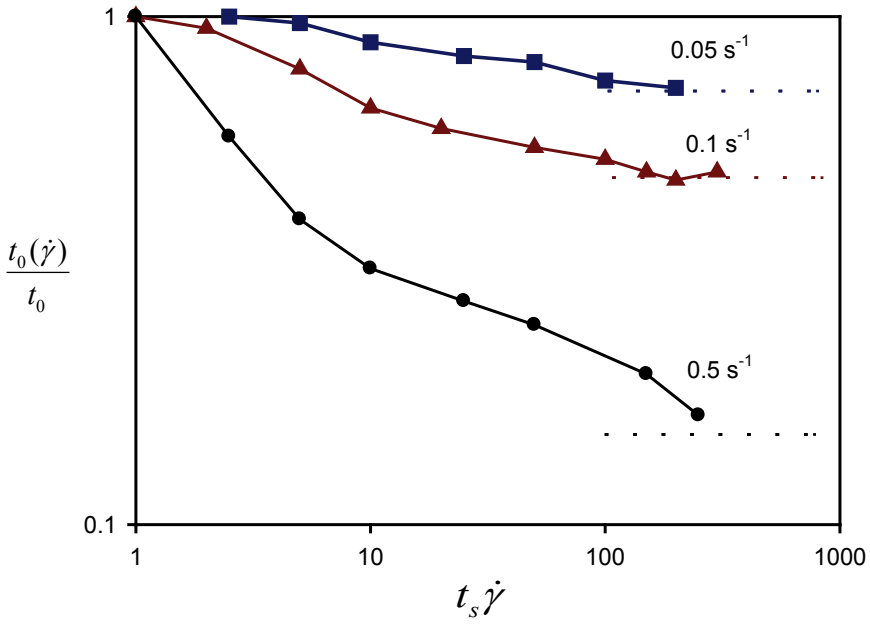

Figure 10.6. The relative induction time after the application of step shear. The temperature was 145 °C. The X axis represents the product of the shearing time and the shear rate. The dashed lines represent a reduced induction time for continuous shear.

Eventually, the most critical parameter for nucleation is maximum achieved degree of orientation of polymer chains. The applied shear causes polymer chain orientation along the shear direction and degree of the orientation depends on both shear rate and the shearing time. Therefore, the induction time steadily decreases with increasing duration of the shear step until maximum alignment is reached. After the

maximum orientation is reached the induction time of the crystallization is equal to that for continuous shear.

10.4. Conclusion

In our study it was found that flow induced crystallization apart of being a complex phenomenon also contains significantly controversial approaches to its studies. It appeared that the biggest concern for FIC studies is a correct determination of the induction time. The absence of scientifically sound approaches to this issue enormously complicates research in this challenging field. Only after such techniques are developed significant progress in FIC studies could be achieved. In this study we attempted to propose such an approach and demonstrated its validity. The standardized residual approach provides a sound research technique which could be applied for all FIC studies. We believe that the use our technique would provide more reliable data which would provide so much needed solid grounds for FIC theory development. Nevertheless further studies using the proposed techniques are needed in order to standardized residual technique become an accepted research practise.

Another significant effect which was largely overlooked in FIC studies is surface crystallization. That is why we have put effort to reveal the existence and magnitude of this phenomenon. Our studies showed that that surface crystallization cannot be neglected in FIC studies. Eventually all FIC studies should include an evaluation of the surface crystallization effects for each particular polymer-surface pair before the FIC study itself can be started.

CHAPTER 11

Conclusions, Contributions, and Recommendations for Future Work

11.1 Conclusions

It was found that while a poly(L-/D-lactide) copolymer exhibits the typical bell-shaped crystallization rate-temperature dependence, poly(L-lactide) exhibits an nonsymmetrical behavior, having two crystallization rate maxima at 105ºC and 130ºC. The different types of crystalline formations exhibited at the surface of polylactide films are shown and discussed. At low supercooling, several different scenarios of individual crystal formation were observed: purely flat-on stacks, purely edge-on stacks, and edge-on crystals flipping to flat-on crystals and vice versa, where flat-on crystals yield edge-on sprouts. The preferred direction of the growth of lamellae of both poly(L-lactide) and poly(D-lactide) was found to be counter-clockwise relative to the free surface. The effects of stereocomplexation on polylactide's growth rate and spherulitic morphology were studied.

The evolution of complex viscosity of a polylactide due to thermal degradation in the absence of crystallization was studied. A simple empirical model was used to characterize the variation of complex viscosity due to thermal degradation and to determine the induction time of homogeneous crystallization at a wide range of degrees of supercooling. The evolution of complex viscosity due to crystallization was measured at several temperatures. Based on the results, a phenomenological model describing the viscosity evolution during homogeneous crystallization was proposed and validated. Finally, the linear viscoselastic data in the early stages of crystallization were shown to be

consistent with gelation due to the formation of a network of tie molecules between spherulites.

Surface nucleation of poly(L/D-lactide) at the interface with aluminium was studied by performing isothermal DSC analysis of amorphous samples of varying thickness between 100°C and 130°C. To ensure complete wetting of the aluminium surface, a hot melt laminating process was used to prepare the samples. Theoretical aspects of surface crystallization kinetics were explored and the resulting model was compared with the results of Monte Carlo simulations. Three stages of surface crystallization were identified depending on the growth geometry: (1) impingement-free growth, (2) increasingly laterally constrained transverse growth, and (3) interstitial growth. By fitting the Monte Carlo simulation to the experimental half-times of crystallization, the surface nucleation concentration and bulk nucleation rate were estimated at four different temperatures. It was found that both surface nucleation concentration and bulk nucleation concentration decrease with increasing crystallization temperature.

The flow-induced crystallization of polylactide was studied using rheological measurements. It was found that the previously validated technique for determination of the induction time is suitable for shear-induced crystallization studies as well. The effect of different setup geometries on measurements was studied and the effect of the surface crystallization on FIC crystallization measurements was evaluated. It was found that the functional dependency of induction time and shear rate on temperature is significantly different from that observed in other studies. This observation was attributed to the new induction time measurement technique which yields results significantly different from

the ones obtained using previous techniques. While it is widely accepted that induction time is inversely proportional to nucleation rate there is still no experimental proof to this concept. Our studies suggest the possibility of a more complex relation of induction time and nucleation rate.

The effect of a static electric field of varying intensity (0-2.4×10^5 V/m) on crystallizing polylactide melt was studied at five different temperatures. The crystallinity enhancement effect increased both with crystallization temperature and applied electric field intensity. The crystallization kinetics at lower temperatures showed no such effect. An XRD analysis demonstrated an identity of crystalline structure of polylactide crystallized in the presence and absence of an electric field, allowing the attribution of the observed effect to increased nucleation density or growth rate. Polarized optical microscopy showed that polylactide continued nucleation during the application of the electric field while nucleation in the control sample was almost entirely simultaneous.

It was found that both flow induced crystallization and electric field induced crystallization facilitate crystallization. However, there are significant differences between these phenomena. The most notable difference is that flow has a pronounced effect on induction time while electric fields do not. Still, it cannot be excluded that electric field could affect the induction time at higher field intensities. While there is no solid experimental proof for flow induced crystallization, it seems that spherulitic growth rate is not affected by the magnitudes of the external fields studied here which allows us to attribute crystallite growth kinetics solely to thermodynamic effects and polymer chain parameters and its properties. It means that at relatively low intensity both flow and electric fields affect the nucleation process but subsequent crystallite growth is

determined mostly by thermodynamic parameters of the melt not affected by external fields.

11.2 Contributions

During this research, various aspects of polylactide crystallization were studied. Most findings and results could be extended to other studies of polymer crystallization.

A new AFM-based technique for the spherulitic growth rate measurements was developed and validated. The isothermal spherulitic growth rate and its dependence on temperature were studied using tapping mode atomic force microscopy and *ex situ* isothermal crystallization. Using this technique, it is possible to extend spherulitic growth rate measurements to a region of significantly higher supercooling, where nucleation concentration makes the use of *in situ* hot stage optical microscopy impossible. The crystallization kinetics of blends of poly(L-lactide) and poly(L/D-lactide) with poly(D-lactide) were studied using the proposed approach. The crystalline long spacing of poly(L-lactide) was also measured directly using tapping mode AFM.

The rheology of the polylactide was extensively studied and modeled using the proposed physical cross-linking model. Linear viscoelastic properties of polymer melts are highly sensitive to any structural changes, including molecular weight changes and the formation and growth of crystallites. This sensitivity was used to study the homogeneous crystallization of polylactide. Since this polymer is rather quickly susceptible to thermal degradation, even at moderate temperatures, it is essentially impossible to study homogeneous crystallization in the absence of degradation. A new

technique for induction time determination was proposed and validated. Unlike existing techniques our technique is based rather on physical effects of crystallization on viscosity than arbitrary changes of parameters. Also, a new theoretical model describing the viscosity dependence on crystallinity was introduced and discussed. This model combines both theoretical and empirical concepts and potentially has significant perspectives for crystallization studies.

Extensive studies of the flow-induced crystallization of polylactide were performed. The range of applicable shear rates for rotational rheometry was investigated. The validity of different approaches to field-induced nucleation were studied and discussed. It was found that the temperature-shear rate dependency of the induction time of crystallization cannot be successfully explained by existing models. This was attributed to the new advanced technique of induction time determination proposed in this study. Experiments suggested that the maximum degree of chain orientation is a decisive parameter for induction time.

For the first time, the enhancement of melt crystallization kinetics of the poly(L-/D-lactide) (A1-type polymer) in the presence of a static electric field was observed through the measurement of the melt viscosity using Small Amplitude Oscillatory Shear (SAOS). It was shown that the nucleation rate of crystallization is significantly accelerated in presence of an electric field. The application of the previously introduced model for relating viscosity to crystallinity was successfully attempted. The analysis using the suggested model demonstrated that enhancement of crystallization is induced by homogeneous nucleation.

11.3 Recommendations for Future Work

There are several directions in which the ideas presented in this research could be extended:

I. The rheological model of polylactide's crystallization could be extended to the crystallization of other polymers. Indeed, the model that was presented here is general by nature and contains all components necessary for application to the crystallization of different polymers. Such research could provide a tool for the rheological measurement of viscosity, which could be used when other techniques (for example, DSC) cannot. The fields where such a technique could be especially successful do include slow crystallizing polymers, when crystallization heat from the polymer sample becomes virtually indistinguishable from the noise level.

II. The technique for determination of induction time, successfully developed and presented in this study, provides a great opportunity to finally get reliable information on the thermodynamics of homogeneous crystallization. It is especially important in the scope of studies on shear-induced crystallization, where correctly determined induction time has a profound effect on the model's outcome.

III. The theoretical model of surface crystallization and its experimental validation opens up numerous possibilities for the reinterpretation of thermal analysis results for various polymers. While surface crystallization is not a new phenomenon and has been described in numerous studies, in many cases, it can significantly affect the results of thermal analysis. The use of relatively small samples makes this

effect especially noticeable. Poorly correlating DSC data were usually explained by nonequilibrium thermal conditions in the sample, and surface crystallization effects were completely missed in most studies. Our studies indicate that even when nonisothermal effects are efficiently eliminated, the surface crystallization has an enormous impact on overall crystallization kinetics.

IV. The simulation program that was created during this study has a huge potential for modelling various aspects of polymer crystallization kinetics. One of the applications could be its use in the modelling of nonisothermal crystallization. It is well known that no nonisothermal crystallization theory can explain the kinetics of crystallization in the vast majority cases, and the Monte Carlo simulation could provide a great help in overcoming of this issue.

V. The studies of the electric field-induced crystallization of polymers containing polar repeat units is a largely unexplored field, and further studies in this direction promise a deeper understanding of the mechanisms of nucleation and molecular dynamics. Especially promising is the application of rheology in these studies.

VI. The rheological studies of polylactide revealed that complex viscosity could be a reliable and sensitive indicator for its degradation. It could be very interesting to use rheology to explore the degradation of polylactide under different conditions. Also, these studies can be of both theoretical interest and significant practical benefits.

Appendix 1

Monte Carlo Simulation of polymer crystallization

A generalized stochastic Monte Carlo simulation schematic is given in Figure A1.1.

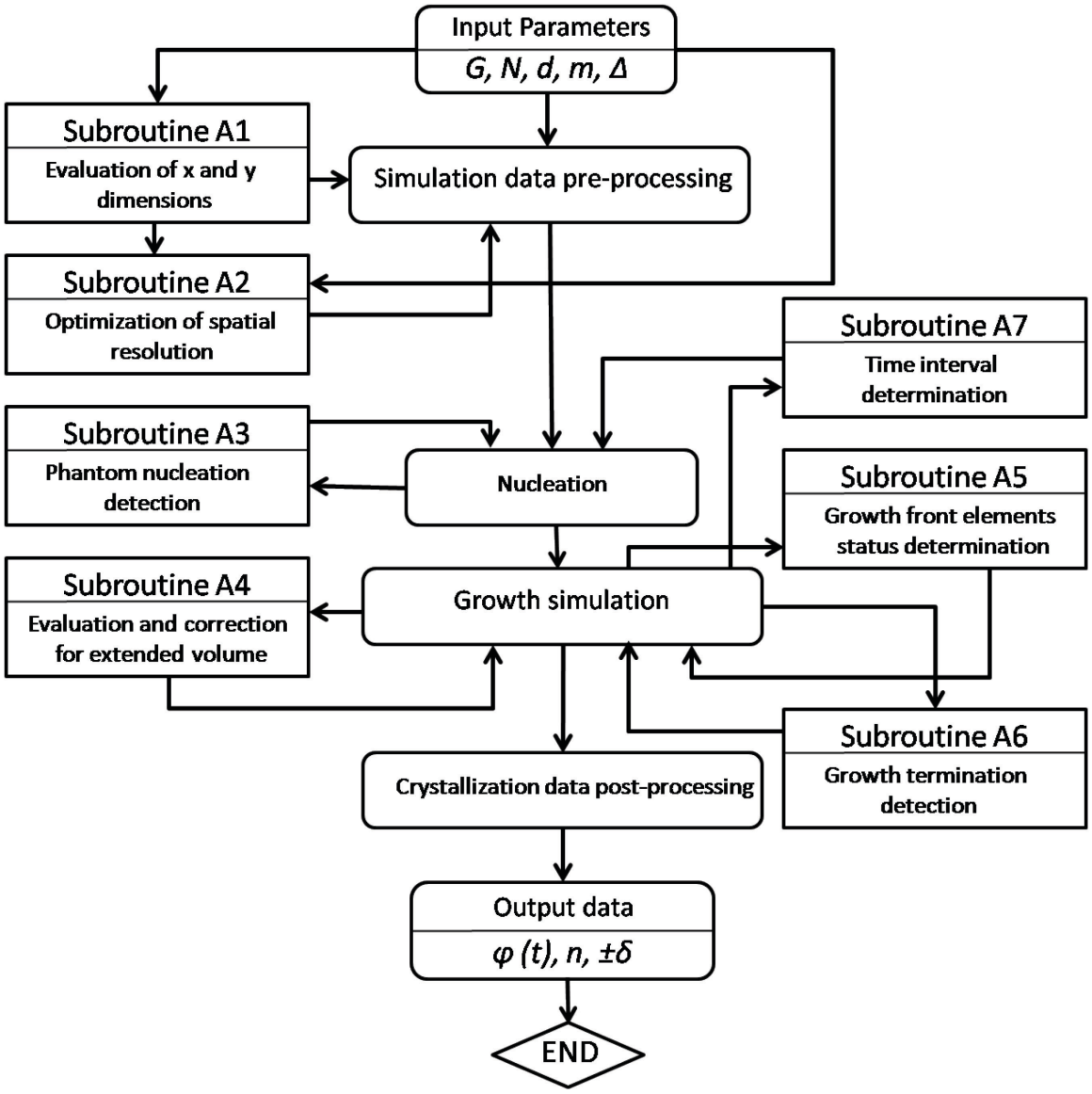

Figure A1.1. A simplified algorithm of the Monte Carlo simulation.

Description of the subroutines

Subroutine A1

This subroutine uses the input parameters to estimate the x and y dimensions so simulated volume mimics the behaviour of infinitely extended plate with preset tolerance Δ regarding to the average Avrami exponent from three simulations. It was considered that x and y dimensions were sufficiently extended and could be considered to be infinite when the change in the average Avrami exponent did not exceed 0.05 after the x and y dimensions were extended by 25%. For this purpose it employs the core simulation engine.

Subroutine A2

This subroutine optimizes the distribution of m elements over all three dimensions to reach the highest possible simulation precision. Since the aspect ratio of the simulation volume can be very high, the assignment of equal resolution in all dimensions would lead to poor resolution in the extended directions. This leads to increased variation in the Avrami exponent between simulations. From a separate study it was found that the size of the element in the constrained dimension a_z should be at least two orders of magnitude smaller than the product of growth rate G and the half time of crystallization $\tau_{1/2}$ to ensure sufficient precision.

Nucleation

All three coordinates of nuclei were independently generated in terms of simulated volume. The coordinates of the nucleus *i* are determined as:

$$x_i = R_x a_x s_x \qquad \text{(A1.a)}$$

$$y_i = R_y a_y s_y \qquad \text{(A1.b)}$$

$$z_i = R_z a_z s_z \qquad \text{(A1.c)}$$

where R_k are random numbers between 0 and 1, s_x, s_y and s_z are the numbers of simulation elements in x, y and z axes respectively. This approach allows for equal probability of formation of a nucleus at any point within the simulation volume.

Subroutine A3

The probability of nucleation in simulated volume is equal for any coordinate and nucleation can happen in already crystallized space (this is the so-called phantom nucleation [93]). This type of nucleation must be eliminated since it would be absorbed by the transformed phase in real conditions. Thus, the status of the newly generated nuclei must be verified prior to being allowed to grow. The probability of newly generated nucleus being phantom is equal to the fraction of transformed volume and therefore ranges from 0 at onset of crystallization to 1 for completely transformed material. When a phantom nucleus is generated, it is rejected and a new nucleus generated until the generated nucleus is placed in untransformed phase.

Growth Simulation

The crystallizing entities are represented as spheres of radius r_i. The growth rate G considered constant and equal for all entities:

$$r_i(t) = G * (t - t_i) \qquad \text{(A1.2)}$$

where t_i is a time of nucleation of nucleus i and t is a absolute simulation time.

Subroutine A4

This subroutine accounts for extended volume appearing during simulation by detecting and accounting for the elements virtually belonging to more than one entity. From the point of view of real crystallization this subroutine handles impingement events. The extended volume concept is well illustrated in ref. [203]. All simulated volume elements are assessed regarding their status regarding all traced crystallizing entities. The input of each element to overall transformed fraction is limited to unity eliminating multiple contributions to crystallinity from each element.

Subroutine A5

Though the precision of the simulation could be increased by increasing the number of elements, in the end it is always determined by the ratio of spherulite size to element size. At the initial stages of crystallization, for each particular entity, the number of its elements which include both crystalline and amorphous phase will be high and we

require a sophisticated algorithm for the evaluation of crystallinity content of such elements. Raabe [129,130] used simple a randomization of crystallinity of those elements regardless of their real position relative to the growth front. Our simulations showed that this approach does not give satisfactory precision mostly because the spherulite border elements are cut by a portion of a sphere which has a convex shape. This leads to the overestimation of the crystallinity of the border elements φ_{el} and a more advanced algorithm was implemented in our A5 subroutine. It employs the following empirical function which we developed to evaluate the degree of crystallinity of the border element using the immersion factor (*IF*). The *IF* is the ratio of the difference between the spherulite radius (r) and the shortest distance from the nuclei coordinate to a corner of the element (c_{min}) to the longest dimension of the element (a_x):

$$\varphi_{el} = \frac{IF}{\sqrt{2 + \left[\frac{a_z}{a_x}\right]^2}} = \frac{(r - c_{\min})/a_x}{\sqrt{2 + \left[\frac{a_z}{a_x}\right]^2}} \qquad \text{(A1.3)}$$

Subroutine A6

While the simulation can be done until crystallization is complete it should be noted that the necessity to trace all growing entities gradually slows down the speed of simulation as crystallinity increases. Since there is no need in complete set of crystallization kinetics data, the A6 subroutine terminates the simulation termination when the simulated crystallinity reaches a preset limit.

Subroutine A7

Each simulation interval is determined by the time of subsequent nucleation. This results in a variable time step where the time of step *i* is defined as:

$$t_i = t_{i-1} + \frac{1}{N(1-\varphi_{i-1})V} \qquad \text{(A1.4)}$$

where t_{i-1} is the absolute time of the preceeding nucleation event and φ_{i-1} is the overall crystallinity at that time.

Crystallization data post-processing

At this stage the obtained crystallization kinetics data are transformed for Avrami fit as *ln t* vs. *ln(-ln(1-φ))* and linear regression is performed. The Avrami exponent is defined as a tangent of resulting linear regression. Finally, the standard deviation δ of the Avrami exponent over five simulations is calculated.

Crystallization parameters and data handling

The probability of the formation of a crystallization site (nucleus) was considered to be equal for all volume of untransformed matter. Nevertheless, it should be noted that there are numerous circumstances associated with surface nucleation which lead to nucleation probability on surface to be higher than average.

Both nucleation *N* and growth rates *G* are governed by thermodynamic parameters of crystallization and the composition and length of the polymer chain and

vary greatly with temperature. For isothermal conditions, N and G can be accepted as constants with significant degree of confidence since the temperature is the only parameter affecting these values for a particular crystallizing polymer. Thus, the nucleation rate N was set to be constant in each particular simulation and the time of each consequent nucleation event was proportional to the nucleation rate and amount of untransformed material. The growth rate G was also set to be constant and equal in all three dimensions ($G_x = G_y = G_z$) and diffusion-independent. This consideration is applicable for most cases of isothermal crystallization. The ratio ρ_c/ρ_l is accepted to be equal to 1 to avoid polymer-specific simulation bias.

References

[1] J. Lunt, A. L. Shafer; Polylactic Acid Polymers from Corn. Potential Applications in the Textiles Industry; Cargill Dow Polymers LLC, Minnetonka, MN 55345.

[2] Ray SS, BousminaM ; Progress in Materials Science 50 (2005) 962–1079

[3] Hoogsteen W, Postema AR, Pennings AJ, Ten Brinke G, Zugenmaier P; Macromolecules, 1990; 23:634.

[4] De Sanctis P, Kovacs AJ; Biopolymers, 1968 ;6:299.

[5] Eling B, Gogolewski S, Pennings AJ; Polymer, 1982;23:1587.

[6] Puiggali J, Ikada Y, Tsuji H, Cartier L, Okihara T, Lotz B; Polymer, 2000 ;41:8921.

[7] Brizzolara D, Cantow HJ, Diedrichs K, Keller E, Domb AJ; Macromolecules, 1996;29:191.

[8] Cartier L, Okihara T, Ikada Y, Tsuji H, Puiggali J, Lotz B; Polymer, 2000 ;41:8909.

[9] Marega C, Marigo A, Di Noto V, Zannetti R; Macromol Chem, 1992;193:1599.

[10] Abe H, Kikkawa Y, Inoue Y, Doi Y; Biomacromolecules, 2001 ; 2:1007.

[11] Iannace S, Nicolais L; J Appl Polym Sci, 1997;4:911.

[12] Ikada Y, Jamshidi K, Tsuji H, Hyon S-H; Macromolecules, 1987 ;20, 904.

[13] Yamane H, Sasai K; Polymer, 2003;44: 2569-2575.

[14] Painter PC, Coleman MM ; Static and Dynamic properties of the Polymeric Solid State ; D. Reidel, Boston, Chaps. 6-8, 1982.

[15] Okihara T, Tsuji M, Kawaguchi A, Katayama K, Tsuji, Hyon H-S, Ikada Y. J Macromol Sci Phys; B30 (1 and 2)1991:119.

[16] Okihara T, Kawaguchi K, Tsuji H, Hyon S-H, Ikada Y, Katayama K, K. Bull. Inst. Chem. Res., Kyoto University, 1988;66:271.

[17] Tsuji H, Ikada Y; Polymer, 1999;40: 6699-6708.

[18] Tsuji H, Hyon S-H, Ikada Y; Macromolecules, 1991;24: 5651-5656.

[19] Urayama H, Kanamori T, Fukushima K, Kimura Y; Polymer, 2003; 44: 5635-5641.

[20] Tsuji H, Ikada Y; Polymer, 1995;36: 2709.

[21] De Santis P, Kovacs AJ. Biopolymers 1968; 6: 299–306.

[22] Okihara T, Tsuji M, Kawaguchi A, Katayama K, Tsuji H, Hyon S-H, Ikada Y. J Macromol Sci Phys 1991; B30: 119–140.

[23] Yamane H, Sasai K, Takano M. J Rheol 2004; 48(3): 599–609.

[24] Anderson KS, Hillmyer Marc A. Polymer 2006; 47: 2030–2035.

[25] Sarasua JR, Arraiza A Lopez, Balerdi P, Maiza I. J Mater Sci 2005; 40: 1855 – 1862.

[26] Xua J, Guoa B-H, Zhoub J-J, Lib L, Wuc J, Kowalczuk M. Polymer 2005; 46: 9176–9185.

[27] Di Lorenzo ML. Prog Polym Sci 2003; 28: 663–689.

[28] Di Lorenzo ML. Eur Polym J 2005; 41: 569–575.

[29] Tsuji H, Tezuka Y, Saha S Kumar, Suzuki M, Itsuno S. Polymer 2005; 46: 4917–4927.

[30] Krumme A. Polymer Testing 2004; 23: 29–34.

[31] Ding Z, Spruiell JE. J Polym Sci Part B Polym Phys 1996; 34: 2783.

[32] Wagner J, Phillios PJ. Polymer 2001; 42: 8999–9013.

[33] Beekmans LGM, Vancso GJ. Polymer 2000; 41: 8975–8981.

[34] Kikkawa Y, Abe H, Fujita M, Iwata T, Inoue Y, Doi Y. Macromol Chem Phys 2003 ;204 :1822–1831.

[35] Fraschini C, Plesu R, Sarasua J-R, Prud'homme RE. J Polym Sci Part B Polym Phys 2005; 43: 3308–3315.

[36] Abe H, Kikkawa Y, Inoue Y, Doi Y. Biomacromolecules 2001; 2:1007–1014.

[37] Baratian S, Hall ES, Lin JS, Xu R, Runt J. Macromolecules 2001;34: 4857–4864.

[38] Alamo RG, Mandelkern L, Stack GM, Krohnke C, Wegner G. Macromolecules 1994; 27: 147–156.

[39] Miyata T, Masuko T. Polymer 1998; 39:5515–5521.

[40] Lauritzen JI, Hoffman JD. J Appl Phys 1973; 44: 4340 –4352.

[41] Di Lorenzo ML. J Appl Polym Sci 2006; 100:3145–3151.

[42] Jang GS, Cho WJ, HA CS. J Polym Sci Part B Polym Phys 2001; 39: 1001–1016.

[43] Kim SH, Ahn SH, Hiraib T. Polymer 44 (2003) 5625–5634.

[44] McLeish TCB. Adv Phys 2002;51:1379–1527.

[45] Dorgan JR, Janzen J, Knauss DM, Hait SB, Limoges BR, Hutchinson MH. J Poly Sci Part B Polym Phys 2005;43:3100–3111.

[46] Glans JH, Turner DT. Polymer 1981;22:1540–1551.

[47] Tsuji H, Ikada Y. Polymer 1999;40:6699–6708.

[48] Wachsen O, Reichert KH, Kriiger RP, Much H, Schulz G. Polymer Degradation and Stability, 1997;55:225.

[49] Wachsen O, Platkowski K, Reichert KH. Polymer Degradation and Stability, 1997; 57: 87.

[50] Liu X, Zou Y, Li W, Cao G, Chen W. Polymer Degradation and Stability 2006; 91:3259.

[51] Jamshidi K, Hyon SH, Ikada Y. Polymer 1988;29:2229.

[52] Zhang X, Wyss UP, Pichora D, Goosen MFA. Polym. Bull. 1992;21:623.

[53] Bigg DM, Society of Plastics Engineers - Annual Technical Conference, 1996; 54(2):2028.

[54] Cam D, Marucci M. Polymer 1997;38:1879.

[55] Gu S-Y, Zhang K, Ren J, Zhan H. Carbohydrate Polymers 2008;74:79.

[56] Ferry JD, Viscoelastic properties of polymers, Third Edition. New York:John Wiley &Sons;1980.

[57] Khanna YP. Macromolecules 1993; 26: 3639–3643.

[58] Kelarakis A, Mai SM, Booth C, Ryan AJ Polymer 2005; 46: 2739–2747.

[59] Voigt W Lehrbuch der Kristallphysik; Teubner: Berlin, 1910.

[60] Reuss AZ angew Math Mech 1929; 9:49.

[61] Kerner EN Proc Phys Soc 1956; B69: 808.

[62] Budiansky BJ Mech Phys Solids 1965; 13: 223.

[63] Lellinger D, Floudas G, Alig I Polymer 2003; 44: 5759–5769.

[64] Coppola S, Balzano L, Gioffredi E, Maffettone PL, Grizzuti N Polymer 2004; 45: 3249–3256.

[65] Yu FY, Zhang HB, Zheng H, Yu W, Zhou C Eur Polym J, 2008; 44: 79–86.

[66] Godara A, Raabe D, Van Puyverde P, Molderaers P Polymer Test, 2006; 25: 460–469.

[67] Nobile MR, Bove L, Somma E, Kruszelnicka E, Sterzynski T Polym Eng Sci 2005; 45: 153–162.

[68] Coppola S, Grizzuti N, Maffettone PL Macromolecules 2001; 34: 5030.

[69] Guo J, Narh KA Adv Polym Tech 2002; 21: 214–222.

[70] Chen Q, Fan Y, Zheng Q Rheol Acta 2006; 48: 305–316.

[71] Zapas LJ, McKenna GB, Brenna A J Rheol 1989; 33: 69.

[72] Bove L, Nobile MR Macromol Symp 2002; 185 : 135–147.

[73] Chaari F, Chaouche M, Benyahial L, Tassin JF Polymer 2006 ; 47: 1689–1695.

[74] Wachsen O, Reichert KH; Kruger RP, Much H, Schulz G Polym Degrad Stab 1997; 55:225–231.

[75] Liu X, Zou Y, Li W, Cao G, Chen W Polym Degrad Stab 2006; 91: 3259–3265.

[76] Jamshidi K, Hyon SH, Ikada Y Polymer 1988; 29: 2229.

[77] Zhang X, Wyss UP, Pichora D, Goosen MFA Polym Bull 1992; 27: 623–629.

[78] YuryevY, Wood-Adams P, Heuzey M.-C, Dubois C, Brisson J Polymer 2008; 49: 2306–2320.

[79] Akima H J Assoc Comput Machinery 1970; 17: 589–602.

[80] Dealy JM, Wissbrun KF Melt Rheology and Its Role in Plastics Processing: Theory and Applications. Kluwer Academic Publishers: Dordrecht, 1999.

[81] Dorgan JR, Janzen J, Knauss DM, Hait SB, Limoges BR, Hutchinson MH J Poly Sci Part B: Polym Phys 2005; 43: 3100–3111.

[82] Dorgan JR, Lehermeier H, Mang M J Polym Environ 2000; 8: 1–9.

[83] Pogodina NV, Lavrenko VP, Srinivas S, Henning Winter H Polymer 2001; 42: 9031–9043.

[84] Hikosaka M, Yamazaki S, Wataoka I, Das NC, Okada K, Toda A, Inoue K J Macromol Sci Phys 2003; B42: 847–865.

[85] Kenny JM, Maffezzoli A, Nicolais L Thermochim Acta 1993; 227: 83–95.

[86] Fokin VM, Yuritsyn NS, Zanotto ED, Schmelzer JWP, Cabral AA J NonCryst Solids 2008; 354: 3785–3792.

[87] Tsuji H, Tezuka Y, Kumar S S, Suzuki M, Itsuno S Polymer 2005; 46: 4917–4927.

[88] Kitano T, Kataoka T, Shirota T Rheol Acta 1981; 20 : 207–209.

[89] Kitano T, Kataoka T, Nadatsuka Y Rheol Acta 1984; 23: 20–31.

[90] Maron SH, Pierce PE J Colloid Sci 1956; 11: 80.

[91] Kataoka T, Kitano T, Sasahara M, Nishijima K Rheol Acta 1978; 17: 149.

[92] Avrami M J Chem Phys 1939; 7: 1103.

[93] Mandelkern L Crystallization of polymers, 2nd ed.; Cambridge University Press: Cambridge, 2004.

[94] He C, Costeux S, Wood-Adams P Polymer 2004; 45: 3747–3754.

[95] Schwittay C, Mours M, Winter HH Faraday Discuss 1993; 101: 93–104.

[96] Horst RH, Winter HH Macromolecules 2000; 33: 130–136.

[97] Isichenko MB Rev Mod Phys 1992 ; 64: 961–1043.

[98] Gatos KG, Minogianni C, Galiotis C Macromolecules 2007; 40: 786–789.

[99] Rubinstein M, Colby RH Polymer Physics; Oxford University Press: New York, 2003.

[100] Binsbergen FL J Polym Sci, Polym Phys Ed 1973; 11:117

[101] Fitchmun DR, Newman S J Polym Sci A-2 1970;8:1545

[102] Billon N, Henaff V, Pelous E, Haudin JM. J. of Appl. Polym. Sci. 2002;86:725-733

[103] Grozdanov A, Bogoeva-Gaceva G. Composite Interfaces 1998;5(2):179-189.

[104] Wang C, Liu CR. Polymer 1999;40(2):289-298.

[105] Feldman A, Gonzalez MF, Marom G. Macromolecular Mater. and Eng. 2003;288(11):861-866.

[106] Wagner HD, Lustiger A, Marzinsky CN, Mueller RR. Comp. Sci. and Techn. 1993;48(1-4):181-184.

[107] Moon CK J. of Appl. Pol. Sci. 1994;54(1):73-82.

[108] Wood JR, Wagner HD, Marom G. J. of Mat. Sci. Lett. 1995;14(22):1613-1615.

[109] Zhang ZY, Zeng HM. J. of App. Pol. Sci. 1993;48(11):1987-1995.

[110] Zhang S, Minus ML, Zhu L, Wong C-P, Kumar S. Polymer 2008;49:1356-1364.

[111] Billon N, Henaff V, Pelous E, Haudin JM. J. of Appl. Polym. Sci. 2002;86:725-733

[112] Billon N, Henaff V, Haudin JM. J. of Appl. Polym. Sci. 2002;86:734-742.

[113] Gadzinowska K, Piorkowska E. Polymery 2003; 48, 11-12:790-799.

[114] Billon N, Haudin JM. Colloid Polym. Sci. 1993;271:343-356.

[115] Chatterjee AM, Price F P, Newman S. J. of Polym. Sci. 1975;13:2369.

[116] Ishida H, Bussi P. Macromolecules 1991;24:3569-3577.

[117] Fokin VM, Yuritsyn NS, Zanotto ED, Schmelzer JWP, Cabral AA. J. of Non-Cryst. Solids, 2008; 354(32): 3785-3792.

[118] Billon N, Esceleine JM, Haudin JM. Colloid & Polymer Sci. 1989;267:668.

[119] Vanden Poel G, Mathot VBF. Thermochimica Acta, 2007;461:107–121.

[120] Piorkowska E, Galeski A. Polymer 1992;33:3985.

[121] Martins JA, Cruz Pinto JJC. J. of Appl. Polym. Sci. 2004;91:125-131.

[122] Janeschitz-Kriegl H, Wippel H, Paulik C, Eder G J Coll. And Polym. Sci. 1993;271:1107-1115.

[123] Wu CH, Eder G, Janeschitz-Kriegl H. Colloid Polym. Sci. 1993;271:1116-1128.

[124] Hargis MJ, Grady BP. Thermochimica Acta 2006;443:147-158.

[125] Hernandez-Sanchez F, del Castillo LF, Vera-Graziano R. J. of App. Polym. Sci. 2004;92:970–978.

[126] Billon N, Magnet C, Haudin JM, Lefebvre D. Colloid Polym. Sci. 1994;272:633-654.

[127] Li JX, Cheung WL, Demin J, Polymer,1999; 40:1219–1222.

[128] Yuryev Y, Wood-Adams P. Macromol Theory Simul, 2010; 19(5):278-287.

[129] Raabe D, Acta Materialia 2004;52:2653.

[130] Raabe D, Godara A, Modelling Simul. Mater. Sci. Eng. 2005;13:733.

[131] Lorenzo AT, Arnal M-L, Albuerne J, Muller AJ. Polymer Testing 2007;26:222–231.

[132] Kenny JM, Maffezzoli A, Nicolais L. Thermochim Acta, 1993; 227: 83-95.

[133] Sarasua JR, Lopez Arraiza A, Balerdi P, Maiza I. J.of Mat. Science 2005;40:1855 – 1862.

[134] Yuryev Y, Wood-Adams P. J. of Polym. Sci. Part B- Polymer Physics 2010; 48(7): 812-822.

[135] Turnbull D, Fisher JC, J. of Chem. Phys., 1949: 17: 71.

[136] Wunderlich B ; Macromolecular Physics I, 1973, Academic press, New York.

[137] Hoffman JD, Davis GT, Lauritzen JI, Treatise of Solid State Chemistry, 1976, Vol.3.

[138] Marand HL, Stain RS, J. of Polym. Sci. Part B; Polym. Phys., 1988; 26 : 452.

[139] Park C, Robertson RE, Polymer, 2001;42: 2597–2609.

[140] Jones AA, Stockmayer WH, Molinari RJ, J. of Polym.Sci. Symp., 1976; 54: 227.

[141] Urakawa O, Adachi K, Kotaka T, Takemoto Y, Yasuda H, Macromolecules, 1994; 27: 7410.

[142] Tynenska B, Galesld A, Kryszewski M, Polym. Bull. 1981; 4:171-177.

[143] Sterzynski T, Garbarczyk J, J. of Mater. Sci., 1991;26 :6357-6361.

[144] Lu FJ, Hsu SL, Macromolecules, 1986;19: 326-341.

[145] Marand HL, Stein RS, Stack GM, J. Polym. Sci, Part B: Polym. Phys., 1988;26:1361-1383.

[146] Hong BK, Jo WH, Hwang IS, Polymer, 1999;37:4183-4191.

[147] Shojaie SS, Greenberg AR, Krantz WB, J. Membr. Sci., 1993; 79:115.

[148] Ye Y, Wnek GE, Krause S, Smith TW, J. Polym. Sci., Part B: Polym. Phys., 1996; 34 :309.

[149] Kawai T, Lee YM, Korea Polymer J., 1998 ; 6 :130-138.

[150] Morkved TL, Lu M, Urbas AM, Ehrichs EE, Jaeger HM, Mansky P, Russell TP, Science, 1996; 273: 931.

[151] Mansky P, DeRouchey J, Russell TP, Mays J, Pitsikalis M, Morkved TL, Jaeger HM, Macromolecules, 1998; 31:4399.

[152] Kolner H, Shiota A, Bunning TJ, Ober CK, Science, 1996; 272:252.

[153] Park C, Robertson RE, J. Mater. Sci., 1998;33:3541.

[154] Amundson K, Helfand E, Davis D, Quan X, Patel SS, Smith SD, Macromolecules, 1991; 24:6546.

[155] Amundson K, Helfand E, Quan X, Smith SD, Macromolecules, 1993;26: 2698.

[156] Wang C, Chien HS, Yan KW, Hung CL, Hung KL, Tsai SJ, Jhang HJ, Polymer 2009; 50: 6100–6110.

[157] Zhou H, Green TB, Joo YL, Polymer 2006; 47: 7497-7505.

[158] Sugita A, Tasaka S, J. Polym. Sci.: Part B: Polymer Physics, 2004 ;42 :4433–4439.

[159] Ziabicki A, Jarecki L, Macromol. Symposia, 1996;104:65-87.

[160] Yuryev Y, Wood-Adams P, Polymer, 2011; 52: 708-717.

[161] Ren J, Urakawa O, Adachi K, Macromolecules, 2003; 36: 210-219.

[162] Watanabe H, Macromol. Rapid Commun., 2001;22:127–175.

[163] Ramalho RR, Soares H, Melo LV, Mat. Sci. & Eng. C-Biomimetic and Sypramolec. Syst., 2007 ;27 :1207-1210.

[164] Graham S, Olmsted PD, Phys. Rev. Lett., 2009;103:115702.

[165] Shen C, Wang Y, Li M, Hu D, J. Polym. Sci.: Part B: Polym. Phys., 2011; 49 :409–413.

[166] Wasanasuk K, Tashiro K, Macromolecules, Article, DOI: 10.1021/ma2017666.

[167] Keller A, Kolnaar JWH, Proc. Polym. In Mat. Sci & Techn. Vol. 18; Meijer HEH Ed., John Wiley & Sons 1997.

[168] Kumaraswamy G, Kornfeld JA, Yeh FJ, Hsiao BS, Macromolecules 2002 ; 35: 1762.

[169] Pogodina NV, Winter HH, Srinivas S, J. Polym. Sci. B, 1999; 37: 3512.

[170] Pogodina NV, Winter HH, Macromolecules, 1998; 31: 8164.

[171] Janeschitz-Kriegl H, Ratajski E, Wippel H, Colloid Polym. Sci. 1999;277: 217.

[172] Janeschitz-Kriegl H, Colloid Polym. Sci.; 1997; 275: 1121.

[173] Graham RS, Olmsted PD, Phys Rev Lett. ; 2009 ; 103: 115702.

[174] Tanner RI, Qi F, J. Non-Newtonian Fluid Mech., 2005; 127:131.

[175] Eder G, Janeschitz-Kriegl H. Colloid and Polym Sci, 1988; 18: 1087-1094.

[176] Eder G, Janeschitz-Kriegl H. In: Meijer HEH, editor. Structure development during processing: crystallization. Materials science and technology, vol. 18. Weinheim: Verlag Chemie; 1997. Ch.5. p. 269–342.

[177] Zheng R, Kennedy PK, J. Rheol.,2004; 48, 823.

[178] Zuidema H, Peters GWM, Meijer HEH, Macromol. Theory Simul., 2001;4, 14.

[179] Coppola S, Grizzuti N, Maffettone PL. Macromolecules 2001;34: 5030.

[180] Coppola S, Balzano L, Gioffredi E, Maffettone PL, Grizzuti N, Polymer, 2004; 45;3249–3256.

[181] Doi M, Edwards SF. The theory of polymer dynamics. Oxford:Clarendon Press; 1986.

[182] Dai SC, Qi F, Tanner RI, Polym. Eng. Sci., 2006; 46: 659–669.

[183] Myung HS, Yoon WJ, Yoo ES, Kim BC, Im SS, J Appl Polym Sci, 2001,80, 2640–2646.

[184] Yu F, Zhang H, Zheng H, Yu W, Zhou C. European Polymer Journal 2008;44;79.

[185] Godara A, Raabe D, Van Puyverde P, Molderaers P. Polymer Testing 2006; 25; 460.

[186] Bove L, Nobile MR, Macromol. Symp. 2002; 180: 169-180.

[187] Nobile MR, Bove L, Somma E, Kruszelnicka E, Sterzynski T. Polymer Engineering and Science 2005; 45:153–162.

[188] Guo J, Narh KA, Advances in Polymer Technology, 2002; 21(3): 214–222.

[189] Narh KA, Roa E, Cohen C, Wang KK, Proc SPE ANTEC, 1995; 41: 2932.

[190] Godara A, Raabe D, Van Puyverde P, Molderaers P. Polymer Testing 2006;25;460.

[191] Chen Q, Fan Y, Zheng Q, Rheol. Acta, 2006; 48: 305-316.

[192] Zapas LJ, McKenna GB, Brenna A, J. Rheol. 1989; 33: 69.

[193] Bove L, Nobile MR, Macromol. Symp. 2002; 185: 135-147.

[194] Lellinger D, Floudas G, Alig I. Polymer 2003; 44: 5759.

[195] Bove L, Nobile MR, Azzurri F, Alfonso GC, Proceedings " 17th Annual Meeting of the Polymer Processing Society (PPS-17)", Montreal, 2001.

[196] Pogodina NV, Lavrenko VP, Srinivas S, Winter HH, Polymer, 2001; 42: 9031.

[197] Gavin PT, Whorlow RW, J. Appl. Polym. Sci. 1975; 19:567.

[198] Pearsom DS, Rochefort WE; J. Polym. Sci. Polym. Phys. 1982; 20: 83.

[199] Gleissle W, Rheol. Acta 1976; 15; 305.

[200] Ishida H, Bussi P, Macromolecules 1991; 24: 3569.

[201] Zeldovich J, J. Exptl. Theor. Phys. 1942; 12: 525.

[202] Becker R, Doering W, Ann. Physik 1935; 24: 719.

[203] Piorkowska E, Galeski A, Haudin JM, Prog. Polym. Sci. 2006; 31: 549.